Dedication

To my family: Mom, Pop, May and Paul for all their unconditional love and support, each who have uniquely contributed to my personal growth, to my other family: Peter who is my refuge and undoubtly provides love and encouragement when I need it most, Katie who continuoulsy brings light and laughter to anything I do, and Emile a constant reminder of the things you live for in life.

Acknowledgements

To those that helped me embark in my pursuit of science: Dwight Herren who first inspired my interests in science. The Herren Foundation and the McNair Program for their financial support, and to my sponsors who made this journey possible.

To those whom I am indebted for my accomplishments: The Neuroscience Program, Roger Albin an incredible mentor and exceptional scientist who has always put my best interests first. The many professors in the greater neuroscience community who have contributed to my scientific growth: Andrew Lieberman, Scott Turner, Geoff Murphy, Jose Esteban, Kirk Fry, Thomas Morrow, Gina Poe, John Fink, Lori Isom, Stephen Fisher, Mohammed Akaaboune, Jack Parent, Matt Lorincz, Henry Paulson, and Rich Hume

To all my friends here in Michigan that have made Ann Arbor a warmer place.

Table of Contents

List of Figures

List of Tables

Chapter I

Introduction

Huntington Disease

Huntington disease (HD) is a progressive and fatal autosomal dominant neurodegenerative disorder characterized initially by incoordination and involuntary movements, and preceded often by cognitive impairment and psychological disturbances (K. Duff et al., 2007; S. A. Johnson et al., 2007; A. C. Solomon et al., 2007). The involuntary movements consist of non-repetitive jerking of the limbs, face, or trunk described as choreic movements. With advancing disease, involuntary movements progressively worsen to include other voluntary movement disorders including bradykinesia, rigidity, and dystonia. Impaired voluntary movements typically occur early in the disease and affect motor speed, fine motor control, and gait. Oculomotor disturbances and motor impersistence also occur early and progressively worsen (S. Warby et al., 2008). Progressive decline of cognition with eventual severe dementia is typical also. Clinical symptoms manifest in mid-life with a mean age of onset between 35 and 44 years (G. P. Bates et al., 2002) with premature death 15 to 18 years after onset of clinical symptoms. Prevalence of HD is between 4-8/100,000 among populations of European decent and is less frequent among non-European ancestry. There are a larger number of individuals at risk for HD (P. M. Conneally, 1984; M. R. Hayden et al., 1986).

HD is caused by a CAG repeat expansion in the first exon of the *huntingtin* (*IT15*) gene on the short arm of chromosome 4 resulting in an expanded polyglutamine domain

1

in the huntingtin protein (htt), a 350 kD protein of unknown function expressed in the cytoplasm of many cell types (T. V. Strong et al., 1993; G. B. Landwehrmeyer et al., 1995; A. H. Sharp et al., 1995). CAG/Polyglutamine (polyQ) expansions exceeding 39 result in full penetrance, while normal repeats contain less than 27 with a median of 18 (B. Kremer et al., 1994; S. Warby et al., 2008). CAG repeats ranging between 36-39 exhibit reduced penetrance and may not present with the HD phenotype. However, it is not clear whether all these individuals would develop HD if given a longer than normal lifespan (D. C. Rubinsztein et al., 1996). Repeats between 27-35 are intermediate allele carriers. Intermediate allele carriers do not develop HD, but show repeat instability upon germline transmission to subsequent generations resulting an increased risk for their offspring to expand >35 CAG repeats and develop HD (A. Semaka et al., 2006). Factors influencing CAG repeat instability include the CAG size, the sex and age of the transmitting parent, family history, and the HD gene and associated polymorphic sequences (A. Semaka et al., 2006). CAG repeat length strongly correlates with the age at which motor symptoms appear such that an individual with longer triplet repeat numbers will develop symptoms earlier (H. D. C. R. Group, 1993b). CAG repeat size accounts for 42-73% of the variability in age of motor onset (S. E. Andrew et al., 1993; O. C. Stine et al., 1993; R. R. Brinkman et al., 1997). The remaining variance in onset of age is attributed to genetic modifiers (S. Metzger et al., 2008), and a small component to environmental factors (N. S. Wexler et al., 2004).

Family of Polyglutamine Disorders

HD belongs to a family of inherited polyglutamine diseases including spinobulbar muscular atrophy (SMBA/Kennedy's disease), dentatorubral-pallidoluysian atrophy

(DRPLA), and spinocerebellar ataxias (SCAs)1, 2, 3, 6, 7, 8 and 17, all of which are less common than HD [Table I.1 (C. J. Cummings and H. Y. Zoghbi, 2000; H. T. Orr and H. Y. Zoghbi, 2007)].

Disease	Gene	Protein	Normal repeat	Expanded repeat	Reference
SMBA	AR	Androgen receptor	9-36	38-62	La Spada, A. 1991
HD	HD	Huntingtin	6-35	36-121	H.D.C.R.G. 1993
DRPLA	DRPLA	Atrophin-1	6-35	49-88	Koide, R. 1994
SCA1	SCA1	Ataxin-1	6-44	39-82	Orr, H. 1993
SCA2	SCA2	Ataxin-2	15-31	36-63	Pulst, S. 1996
SCA3	SCA3	Ataxin-3	12-40	55-84	Kawaguchi, Y. 1994
SCA6	SCA6	Ataxin-6	4-18	21-33	Zhuchenko, O. 1997
SCA7	SCA7	$_{1A}$-voltage-dependent calcium channel subunit	4-35	37-306	David, G. 1997
SCA8	SCA8	Ataxin-8	16-34	>74	Moseley, M. 2006
SCA17	SCA17	TATA-binding protein	29-42	47-55	Nakamura, K. 2001

Table I.1 Family of polyglutamine diseases.

Recently, another dominant ataxia, SCA8, previously identified as caused by an untranslated CTG expansion, has been recognized as having a bidirectional CAG repeat that is thought to contribute to the disease (M. L. Moseley et al., 2006). Following generation of a transgenic mouse model of SCA8 overexpressing the entire human ataxin 8 locus, the authors unexpectedly discovered polyglutamine-containing inclusions within neurons. Further analyses confirmed transcription in the reverse direction, producing a

pathogenic CAG-containing transcript that encodes expanded polyglutamine. All these diseases are dominantly inherited with the exception of SMBA, which is X-linked, and share an abnormal CAG expansion beyond the normal range in the coding region of the gene, producing an altered form of the normal protein. Because the family of polyglutamine diseases all share an abnormally expanded polyglutamine repeat (polyQ) in unrelated proteins and are all autosomal dominant disorders with the exception of X-linked SMBA, it is likely that the expanded CAG domain is the driver of pathogenesis (see Table I.2 for shared commonalities).

CNS disease
Dominant Inheritance (except for X-linked SMBA)
Regionally selective pathology
CAG repeat length dependent age of onset
Anticipation through paternal transmission

Table I.2 Commonalities of polyglutamine diseases.

A classic study by Ordway and colleagues addresses the primacy of expanded CAG repeats in the genesis of polyQ disorders. This group demonstrated that CAG repeats need not be in one of the classic trinucleotide repeat disorder genes to produce a neurotoxic effect. By introducing a 146-unit CAG repeat into the mouse hypoxanthine phosphoribosyltransferase locus (*HPRT*), a gene normally without a CAG repeat domain, they created a novel disease that replicated features of CAG repeat disorders, such as polyglutamine-containing inclusions and premature death (J. M. Ordway et al., 1997).

4

The expanded polyQ domains are thought to cause a common neuropathologic hallmark of cytoplasmic and neuronal intranuclear inclusions (NIIs) containing pathogenic protein [full length or proteolytic fragments; (M. DiFiglia et al., 1997)]. There is debate as to whether these aggregates contribute to pathogenesis (I. A. Klement et al., 1998; F. Saudou et al., 1998; C. J. Cummings et al., 1999), but they are useful markers of abnormal protein processing. Beyond these commonalities, the CAG/polyglutamine family of diseases displays a range of clinical manifestations that appear to be protein context dependent. The differences in the regionally selective pattern of neuropathology observed in this family of diseases are likely to be mediated by the amino acid sequences surrounding the polyQ tract. For example, *huntingtin* and several of the SCA causing loci have widespread expression in many neuronal and non-neuronal cells. However, in HD there is selective degeneration of striatal neurons and SCAs exhibit selective degeneration of cerebellar and pontine neurons (A. H. Sharp et al., 1995; B. W. Soong and H. L. Paulson, 2007). In general, the pattern of protein expression in polyQ disorders does not correlate with the regional pattern of pathology. Because different proteins contain different interaction domains, cleavage sites, and phosphoregulation sites, these differences are likely to influence the functional consequences of expanded polyQ/CAG repeat expansions. Despite the widespread expression of all ten genes, only a certain subset of neurons is vulnerable to degeneration, suggesting that protein context may be responsible for the selective neuronal vulnerability.

Neuropathology

Regional Selective Neurodegeneration and Loss of Dopamine (DA) Receptors

The striatum contains a large number of medium-sized neurons with spiny dendrites and long axons (projection neurons), as well as small subsets of medium and large-sized neurons with smooth dendrites and short axons (interneurons). The medium spiny projection neurons are the main afferent neurons of the basal ganglia, compared to the aspiny interneurons, which receive only sparse innervation (G. A. Graveland et al., 1985). Striatal interneurons are subdivided by expressed neurotransmitters/neuropeptides. Important interneuron subpopulations include cholinergic interneurons, and interneurons containing somatostatin (SS) and neuropeptide Y (NPY). There are four types of striatal projection neurons that are subdivided based on their primary projection target. All striatal projection neurons express GABA as their primary neurotransmitter. Projection neurons to the external segment of the globus pallidus (GPe) are typically enkephalin (ENK) enriched and mainly devoid of substance p (SP). Striatal neurons primarily projecting to the internal segment of the globus pallidus (GPi) are primarily substance P (SP) expressing with little expression of ENK. Striatal neurons projecting to the substantia nigra pars reticulata (SNr) and pars compacta (SNc) also are rich in SP and typically poor in ENK (S. N. Schiffmann and J. J. Vanderhaeghen, 1991; J. S. Fink et al., 1992). The dendrites of striato-GPe neurons are enriched in D2 dopamine receptors, while the dendrites of striato-GPi neurons are enriched in D1 dopamine receptors, as are the dendrites of striatonigral neurons and their terminals in the SN (S. N. Schiffmann and J. J. Vanderhaeghen, 1991; J. S. Fink et al., 1992).

The striatum receives abundant excitatory afferents from the cortex, thalamus, and subthalamic nucleus (STN). Striatal afferents also include dopamine-containing fibers from the pars compacta of the substantia nigra. GPi and SNr represent the major output nuclei of the basal ganglia (R. L. Albin et al., 1989; M. R. DeLong, 1990). Output from the basal ganglia is directed primarily to the thalamus, which projects to cortical regions such as the prefrontal and motor cortices.

Neuropathologic examination of postmortem HD brains reveals early and marked degeneration of GABAergic medium spiny neurons (MSNs) of the striatum (J. P. Vonsattel and M. DiFiglia, 1998), and because the striatum is composed primarily of these projection neurons, their vulnerability in HD is responsible for the pronounced atrophy of the striatum observed by late HD (A. M. Graybiel, 1990). Selected cortical regions such as the primary motor cortex are affected to a lesser extent, while other regions of the brain, such as the cerebellum, remain relatively unaffected. In early stages of HD, ENK-containing MSNs of the striato-GPe pathway degenerate, explaining the typical hyperkinetic, choreiform movements of HD (R. L. Albin et al., 1989; G. E. Alexander and M. D. Crutcher, 1990). In later stages of the disease, MSNs coexpressing SP projecting to the GPi are also severely affected (see Figure I.1). These neurons are responsible for the initiation of voluntary movements and death of these neurons results in the dystonic and parkinsonian symptoms observed at end-
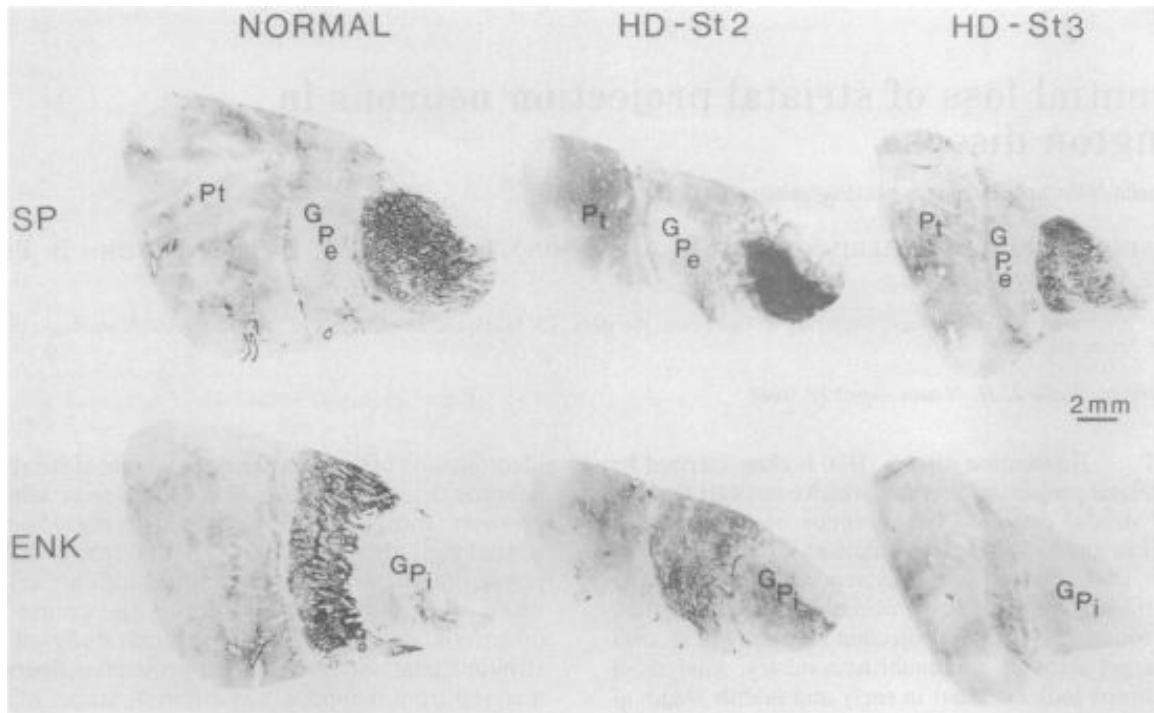
Figure I.1 Preferential loss of HD pathology. Immunohistochemical sections showing GPi of normal control in early (HD-St2) and late stage HD (HD-St3) stained for SP (*upper panel*) and ENK (*lower panel*). Early stage exhibits gross atrophy of GPe and subsequently in later stages with prominent reductions in SP and ENK containing fibers in GPe and GPi (Reiner A. et al., 1988).

stage of the disease (V. Macdonald and G. Halliday, 2002). However, degeneration of striatal neurons is not uniform. Interneurons coexpressing NPY and SS are relatively preserved, and cholinergic interneuron perikarya are also spared [see table I.3 for summary of striatal pathology; (D. Dawbarn et al., 1985; A. Reiner et al., 1988)].

Relative Sparing of striatal dopaminergic afferents
Interneurons: - SS/NPY/NOS spared   - Cholinergic interneuron spared but dysfunctional

Projection neurons: sequential/subsequent degeneration
              Early: Str-GPe, Str-SNr
              Late: Str-GPi, Str-SNc

Degenerative-Regenerative Changes:
     abnormal dendritic growth (branches and spines)
     density of spines may be unchanged, severely reduced, or markedly increased

8

Table I.3 Striatal degeneration in HD.

Expression of htt is widespread and there is no clear correlation between htt expression and the initial selective pathology (T. V. Strong et al., 1993; G. B. Landwehrmeyer et al., 1995; A. H. Sharp et al., 1995; S. Kuemmerle et al., 1999). End-stage disease postmortem HD brains reveal up to a 90% neuronal loss in the striatum and a 40% loss in the cortex. Even in early stages of the disease, imaging studies have also revealed marked striatal and cortical atrophy in preclinical HD (E. H. Aylward et al., 2000; E. H. Aylward et al., 2004; L. J. Beglinger et al., 2005; H. D. Rosas et al., 2005), suggesting that neuronal degeneration occurs early in the disease process prior to motor symptoms. Concurrent atrophy of the cortex and striatum is not surprising given the highly complex interconnections of the corticostriate pathway. Support for early distinct cortical degeneration is consistent with the detection of htt aggregates in cortex of HD postmortem brains prior to clinical symptoms, and the detection of NIIs in select cortical regions prior to motor deficits in mouse models of HD (C. A. Gutekunst et al., 1999; L. B. Menalled et al., 2003). Recent evidence provides support for cortical degeneration and its involvement in distinct motor phenotypes and disease progression that has been previously attributed to degeneration of the striatum (H. D. Rosas et al., 2004b; H. D. Rosas et al., 2005). Differential topographic corticostriate degeneration may explain the clinical heterogeneity observed in HD. Whether cortical atrophy precedes, results from, or is independent of striatal degeneration remains to be further investigated. Striatal degeneration is accompanied by DA receptor loss. Imaging studies exhibit loss of striatal dopamine receptors in presymptomatic HD mutation carriers and are consistent with mouse models of HD (R. A. Weeks et al., 1996; J. H. Cha et al., 1998; L. Kennedy et al.,

2005; J. C. H. van Oostrom et al., 2005; M. Y. Heng et al., 2007). DA receptor declines in HD brains progressively worsen and became more widespread to include extrastriatal regions (N. Pavese et al., 2003).

Neuronal Intranuclear Inclusions (NIIs) and Cytoplasmic Aggregates

NIIs and cytoplasmic aggregates are a characteristic feature of HD and other polyQ diseases (M. DiFiglia et al., 1997; H. L. Paulson et al., 1997; M. L. Maat-Schieman et al., 1999; R. de Pril et al., 2004). The hydrophobic polyQ tract is thought to result in the formation of protein aggregations within the cell (M. F. Perutz et al., 2002). Because these aggregates and NIIs harbor components of the ubiquitin proteasome system and sequester other proteins - important transcription factors or regulatory elements - the accumulation of these aggregates is suggested to be toxic and pathogenic. How these abnormal inclusions form and whether they are protective, pathogenic, or possibly both over the course of disease is not well understood.

Inclusions often precede onset of symptoms and have been proposed to be involved in the pathogenesis of polyQ disorders including HD (M. DiFiglia et al., 1997). There is a strong correlation between brain regions most affected and NII formation; striatal regions exhibiting highest levels of of NIIs and neuropil inclusions correlate with greatest pathology in HD (M. L. Maat-Schieman et al., 1999). Consistent with human observations, aggregates are found in brain regions containing neurons that degenerate in mouse models of HD as well as in other polyQ disorders (H. L. Paulson et al., 1997; I. A. Klement et al., 1998). Aggregation results from a fibrillar beta-pleated sheet conformation, while no aggregation occurs with normal htt expression (A. Lunkes and J. L. Mandel, 1997; E. Scherzinger et al., 1997; J. K. Cooper et al., 1998; H. Li et al., 1999).

10

A conditional mouse transgenic model of HD that allowed reduced expression of the mutant Htt in symptomatic mice led to a disappearance of NIIs and an amelioration of the behavioral phenotype (A. Yamamoto et al., 2000).

Whether inclusions are pathogenic or protective is debated. Some emerging evidence has shown that striatal neurons not containing NIIs are more susceptible to death compared to those that contain NIIs (M. Arrasate et al., 2004), suggesting that NIIs may be protective. Additional studies also show that aggregate formation does not necessarily result in cell death (M. W. Becher et al., 1998; E. J. Slow et al., 2005; E. J. Slow et al., 2006). Whether disease causing or not, NIIs are a marker of neuronal involvement.

Mechanisms of Pathogenesis

The mechanisms of pathogenesis are complex, as mutant htt is implicated in several cellular dysfunctions, from transcriptional dysregulation to glutamate excitotoxicity (see Table 1.4 for summary of mechanisms). The altered interactions of htt and its binding partners as a result of the expanded polyglutamine tract has led to the hypothesis of the direct disruption or loss of function (haploinsufficiency) as a result of altered binding of interacting proteins (G. Morfini et al., 2005; W. Zhai et al., 2005).

Gain of Function Toxicity
Impaired UPS and Hsp function
Transcriptional dysregulation
Altered Ca^{2+} signaling
Impaired energy metabolism
Glutamate excitotoxicity
Loss of Function/Haploinsufficiency
Loss of REST/NRSE activity
Loss of axonal transport

Table I.4 Summary of possible mechanisms involved in HD.

Loss of function/Haploinsufficiency Versus Gain of Function Toxicity

Loss of REST/NRSF function: Zuccato and colleagues provided evidence for a possible form of haploinsufficiency in cell culture model systems demonstrating that wild type htt interacts with repressor element-1 transcription factor/neuron restrictive silencer factor (REST/NRSF) by maintaining its localization to the cytoplasm, thus reducing its transcriptional availability to suppress transcription of important neuronal genes such as brain-derived neurotrophic factor (BDNF), and consequently enhancing transcription of these genes. Conversely, mutant htt reduced cytosolic REST/NSF residence and increased nuclear REST/NRSF activity and reduced expression of trophic factors. This experiment demonstrates wild type htt mediated regulatory activity on gene transcription and loss of function mediated toxicity (C. Zuccato et al., 2003).

Loss of axonal transport : Htt is a relatively large protein containing multiple motifs involved in many cellular functions, and one such motif may be involved in cytoplasmic transport (M. A. Andrade and P. Bork, 1995). Htt is also known to interact with various proteins involved with axonal transport, such as clathrin-coated vesicles,

12

microtubules, and cytoplasmic granules (M. DiFiglia et al., 1995; C. A. Gutekunst et al., 1995; E. Sapp et al., 1997; G. Szebenyi et al., 2003). Loss of normal intracellular transport as a result of the polyQ expansion in HD is plausible. Huntingtin-associated protein 1 (HAP1), an interacting protein of htt, has been implicated in axonal transport. Unlike the widespread expression of htt, HAP1 is predominantly expressed in neurons (X. J. Li et al., 1995; C. A. Gutekunst et al., 1998). Mutant htt enhances binding to HAP1. The resulting alteration in HAP1 function inhibits axonal transport (X. J. Li et al., 1995; L. R. Gauthier et al., 2004). The interaction of HAP1 and wild-type htt normally facilitate the transport of brain derived neurotrophic factor (BDNF), a trophic factor produced by cortical neurons that is essential for the survival and maintenance of striatal neurons (J. M. Canals et al., 2001). Cumulative studies of HD postmortem brains exhibit significant reductions in cortical BDNF mRNA and protein compared to controls (C. Zuccato et al., 2007) as well as up to a 50% loss of BDNF protein in the striatum, regions of the brain that exhibit the greatest neurodegeneration (I. Ferrer et al., 2000). Impaired BDNF delivery resulting from the loss of wild-type htt has previously been proposed as a mechanism by which striatal neurons become injured (C. Zuccato et al., 2001; J. M. Canals et al., 2004; L. R. Gauthier et al., 2004; A. D. Strand et al., 2007). Consistent with general impaired transport, mutant htt also impairs the motility of mitochondria (E. Trushina et al., 2004). Whether mitochondrial immobility is central to HD is not clear. It is possible, however, that mitochondrial immobility could result in insufficient delivery of ATP or reduced capacity to buffer intracellular/extracellular increases of cytosolic Ca^{2+}.

However, the dominant nature of the shared expanded polyQ domain in all 10 polyglutamine disorders suggests a gain of function toxicity. Several key experiments corroborate this. White et al. showed that dramatic reduction of wild type htt results in aberrant brain development and perinatal lethality. These abnormalities were rescued by expanded mutant htt, indicating that the polyQ tract does not exert a dominant negative effect, as well as showing that abnormal neuronal development and perinatal lethality does not mimic the HD phenotype, supporting a gain of function mechanism (J. K. White et al., 1997). Experimental studies also demonstrate gain of function toxicity by linking an expanded polyQ tract to an otherwise inert and normal protein producing neurological abnormalities and NIIs in rodents, directly linking toxicity to polyQ length (J. M. Ordway et al., 1997; K. L. Moulder et al., 1999). These findings are also consistent with other polyQ disorders. The selective neuronal loss particular to each disease occurs only when the full-length protein harboring an expanded glutamine tract is expressed, indicating that these diseases are caused by a gain of function mechanism and that the expanded polyQ tract are at the core of pathogenesis (X. Lin et al., 1999; H. Y. Zoghbi and H. T. Orr, 1999).

It is possible that mutant htt imposes both loss of function and gain of function mechanisms, and that a subtle loss of function/haploinsufficiency acting concomitantly with gain of function toxicity is sufficient to achieve pathogenesis on multiple levels that could be causal for the distinctive regional pathologies in these diseases. Recent findings report dual pathogenic mechanisms in SCA1 showing that the expanded polyQ Ataxin-1 favors formation of a particular protein complex exerting a gain of function toxicity,

while at the same time the polyQ domain attenuates the formation of another protein complex contributing to a partial loss of function mechanism (J. Lim et al., 2008).

Impaired Ubiquitin Proteasome System (UPS) and Heat Shock Proteins (Hsp)

Cytoplasmic and NIIs sequestration of components of the UPS and critical Hsps has implicated impaired protein quality control as a mechanism of polyQ induced cell death. The UPS and molecular chaperones are important in maintaining protein quality control by facilitating refolding or degradation of misfolded polypeptides, thus reducing the levels of soluble abnormal proteins (M. P. Hinault et al., 2006). Hsp 40 and Hsp70 are both involved in the clearance of misfolded proteins through the ubiquitin-proteasome pathway and were found to associate with nuclear aggregates in HD cell culture and transgenic mouse models of HD. Overexpression of Hsp and associated co-chaperones reduce aggregate formation (B. Bercovich et al., 1997). These findings suggest that cytoplasmic aggregates and NIIs may contribute to toxicity by sequestering important regulators of protein homeostasis; thus making it more difficult to respond to the constant accumulation of misfolded proteins and possibly the functional recruitment of these proteins making them less available for other cellular processes. Experimental studies have examined the rate of degradation and have found that it has a functional consequence on normal UPS function. Htt with an expanded pathogenic polyQ tract EGFP-tagged exhibited slower aggregation formation and increased cellular toxicity compared to a non-toxic polyQ tract, indicating that the half-life of the soluble htt was dependent on the polyQ tract length (M. D. Kaytor et al., 2004). Consistent with these findings, Hunter and colleagues found that mutant htt expressing cells exhibited a functional decrease of UPS activity and degradation of ubiquitylated substrates (J. M.

Hunter et al., 2007), supporting UPS dyfunction as a consequence of the mutant htt PolyQ expansion. Whether chaperones are directly involved in aggregation is not clear. Ubiquitination of NIIs may merely represent end products of an upstream toxic event.

Transcriptional Dysregulation

Data indicates nuclear localization of mutant species of the expanded polyQ protein is necessary for toxicity (LaSpada 2002 Neuron; Klement I.A Cell 1998; W.Jackson HMG 2003). Perhaps expanded polyQ exerts toxicity by altering normal transcription in the nucleus. Alterations in mRNA transcripts have been reported in HD postmortem brains as well as in brains of mouse models of HD (E. A. Thomas, 2006; J. H. Cha, 2007; A. Kuhn et al., 2007; G. D. R. Kuhn A., Hodges A., Strand A.D., Sengstag T., Kooperberg C., Becanovic K., Pouladi M.A., Sathasivam K., Cha J.H., Hannan A.J., Hayden, M. R., Leavitt B.R., Dunnett S.B., Ferrante R.J., Albin, R. L., Shelbourne P., Delorenzi M., Augood S.J., Faull R.L., Olson J.M., Bates B.P., Jones, L., Luthi-Carter R., 2007). Transcription factors, such as CREB-binding protein (CBP), TATA box binding protein (TBP), specificity protein 1 (SP1), and p53 are present with mutant htt in aggregations and NIIs (J. S. Steffan et al., 2000; F. C. Nucifora, Jr. et al., 2001; P. Harjes and E. E. Wanker, 2003; S. H. Li and X. J. Li, 2004). These findings suggest sequestration and depletion of important transcription factors by the mutant protein, which could contribute to a cascade of perturbed signaling pathways. Similarly, mutant htt could alter gene transcription by directly binding to transcription factors and inhibiting their normal function. For example, recent work shows that mutant htt binding to NF-Y transcription factor results in the negative regulation of HSP70 (T. Yamanaka et al., 2008). Alterations in gene expression is an important question related to disease

pathogenesis in HD (J. H. Cha, 2007; M. O. Kim et al., 2008) whether it is sequestration

of critical transcription factors by NIIs or direct interaction of mutant huntingtin that

leads to transcriptional dysregulation.

Altered Ca^{2+} Homeostasis

Expanded polyQ htt may perturb important regulators of intracellular Ca^{2+}

homeostasis. Altered N-methyl-D-aspartate (NMDA) receptor dysfunction is one

contributing factor to intracellular Ca^{2+} homeostasis. Intracellular Ca^{2+} storage sites such

as the endoplasmic reticulum are key regulators of Ca^{2+} homeostasis (T. S. Tang et al.,

2003b; H. B. Fernandes et al., 2007). *In vitro* experiments suggest that direct binding of

mutant htt causes abnormal sensitization and activation by type 1 inositol 1,4,5-

trisphosphate receptor (InsP3R1). This intracellular Ca^{2+} release channel, located on the

endoplasmic reticulum predominantly and expressed in the brain, results in the

detrimental overload of cytosolic Ca^{2+} in MSNs compared to wild type htt (T. S. Tang et

al., 2003b). These findings link htt and InsP3R1-mediated neuronal Ca^{2+} signaling and

provide an additional explanation for how mutant htt contributes to the unbalanced Ca^{2+}

signaling in HD. Expanded polyQ htt may exert other multiple actions on neuronal Ca^{2+}

homeostasis by altering mitochondrial dysfunction (M. F. Beal, 1992b; J. M. Oliveira et

al., 2007).

Impaired Energy Metabolism

There is also evidence for mitochondrial dysfunction and altered energy

metabolism in HD. The most compelling evidence stems from the initial discovery that

the accidental ingestion of the mitochondrial toxin 3-nitropropionic acid (3NP) produces

preferential degeneration of the putamen and caudate similar to HD (S. E. Browne et al.,

1997; E. Brouillet et al., 2005). 3NP inhibits complex II/succinate dehydrogenase

activity in the mitochondria, which is consistently reduced in the striatum of patients with

HD (M. Gu et al., 1996; S. J. Tabrizi et al., 1999). These findings have been replicated

using 3NP and malonate in non-human primates and rodents, causing striatal lesions

similar to HD (M. F. Beal et al., 1991; M. F. Beal, 1994; O. A. Andreassen et al., 2000).

Postmortem HD brains show deficiencies in mitochondrial complex II, III, and IV,

particularly in the caudate (V. M. Mann et al., 1990; M. Gu et al., 1996), suggesting an

important role for mitochondrial energy metabolism in pathogenesis. There is also

evidence for the direct interaction of mutant htt and mitochondria. Direct binding of

mutant htt lowers the threshold of the mitochondrial membrane potential resulting in a

lower Ca^{2+} response of the mitochondrial permeability transition pores (MT-PTP).

Isolated mitochondria from lymphoblasts of HD patients and striatal neurons from animal

models of HD consistently show more sensitivity in opening of the MT-PTP in response

to calcium compared to controls. These perturbations in mitochondrial membrane

depolarization, largely resulting in caspase activation and pro-death pathways, and can be

ameliorated by Cyclosporin A (CsA), a specific MT-PTP inhibitor (A. Sawa et al., 1999;

A. V. Panov et al., 2002; M. M. Zeron et al., 2004; A. V. Panov et al., 2005).

Dysfunction of mitochondrial energy metabolism leads to reduced ATP production,

increase lactate levels, perturbed calcium signaling, and the increased generation of

reactive oxygen species. These findings of impaired mitochondrial energy metabolism

have recently been challenged. Powers et al. reported that measurements of the cerebral

oxygen metabolism to cerebral glucose metabolism ratio in HD patients were inconsistent

with impaired energy metabolism as a result of defects in mitochondrial electron

transport chain (W. J. Powers et al., 2007a; W. J. Powers et al., 2007b). Although

possibly involved in some way with HD pathogenesis, mitochondrial dysfunction may be

only one factor that alters Ca^{2+} homeostasis in HD.

Glutamate Excitotoxicity

Another promising line of research implicates altered N-methyl-D-aspartate

receptor (NMDAR) function as a likely contributor to perturbed intracellular Ca^{2+}

homeostasis in HD (T. Milakovic et al., 2006; H. B. Fernandes et al., 2007). Growing

evidence links NMDAR excitoxicity with selective degeneration in HD [see table 1.3 for

HD comparison to glutamate excitotoxicity (L. Li et al., 2003; T. S. Tang et al., 2003b;

A. J. Starling et al., 2005; E. Perez-Navarro et al., 2006)]. Coyle and Schwarcz and the

McGeers developed the first model of HD with demonstrations that acute intrastriatal

administration of the glutamate agonist kainate produced neurodegeneration with features

of HD (J. T. Coyle and R. Schwarcz, 1976; E. G. McGeer and P. L. McGeer, 1976). This

spurred subsequent work with NMDAR selective agonists resulting in acute striatal

lesions that reproduced more features of striatal pathology in HD (M. F. Beal et al., 1986;

T. J. Bazzett et al., 1993). Other studies have shown that cultured striatal neurons from

mouse models of HD exhibited a polyglutamine length-dependent enhancement of peak

NMDAR current compared to wild type. This was not observed in cortical neurons from

HD mice, suggesting a mechanism by which striatal neurons selectively degenerate (J.

Shehadeh et al., 2006; M. M. Fan and L. A. Raymond, 2007). Zeron and colleagues

demonstrated that striatal neurons from a transgenic mouse model of HD were more

vulnerable to NMDAR-mediated death. Excitotoxic death of these neurons was

increased after instrastriatal injection of quinolinic acid and NMDA but not AMPA and

moreover, was not observed in extrastriatal regions (M. M. Zeron et al., 2002). The

NR2B subunit of the NMDAR, known to mediate pro-death pathways, is highly

expressed in the striatum compared to other regions of the brain (K. D. Kuppenbender et

al., 2000), supporting a role for NR2B NMDAR-mediated excitotoxicity. Consistent

with these findings is the increased NR1/NR2B composition of NMDA receptors at the

cell surface of striatal neurons in a transgenic model of HD, supporting the hypothesis

that mutant htt alters NMDA receptor function via the NR2B subunit [see Fig. 1.2 for

proposed mechanism of action; (N. Chen et al., 1999; M. M. Fan et al., 2007).

Glutamate excitotoxic lesions reproduce many of the neuropathological changes

of HD, such as marked degeneration of the striatum specifically long projecting ENK/SP

containing MSNs while sparing short SS/NPY/NOS containing aspiny interneurons and

cholinergic interneurons (see Table I.5 for complete comparison). Because excitotoxic

lesions recapitulate HD striatal pathology and because of convergent evidence of altered

Ca^{2+} signaling tied to aberrant NMDA receptor function, glutamate excitotoxicity is a

strong candidate for a proximate cause of neurodegeneration in HD.

Relative sparing of dopaminergic afferents	yes
Sparing of SS/NPY/NOS interneurons	yes
Sparing of cholinergic interneuron's with loss of ChaT activity	yes
Loss of Parvalbumin interneuron	yes
Degenerative/regenerative changes in striatal projecting neurons	yes
Preferential loss of striato-GPe and striatonigral projection neurons	no

Table I.5 Similarities between HD pathology and excitotoxic lesions.
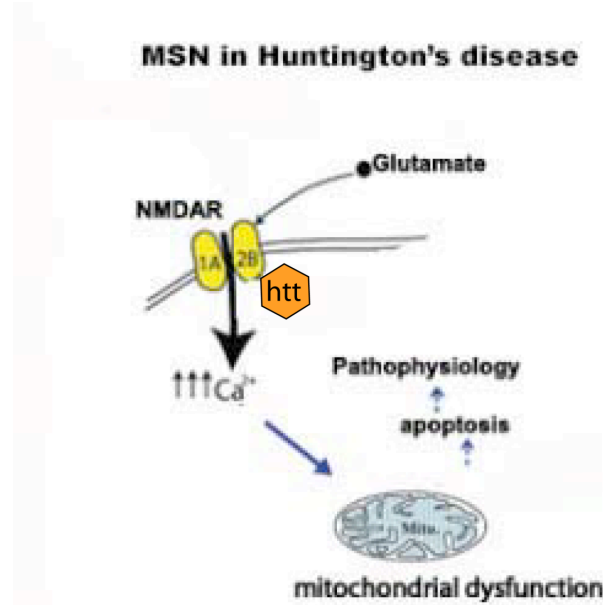
Figure I.2 Proposed mechanism of NR2B NMDA receptor-mediated excitotoxicity. Model demonstrates sensitzation of the NMDAR via binding of mutant htt to the NR2B subunit resulting in toxic levels of Ca^{2+} entry.

Summary of Mechanisms

All these hypotheses have some experimental support. The mechanism(s) by which mutant htt exerts neuronal dysfunction and eventually neurodegeneration in HD may begin with one event cascading to multiple toxic events. Neuronal dysfunction may begin with the accumulation of cytoplasmic aggregates and NIIs sequestering important neuronal transcription factors leading to transcription dysregulation and at the same time overwhelming the UPS involved in protein quality control. These additive insults, along with senescence, may subsequently cascade and weaken other cellular processes such as impaired axonal transport, reduced delivery of critical neuronal trophic factors, and

disruption of membrane potential resulting in deranged Ca^{2+} regulation from extracellular and intracellular sources, such as the NMDA receptor and mitochondria.

It is possible that expanded mutant htt is neurotoxic because it has multiple deleterious effects. However, it is important to consider whether these individual events are primary or secondary, and whether these perturbations are a necessary step in the pathophysiologic cascade leading to neurodegeneration in HD. Whether there is one pathway leading to neurodegeneration in HD or an overlapping network of expanded polyQ effects resulting in neurodegeneration remains unclear. Important to clinically relevant HD research is the elimination of potential pathways that may be irrelevant to the disease while narrowing the search for more promising therapeutic intervention. By doing so, we will also provide a better understanding of the normal function of htt and gain of function or loss of function properties of the mutant htt protein.

Murine Models of HD

Since the cloning of HD, various murine models have emerged and become useful tools in studying HD (see table II.1 for complete summary and comparison). However, a valid murine model of HD is crucial. Differences in findings between murine models are debated and attributed to differences in genetic design. Furthermore, some pharmacological interventions shown to ameliorate symptoms and pathological progression in some murine models fail to translate to positive results in human clinical trials (H. S. Group, 2001). A valid murine model of HD should recapitulate the key features of HD. These include progressive motor impairments, early loss of striatal projection neurons, and the regional striatal specific expression of NIIs and cytoplasmic

22

aggregates. More *in vivo* testing would be the most rigorous route to refine mechanisms of pathogenesis and with validated murine models of HD.

There are two categories of murine models of HD: transgenic murine models (overexpressing truncated or full length human mutant HD allele) and knock-in murine models (expressing human or mouse HD allele with various CAG repeat lengths inserted into the murine Hdh homologue). These models vary in the onset of behavioral motor phenotypes and neuropathological abnormalities, as well as additional non-HD abnormalities. Knock-in models have proven to be the most honest model of HD with age-appropriate onset, behavioral and neuropathology closer to HD and mutant htt expression in an appropriate genomic and protein context. Extensive evaluation and cross comparison of these models is discussed in the following chapter (Chapter II).

Research Objectives

The studies in this dissertation were performed to test the following hypotheses: The first is to assess the validity of the $Hdh^{(CAG)150}$ knock-in murine model of HD by providing the first prospective behavioral and neuropathological study (Chapter III). The $Hdh^{(CAG)150}$ knock-in murine model proves to be a faithful model of HD mimicking important features of the human disorder marked by progressive striatal specific degeneration concomitant with progressive motor abnormalities. The second is to use the established model to rigorously test the proximate hypothesis of glutamate excitotoxicity in HD (Coyle and Schwarcz and the McGeers), essentially providing the first *in vivo* evidence of glutamate excitotoxicity as an underlying mechanism of pathogenesis in HD (Chapter IV) as well as establishing the NR2B subunit of the NMDA receptor as a mechanistic means of glutamate excitotoxicity in HD.

Chapter II

Murine Genetic Models of Huntington Disease

Abstract

Huntington disease (HD) is a dominantly inherited human neurodegenerative disorder characterized by motor deficits, cognitive impairment, and psychiatric symptoms leading to inexorable decline and death. Since the identification of the *huntingtin* gene and the characteristic expanded CAG repeat/polyglutamine mutation, multiple mouse models have been generated. These models fall into two general categories: transgenic models with ectopic expression of the characteristic expanded CAG codon mutation, and knock-in models with expression of mutant *huntingtin* under control of endogenous regulatory elements. Murine genetic models are valuable tools for studying mechanisms of pathogenesis in HD and for preclinical evaluation of possible therapies. In this review, we provide a concise comparative summary of murine genetic models of HD.

Introduction

Huntington disease (HD) is an adult-onset, dominantly inherited human neurodegenerative disorder characterized by progressive motor impairment, involuntary movements, cognitive decline, and psychiatric disturbances. HD is caused by pathologic expansion of polymorphic CAG repeats in exon 1 of the *huntingtin* gene, translated as an expanded polyglutamine domain. *Huntingtin* encodes a widely expressed protein (huntingtin; Huntington's Disease Collaborative Research Group, (H. D. C. R. Group,

24

1993a) and huntingtin (htt) is a large, approximately 350 kD protein of unknown function, predominantly cytoplasmic localization, and expressed in virtually all neurons and some extra-neuronal tissues (T. V. Strong et al., 1993; G. B. Landwehrmeyer et al., 1995; A. H. Sharp et al., 1995). Disease-causing polyglutamine repeat mutations occur in eight other neurodegenerative disorders of unrelated proteins and exhibit regionally distinctive patterns of neurodegeneration (H. T. Orr and H. Y. Zoghbi, 2007). Since the discovery of *huntingtin* and the characteristic mutation in 1993, a variety of murine genetic models have been generated (Table II.1). Murine genetic models are potentially valuable as tools for exploring the pathogenesis of HD, in enabling the search for potential therapeutic targets, and in preclinical evaluation of potential therapies. Selection of experimental models depends on the validity of models, characteristics of models, and the type of experiments planned. In this review, we provide a comparative summary of the most widely used murine genetic models of HD. The available murine models can be separated into two categories: transgenic models (ectopic expression of the *huntingtin* mutation) and knock-in models (expression of the mutant *huntingtin* gene under the control of endogenous regulatory elements). These models vary in repeat length, level of expression of mutant htt protein, and whether the mutant allele is truncated or full length and human or murine (Table II.1).

HD Clinical Features and Pathology

The clinical features and pathology of HD provide the standards for assessing fidelity of murine genetic models. In humans, median age of onset of HD occurs around 40 years with premature death approximately 15-20 years after onset of symptoms (S. Warby et al., 2008). Prevalence in populations of European ancestry is approximately 4-

8 people per 100,000 (P. S. Harper, 1992) with a significantly larger number of individuals at risk for HD (P. M. Conneally, 1984). HD is much less common in populations of non-European ancestry. Normal *huntingtin* alleles contain less than 27 CAG repeats with a median around 18 (B. Kremer et al., 1994; S. Warby et al., 2008). Repeat numbers exceeding 39 result in full penetrance, and alleles with 36-39 CAG repeats are associated with reduced penetrance (D. C. Rubinsztein et al., 1996). Intergenerational transmission of mutant alleles often results in repeat number expansion and individuals with alleles carrying 27-35 CAG repeats will not develop HD but have increased risk of HD in their children (A. Semaka et al., 2006). There is a strong inverse correlation between CAG repeat length and age of onset of HD. CAG repeat length accounts for 42-73% of the variance in age of onset with 60 or more CAG repeats resulting in disease onset at 20 years of age or younger (S. E. Andrew et al., 1993; H. D. C. R. Group, 1993b; O. C. Stine et al., 1993; J. F. Gusella and M. E. MacDonald, 1995; D. R. Langbehn et al., 2004; J. M. Andresen et al., 2007). Manifest HD is defined clinically by the presence of a movement disorder, usually chorea but sometimes dystonia or bradykinesia. Data from the PREDICT-HD study of presymptomatic mutant allele carriers confirms clinical impressions and data from prior studies suggesting that onset of manifest HD is preceded by behavioral and cognitive changes (K. Duff et al., 2007; S. A. Johnson et al., 2007; A. C. Solomon et al., 2007). It is likely that behavioral and cognitive changes are followed by and or accompanied by relatively subtle declines in coordination. Incoordination progressively worsens and motor deficits eventually include dysarthria, dysphagia, and immobility (J. B. Penney, Jr. et al., 1990). End-stage HD patients are profoundly debilitated and demented.

Neurodegeneration within the central nervous system exhibits a regionally selective pattern in HD, with medium spiny neurons (MSNs) of the striatum exhibiting the earliest degeneration and atrophy (J. P. Vonsattel et al., 1985). Cortical degeneration occurs also in early phases of HD (H. D. Rosas et al., 2002; H. D. Rosas et al., 2005). Striatal and cortical degeneration and atrophy are ultimately profound (G. M. Halliday et al., 1998). Careful neuropathologic evaluations of more advanced HD specimens reveal evidence of neurodegeneration in many brain regions. Expression of *huntingtin* is widespread and probably universal among neurons, and there is no clear correlation between *huntingtin* expression and the regional pattern of initial pathology in HD (T. V. Strong et al., 1993; G. B. Landwehrmeyer et al., 1995; A. H. Sharp et al., 1995; G. M. Halliday et al., 1998). As with other polyglutamine diseases, HD is marked by expression of neuronal intranuclear inclusions (NIIs) and cytoplasmic inclusions containing aggregated expanded repeat htt and other proteins (M. DiFiglia et al., 1997; M. W. Becher et al., 1998; M. L. Maat-Schieman et al., 1999).

Neuropathologic analysis is necessarily post-mortem analysis, but there is strong *in vivo* evidence of the inferred early changes in striatum and cortex. Imaging studies of pre-manifest and early manifest HD reveal substantial striatal and cortical atrophy (E. H. Aylward et al., 2000; E. H. Aylward et al., 2004; L. J. Beglinger et al., 2005; H. D. Rosas et al., 2005), as well as decreases in striatally enriched dopamine D1 and D2 receptors (A. Antonini et al., 1996; R. A. Weeks et al., 1996). In pre-manifest HD mutant allele carriers, striatal atrophy may occur years prior to predicted age of onset of manifest HD (E. H. Aylward et al., 2000; E. H. Aylward et al., 2004).

Murine Models of HD

A valid murine model of HD should recapitulate key features of HD. These include mid- to late-life onset, progressive motor impairment, selective early loss of striatal projection neurons, and expression of NIIs and cytoplasmic aggregates in an appropriate anatomic distribution. A valid model should exhibit measurable progressive pathology. Other possible criteria can be entertained but may not apply to mice. Chorea, for example, is probably a phenomenon restricted to primates. HD is characterized by early cognitive and psychiatric abnormalities but determining their precise rodent analogues is problematic. Following are summaries of the behavioral phenotypes and pathologic features of selected murine genetic models of HD (Table II.1; Figure II.1).

Transgenic Murine Models

R6/2: Of the transgenic chimeric models that express truncated forms of the human mutant HD allele, the R6/2 line is the most widely used. This line expresses an exon 1 fragment of htt with a range of 148-153 repeats, expressed from an unknown chromosomal location in the mouse genome. The R6/2 line displays an aggressive phenotype and provides clear experimental endpoints. R6/2 mice exhibit behavioral deficits by 5 weeks, neuroanatomic abnormalities including progressive reduction in brain and striatal volume, substantially reduced striatal neuron number by 12 weeks, and death by 12-15 weeks (L. Mangiarini et al., 1996; M. A. Hickey et al., 2005; A. J. Morton et al., 2005; E. C. Stack et al., 2005). Mice normally reach sexual maturity by 6 weeks and live beyond 2 years of age. Evaluation with learning and memory tasks shows abnormalities as early as 3.5 weeks of age, and simple motor tasks such as the rotorod and beam walking reveal deficits by 5 weeks of age (R. J. Carter et al., 1999; L. A. Lione

et al., 1999; E. C. Stack et al., 2005). NIIs are present as early as post-natal day 1 in R6/2 striatum, somatosensory cortex, and hippocampal formation. These NIIs increase steadily in number, size, and distribution (A. J. Morton et al., 2005; E. C. Stack et al., 2005). Within the striatum, NIIs appear first in the matrix compartment (Morton et al., 2000). At disease endstage, R6/2 brains reveal widespread neuronal nuclear inclusions (NIIs) and neuropil aggregates (A. J. Morton et al., 2005; E. C. Stack et al., 2005). Total brain weight is decreased at 30 days (E. C. Stack et al., 2005). By 12 weeks, there is a 26% reduction in striatal neuron number and a 41% reduction in striatal volume. However, total brain volume is reduced by 44% (E. C. Stack et al., 2005). The reduction in total brain volume is too large to be accounted for by the reduction in striatal volume alone, supporting the inference that there is diffuse loss of neurons in R6/2 brain. Striatal dopamine D1 and D2 receptors, highly enriched on dendrites of striatal projection neuron, are decreased as early as 8 weeks, consistent with both early striatal neuronal dysfunction and neurodegeneration (J. H. Cha et al., 1998). Other neurotransmitter receptors are decreased at 12 weeks and some receptor mRNA expression levels are decreased as early as 4 weeks (J. H. Cha et al., 1998, 1999).

The aggressive phenotype makes R6/2 mice very useful for preclinical pharmacology, but it is not an exact genetic or neuropathological analogue of adult-onset HD. R6/2 mice have widespread NII expression, a high incidence of epilepsy, diabetes, cardiac dysfunction, peripheral neuropathy, and neuromuscular junction abnormalities, none of which are characteristic of typical adult-onset HD (M. S. Hurlbert et al., 1999; C. A. Meade et al., 2002; R. R. Ribchester et al., 2004; M. J. Mihm et al., 2007). As the R6/2 model exhibits severe, early onset and diffuse pathology, it is potentially a good

model of juvenile-onset HD, where effects of expanded polyglutamine htt occur in the context of a developing brain. Epilepsy, for example, is common in juvenile-onset HD (S. Seneca et al., 2004).

YAC128: The YAC128 is a widely used yeast artificial chromosome full-length human mutant HD transgenic model generated and characterized by the Hayden laboratory (E. J. Slow et al., 2003; J. M. Van Raamsdonk et al., 2005a). YAC128 mice exhibit motor abnormalities as early as 3 months with increased open field activity, followed by rotorod performance abnormalities at 6 months. Behavioral deficits are progressive and by 12 months, open field activity is diminished significantly in comparison with controls. Van Raamsdonk et al. (J. M. Van Raamsdonk et al., 2005b) evaluated YAC128 mice with a variety of more cognitively oriented tests, demonstrating abnormalities which precede and then parallel the progression of simpler motor function tests. Modest striatal atrophy is found at 9 months with both striatal and cortical atrophy at 12 months (10-15% and 7-8% decreases in volume, respectively). Unlike R6/2 mice, where there is probably diffuse loss of brain, other brain regions such as the cerebellum and hippocampal formation exhibit normal volume (J. M. Van Raamsdonk et al., 2005b). A modest degree of striatal neuron loss, approximately 15%, is found at 12 months. Although NIIs are not found until 18 months, abnormally high nuclear htt immunoreactivity is present within striatal and other neurons from 2 months onwards. Nuclear htt immunoreactivity is abundant in striatal neurons at 3 months of age and found in a significant number of cortical, hippocampal, and cerebellar neurons at the same age. By 6 months, nuclear htt immunoreactivity is present in many neurons (J. M. Van Raamsdonk et al., 2005b). Surprisingly, twelve month old YAC128 mice, despite the

presence of behavioral abnormalities and evidence of striatal neuron loss, exhibit no decreases in a wide array of striatal neurotransmitter receptor binding sites (C. L. Benn et al., 2007). YAC128 mice display glutamate receptor binding site increases in some extrastriatal regions. NMDA receptor binding is increased in the hippocampus and cortical layers, AMPA receptor binding is increased in the cerebellum, and group 2 metabotropic glutamate receptor binding is increased in the dentate gyrus of the hippocampus (C. L. Benn et al., 2007). The apparently normal striatal neurotransmitter receptor expression is different from results with other murine genetic models and probably also HD, where neurotransmitter receptor expression appears to be a reliable indicator of striatal neuron dysfunction/degeneration.

Knock-In Murine Models

In contrast to the transgenic murine models of HD, knock-in models express mutant htt in an appropriate genomic and protein context. A number of knock-in models have been generated (L. B. Menalled, 2005). Experience with these models was initially disappointing as they did not develop the marked phenotype of transgenic fragment models like R6/2. Careful analyses and generation of knock-in models with longer repeat lengths demonstrated behavioral and histological abnormalities in several knock-in models. In general, these models tend to show normal life span, milder initial behavioral abnormalities, development of more robust behavioral abnormalities at later ages, and expression of aggregate pathology more selectively localized to striatal neurons (L. B. Menalled, 2005); Table II.1). There are several prospectively characterized knock-in models with larger CAG expansions and overt behavioral and neuropathological abnormalities (L. B. Menalled, 2005); Table II.1; Figure II.1).

HdhQ94 and Hdh Q140: The HdhQ94 and HdhQ140 lines are based on a gene targeted replacement of exon 1 of the mouse *huntingtin* homologue, *Hdh*, with a chimeric mouse/human exon 1 encoding approximately 94 or 140 CAG repeats. In HdhQ94 mice, increased repetitive rearing is found at 2 months of age with decreased locomotion at 4 and 6 months of age (L. B. Menalled et al., 2002). Diminished striatal enkephalin mRNA expression is found at 4 months of age. In 18 to 26 month old mice, striatal volume is decreased by approximately 15% but striatal neuron number is normal. Nuclear htt immunoreactive microaggregates, which may be small NIIs, are observed in many striatal neurons by 6 months of age; these are found in striosome compartment neurons. Only rare nuclear microaggrates are described in cortex at 6 months and none in the hippocampal formation. Typical large striatal NIIs do not appear until 18 months of age and there are no reports of NII or cytoplasmic aggregates in other regions.

HdhQ140 mice exhibit similar but more pronounced features (L. B. Menalled et al., 2003). Increased repetitive rearing occurs at 1 month of age with diminished locomotor activity at 4 months of age. Footprint analysis at age 12 months reveals significant changes in mutant mouse gait. Striatal htt nuclear immunoreactivity is observed at 2 months with some nuclear microaggregates expressed. By 4 months, nuclear htt immunoreactivity becomes more intense and nuclear microaggreates are common. Other brain regions, including olfactory bulb, anterior olfactory nucleus, and piriform cortex, exhibit strong nuclear htt immunoreactivity. By 6 months, nuclear htt immunoreactivity and some microaggregates/NIIs are present in several brain regions; striatal nuclear htt immunoreactivity is more intense and large NIIs are expressed. Neuropil htt immunoreactive aggregates, presumably cytoplasmic inclusions, appear in

striatum and other regions by 4 months and increase in density by 6 months of age. Neuropil aggregates are particularly prominent in the hippocampal formation, some cortical laminae, the globus pallidus, entopeduncular nucleus, and substantia nigra pars reticulata. In the latter three regions, they may be expressed in striatal neuron terminals. Striatal neuron loss and atrophy has not been demonstrated.

HdhQ111: Like the HdhQ94 and HdhQ140 lines, HdhQ111 is a knock-in model based on a chimeric human/mouse exon 1 construct (V. C. Wheeler et al., 2000; V. C. Wheeler et al., 2002). In this line, subtle motor deficits are detected by footprint analysis at 24 months of age. At this age, small numbers of degenerating striatal neurons are observed with reactive gliosis (V. C. Wheeler et al., 2002). In HdhQ111 homozygotes, clusters of ventral striatal neurons exhibit nuclear htt immunoreactivity at 1.5 months of age. By 4.5 months of age, there is strong nuclear htt immunoreactivity in many MSNs with some small NIIs formed. In HdhQ111 heterozygotes, prominent nuclear htt immunoreactivity is observed at 5 months of age. In both homozygotes and heterozygotes, older mice display prominent NIIs, and neuropil htt immunoreactive aggregates are found in the globus pallidus and substantia nigra pars reticulata by 17 months of age.

Hdh^(CAG)150: The *Hdh*^(CAG)150 knock-in mouse lacks foreign DNA sequences or selectable markers and is purely murine with approximately 150 CAG repeats inserted into exon 1 of the murine *huntingtin* homologue (C. H. Lin et al., 2001; S. J. Tallaksen-Greene et al., 2005; M. Y. Heng et al., 2007). *Hdh*^(CAG)150 mice exhibit an apparently normal phenotype until greater than a year of age. At 100 weeks of age, homozygous *Hdh*^(CAG)150 mice exhibit weight loss, diminished activity, and abnormal rotorod

performance. Both 100 week old homozygous and heterozygous $Hdh^{(CAG)150}$ mice display abnormal performance on a balance beam task and with footprint analysis. Qualitative changes in gait are apparent on the beam task in some homozygous mutants as early as 50 weeks of age. Evaluation of younger $Hdh^{(CAG)150}$ mice, less than 1 year of age, with the Morris water maze, fear conditioning, and open field testing did not show any abnormalities (Heng et al., unpublished data). At 100 weeks of age, stereological analysis demonstrates approximately 50% loss of neurons in heterozygous and homozygous $Hdh^{(CAG)150}$ mice, though only the homozygous $Hdh^{(CAG)150}$ mice exhibit loss of striatal volume (M. Y. Heng et al., 2007). The latter fact suggests neuronal dysfunction rather than death in $Hdh^{(CAG)150}$ heterozygotes. Ultrastuctural study of 14 month old $Hdh^{(CAG)150}$ heterozygotes demonstrated striatal axonal degeneration (Z. X. Yu et al., 2003). Assessment of striatal D1 and D2 receptor binding sites in 100 week old heterozygous and homozygous $Hdh^{(CAG)150}$ mice shows significant declines in these binding sites, greater in homozygous than heterozygous mutants. At 70 weeks of age, stereologic analyses showed normal striatal volume and striatal neuron number in both homozygous and heterozygous $Hdh^{(CAG)150}$ mice. Striatal D1 and D2 receptor binding sites are, however, diminished in 70 week old heterozygous and to a greater extent, homozygous $Hdh^{(CAG)150}$ mice. Normal striatal neuron number and volume in 70 week old $Hdh^{(CAG)150}$ mice, coupled with the presence of striatal D1 and D2 receptor binding deficits and behavioral changes, supports the inference that a period of neuronal dysfunction precedes neurodegeneration. As with other knock-in models, nuclear localization of htt immunoreactivity precedes NII formation. Nuclear htt immunoreactivity is found at 27-29 weeks of age. At approximately 40 weeks of age,

some striatal neurons express NIIs, and by 70 weeks of age, NIIs are expressed by most striatal neurons. NIIs initially appear in clusters of striatal neurons predominantly within the matrix compartment. Around 100 weeks of age, almost all striatal neurons express NIIs. Even at this advanced age, NIIs are found in only a small minority of neurons in most other brain regions. Only piriform cortex and layer 4 of primary somatosensory cortex exhibit high percentages of neurons with NIIs. Neuropil aggregates are abundant in the globus pallidus and substantia nigra pars reticulata, suggesting localization within striatal neuron terminals. The relatively selective distribution of NIIs in $Hdh^{(CAG)150}$ mice suggests preferential striatal pathology. This inference is consistent with GABA-A/benzodiazepine receptor binding studies in 100 week old $Hdh^{(CAG)150}$ mice. Extrastriatal regions that express high levels of GABA-A/benzodiazepine receptor binding sites exhibit normal binding.

Validity

Extrapolating from murine models to HD depends on the validity of the model. Murine genetic HD models can be assessed with the three criteria proposed by Paul Willner (P. Willner, 1991) with the goal of increasing the odds that results in the model will predict similar results in humans. First is face validity: does the phenotype of the model recapitulate the clinical manifestations of the disease of interest? Second is construct validity: do the experimental manipulations produce similar underlying mechanisms of pathogenesis as observed in the disease of interest (this may be the most challenging to establish, and is critical since a model can have face validity driven by an irrelevant molecular mechanism). Third is predictive validity: is the model able to predict pathological outcomes known to exacerbate or ameliorate physiological states in

35

the disease of interest (such as the response to therapeutic drugs)? There are difficulties in creating a valid model of HD when the disease itself is not fully understood. However, these criteria provide a framework to evaluate a wide range of models and allow systematic assessment of murine genetic models (Table II.2).

Face validity can be assessed by comparison with the clinical and pathologic features of HD. Transgenic fragment, transgenic full length, and knock-in models all possess at least some face validity in that they recapitulate some of the phenotypic features of HD. All result in progressive motor dysfunction, and where assessed, progressive pathologic changes. In terms of behavioral features, the mid- to late-life onset of transgenic full length and knock-in models appear to replicate typical adult-onset HD best. In terms of pathology, transgenic full length and knock-in models appear to replicate best the features of adult-onset HD with more selective striatal involvement than the R6/2 line. As mentioned above, however, the R6/2 line may resemble the more aggressive juvenile-onset form of HD.

Transgenic fragment, transgenic full length, and knock-in models all possess considerable construct validity. All express the expanded polyglutamine repeat domain that is the core cause of neurodegeneration in HD and other polyglutamine diseases (J. M. Ordway et al., 1997). Recent results, however, indicate that the specific regional pathology of individual polyglutamine diseases is a function of the biology of the protein carrying the pathologically expanded polyglutamine repeat (H. T. Orr and H. Y. Zoghbi, 2007). Transgenic fragment models may be more models of generalized expanded polyglutamine repeat pathogenesis than of any specific polyglutamine disease. The expedience of an aggressive phenotype therefore must be balanced against the possibility

that the phenotype may be driven by molecular processes that do not mimic HD. For this reason, transgenic full length and knock-in models appear to possess a greater degree of construct validity. Theoretically, knock-in models possess a yet higher degree of construct validity than transgenic full length models because the expanded CAG repeat sequence is expressed in its native biologic context. Huntingtin and its murine homologue are very similar proteins and likely to have similar functional properties.

Predictive validity is the most pragmatically important of Willner's criteria. The R6/2 line has been the major vehicle for preclinical pharmacology for HD. A substantial number of interventions have been evaluated with this line. Assessment of predictive validity requires comparison of model and human trial outcomes. The human experience is limited to date. The first large efficacy trial for HD, Coenzyme Q10 and Remacemide Evaluation in HD (CARE-HD), evaluated 600 mg per day of coenzyme Q10 and 600 mg per day of remacemide, a non-selective NMDA receptor antagonist (H. S. Group, 2001). Neither compound was effective though there was a trend towards efficacy with coenzyme Q10. Both compounds were evaluated subsequently in R6/2 mice and both treatments produced modest but significant amelioration of the R6/2 phenotype (R. J. Ferrante et al., 2002). On a mg/kg basis, mice in this study received much higher doses of coenzyme Q10 and remacemide than participants in the CARE-HD trial. Comparison of mouse and human results is confounded by probable differences in pharmacokinetics and effective doses. Mice in the simple cage environment, for example, may tolerate relatively higher doses of a psychoactive compound like remacemide. A second major efficacy study of coenzyme Q10, Coenzyme Q10 in Huntington Disease (2CARE), is in progress. 2CARE uses a substantially higher dose of coenzyme Q10 and may provide a

37

definitive answer about the neuroprotective value of coenzyme Q10 in HD. 2CARE and other human efficacy trials may provide useful information about the predictive validity of the R6/2 model.

Comparing Models

While predictive validity of HD murine genetic models is unknown, transgenic full length and knock-in models appear to possess better face and construct validity than transgenic fragment models. Accumulating human data to assess predictive validity will take years. In the interim, useful data might be gleaned by selective evaluation of compounds that succeed in R6/2 by further testing in transgenic full length or knock-in models. The practical advantages of the strong R6/2 phenotype makes it unlikely that it will be replaced as the preferred model for preclinical pharmacology, however, transgenic full length and knock-in models are preferable models for experiments examining the pathogenesis and pathophysiology of HD.

Among transgenic full length and knock-in models, the YAC128 and $Hdh^{(CAG)150}$ lines offer the advantages of well characterized natural history and well characterized behavioral and pathologic endpoints. The $Hdh^{(CAG)150}$ line may exhibit a period of neuronal dysfunction prior to neurodegeneration that should be especially valuable for examining early events in HD pathogenesis (A. Kuhn et al., 2007) compared striatal gene expression changes in several murine genetic models of HD, including R6/2, YAC128, and $Hdh^{(CAG)150}$ (termed CHL2 in Kuhn et al., 2007) with striatal gene expression changes in HD. All murine genetic models had significant correlation with human striatal gene expression changes. The highest correlations were found with 22 month old $Hdh^{(CAG)150}$ homozygotes and 12 week old R6/2 mice. The most marked similarities

between HD and murine genetic models occurred with down regulated transcripts. Similar results were obtained with a limited number of transcripts by Woodman et al. (B. Woodman et al., 2007). This may reflect that fact that $Hdh^{(CAG)150}$ homozygous and R6/2 mice of these ages exhibit the greatest degree of striatal degeneration among murine genetic models of HD.

Summary

A variety of murine genetic models of HD are available. The different features of these models confer different advantages and disadvantages, depending on specific experimental aims. While none of the models fulfill all Willner criteria, transgenic full length and particularly knock-in models appear to be the highest-fidelity model of HD with age-appropriate onset, and behavioral deficits and neuropathology similar to HD. The milder phenotype and late onset of behavioral abnormalities of transgenic full length and knock-in models make them difficult to use for preclinical pharmacology. Knock-in models exhibit a natural history of behavioral deficits and striatal dysfunction followed by degeneration, allowing examination of early events in the pathogenesis of HD. Transgenic fragment models like R6/2 provide robust endpoints for preclinical pharmacology, but may involve pathophysiologic processes not typical of HD. Additional comparative studies of murine genetic HD models and with human trial data are needed to evaluate model validity completely.

Acknowledgements

LINE	CAG EXPANSION AND GENETIC EXPRESSION	AGE OF ONSET AND BEHAVIORAL PHENOTYPE	NEUROPATHOLOGY	SURVIVAL	ADDITIONAL PHENOTYPES	REFERENCES
N171-82Q (fragment transgenic) C57BL/6JxC3H/HeJ	N-terminal fragment expressing first 171 amino acids of *htt*; 82 CAG repeats. Mouse PrP promoter.	Progressive weight loss beginning 4-6 wks before death as well as tremor and hypokinesis, and clasping. Progressive Acc. rotarod deficit beginning at 12 wks. No seizures reported.	NIIs >50% observed in the cortex, hippocampus, amygdala, but less in the striatum. Astrocytic reactive gliosis and neuropil aggregates (GFAP, EM48-16 wks). Neuronal loss and neurodegeneration in the cortex and sriatum, 20 wks (TUNEL, cresyl violet staining, and EM).	20-24 wks.	20-24 wks. No seizures observed.	Schilling G. (1999) Yu ZX. (2003)
R6/2 (fragment transgenic) CBAxC57BL/6 mix background strain	Exon 1N-terminal fragment: ~150 CAGs. HD promoter.	Progressive weight loss by ~8 wks. Acc. rotarod deficit visible at 5 wks. Clasping, 6 wks. Increase limb movement, 10 wks (video capture). Decrease in grip strength, 11 wks (grip strength meter). Circling behavior, 12 wks. Cognitive deficits: water morris maze (3.5 wks), T-maze (5 wks), two choice swim tank (6.5 wks), visual discriminate learning (7-8 wks).	Onset of decreased brain weight, 4 wks. 44% decrease in brain volume, 41% decrease in striatal volume, ~ 6-fold increase in ventricular volume, 12 wks. Htt positive aggregates present by postnatal day 1 in cortical layers II, V, VI, neostriatum and greatest in the hippocampus. 25% reduction in striatal neuron number, 60% decrease in striatal neuron area and increase in reactive astrogliosis, 12 wks. Widespread NIIs and neuropil aggregates, 12 wks. Decrease in dopamine D1 and D2 receptors in striatum. Decrease in mGluR II, AMPA and kainate receptors in striatum and cortex, 12 wks. Decrease A2a adenosine receptors, 4 wks.	12-15 wks.	Seizures, diabetes, NMJ and cardiac dysfunction.	Carter RJ. (1999, 1998) Cha JH. (1998) Davies SW. (1997) Hickey MA. (2005) Hurlbert MS. (1999) Lione LA. (1999) Mangiarini L. (1996) Meade CA. (2002) Mihm MJ. (2007) Ribchester RR. (2004) Stack EC. (2005)
Full length *HD* cDNA (full length transgenic) FVB/N background strain	CMV promoter: 89 CAGs.	Clasping, 8 wks. Hyperactive, unilateral rotation, excessive grooming, 20 wks. Decrease exploratory and locomotor activity, 24 wks (by general monitoring).	PolyQ aggregates, 12 wks. NIIs in cerebellum, cortex, hippocampus, thalamus, and <1% in striatum. Astrocytic reactive gliosis (GFAP).~20% fewer striatal MSNs in homozygous (H & E and TUNEL staining).	Normal lifespan	urinary incontenence	Reddy PH. (1998)
YAC 128 (full length transgenic) FVB/N background strain	Chimeric full length *HD*/mouse exon 1: 120 CAGs HD promoter	Hyperkinetic, 12 wks and hypokinetic, 48 wks (open field). Acc. rotarod deficit, 24 wks. Progressive cognitve deficits, 8 wks (acc. rotarod), 32 wks (water morris maze, open-field habituation, and T-maze).	10.4% - 15% reduction in striatal and 7% - 8.6%, reduction in cortical volumes, 48 wks. 9.1% reduction in striatal neuron number and 8.3% reduction cortical neuron number, 48 wks (stereology). Diffuse striatal htt nuclear immunoreactivity, 12 wks (EM48) > cortex, hippocampus, and cerebellum progressed and became more widespread but no NIIs detected, 48 wks. EM 48 positive inclusions detected in striatal cells, 72 wks. Increase in NMDA receptor binding (dentate gyrus, inner cortex, and whole brain), increase in AMPA (cerebellum and whole brain), mGluR I (whole brain) and mGluR II receptor binding (dentate gyrus and whole brain). No change in striatal dopamine, GABA A/B or adenosine receptor binding at 48 wks.	Normal lifespan.	None reported.	Benn CL. (2007) Hodgson JG. (1999) Slow EJ. (2003) Van Raamsdonk JM. (2005a, 2005b)
Hdh/Q72-80 (knock-in) 129/SvxC57BL/6 mix background strain or 129/Svx FVB/N mix background strain	*Hdh* promotoer: 72-80 CAGs.	Increased male aggression and a lesser extent in females, 12wks. No observed weight loss compared to WT, 72 wks. Rotarod (non-accelerated) deficit beginning at 16 wks (C57BL/6 N6 generation)	H&E, Nissl stains, and GFAP immunoreactivity revealed no neuron loss or reactive gliosis. No NIIs detected. No loss in enkephalin or calbindin immunoreactivity, 72 wks. Neuropil aggregates, 28-96 wks. Striatal nuclear htt aggregates, 96 wks (C57BL/6 N6-7 generation or FVB/N N4 generation). Decrease in dopamine D2 receptor binding and increase in GABA/benzodiazepine receptor binding in the striatum and cortex, 68-72 wks.	Normal lifespan.	None reported.	Kennedy L. (2005) Shelbourne PF. (1999)
HdhQ111 (knock-in) 129/CD1 mix background strain	Chimeric human/mouse exon1: 109 CAGs	Gait impairment 96 wks (painted-feet). However, no acc. rotarod deficits.	Diffuse striatal nuclear-reactivity, 6 wks (EM48). NIIs, 48 wks. Striatal neuropil aggregates, 68 wks. Neurodegeneration and reactive gliosis, 96 wks (toluidine blue GFAP).	Normal lifespan	None reported.	Wheeler VC. (2000, 2002)
HdhQ140 (knock-in) 129Sv/C57BL6 mix background strain	Chimeric human/mouse exon1: 140 CAGs.	No obvious abnormal behavior up to 48 wks. No abnormal weight loss. Decrease locomotor activity, 8-24 wks (open-field). Hyperactivty, 4 wks and hypoactivity, 12 wks. Gait abnormalities, 48 wks (painted-feet).	Striatal htt nuclear staining beginning at 8 wks and becoming more widespread by 24 wks. nuclear and neuropil aggregates prominent at 16 wks in the striatum, nucleus accumbens, olfactory tubercle (EM48), as well as widespread nuclear staining including cortical layers II/III, and V., hippocampus, and regions of the olfactory system.	Normal lifespan.	None reported.	Menalled LB. (2003)
Hdh(CAG)150 (knock-in) 129/Ola and C57BL/J6 mix background strain	Murine Hdh: 150 CAGs.	Motor abnoralities: Acc. Rotarod, Balance beam, painted feet, 70-100wks. Resting tremor and ataxic, 100 wks.	Striatal nuclear htt immunoreactivity, 28 wks. Striatal NIIs, 37 wks. Reactive astrocytic gliosis, 56 wks. Robust striatal NIIs and striatal neuron receptor loss, 70-100 wks. Loss of striatal perikarya and volume, 100 wks. Decrease in striatal dopamine D1 and D2 receptors and dopamine uptake sites (DAT).	Normal lifespan.	None reported.	Heng MY. (2007) Lin CH. (2001) Tallaksen-Greene S. (2005)

Table II.1Summary of murine models of HD.

.

R6/2
(fragment transgenic)

Htt immunoreactive aggregates present at birth
Cognitive deficits
Onset of decreased brain weight
Motor abnormalities
Widespread NIIs and neuropil aggregates, striatal degeneration, reactive astrogliosis, striatal dopamine receptor loss
Death

3.5 weeks
4 weeks
5 weeks
12 weeks
12-15 weeks

YAC 128
(full length transgenic)

Cognitive deficits
Hyperkinetic, diffuse striatal htt nuclear immunoreactivity
Motor deficits
Hypokinetic, decrease in striatal and cortical volume, striatal degeneration, but No NIIs detected. Alterations in extrastriatal glutamate receptors, no change in striatal dopamine receptors
Small htt positive striatal inclusions

8 weeks
12 weeks
24 weeks
48 weeks
72 weeks

Hdh(CAG)$^{150/150}$
(knock-in)

Striatal htt nuclear immunoreactivity
Striatal neuron htt NIIs
Motor behavior abnormalities, weight loss
Robust striatal htt NIIs
Striatal dopamine receptor loss
Loss of striatal perikarya and striatal volume
Increased striatal DA receptor loss and loss of striatal DAT

28 weeks
37 weeks
70 weeks
100 weeks

Hdh(CAG)$^{150/+}$

Striatal neuron nuclear htt immunoreactivity
Striatal neuron htt NIIs
Robust striatal htt NIIs
Striatal dopamine receptor loss
Motor behavior abnormalities, weight loss
Increased striatal DA receptor loss
Loss of striatal NeuN immunoreactivity
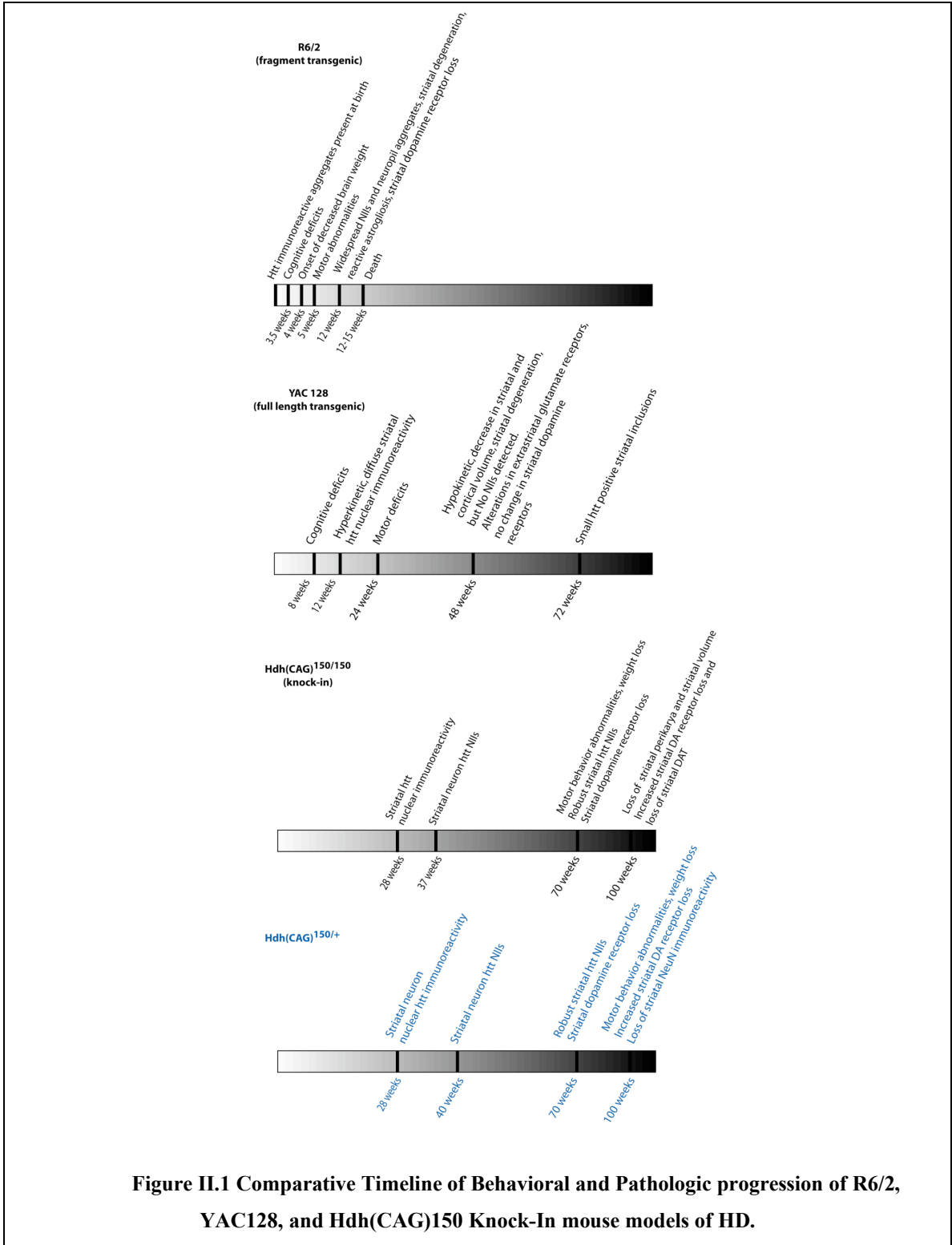
28 weeks
40 weeks
70 weeks
100 weeks

Figure II.1 Comparative Timeline of Behavioral and Pathologic progression of R6/2, YAC128, and Hdh(CAG)150 Knock-In mouse models of HD.

41

Similarity of Model to HD	Phenotypic	Molecular Mechanism	Therapeutic Response
Willner Criteria	**Face Validity**	**Construct Validity**	**Predictive Validity**
R6/2	+	++	U
	Progressive motor phenotype. NII and cytoplasmic aggregate pathology	Core feature – polyQ expansion.	Coenzyme Q10 and remacemide unsuccessful in HD, efficacious in R6/2. Higher dose Q10 trial in progress.
	Very early onset and widespread pathology. Extra-CNS features not typical of HD.	Lacks appropriate surrounding protein context and regulatory elements. Transcriptome alterations similar to HD.	
YAC128	++	++1/2	U
	Progressive motor phenotype, adult onset, early cognitive features. Preferential striatal and cortical atrophy. Early nuclear htt immunoreactivity with late NIIs.	Core feature – polyQ expansion. Appropriate surrounding protein context.	
	No HD-like striatal neurotransmitter receptor changes.	Ectopic location, lacks native murine regulatory elements.	
Hhd(CAG)150	+++	+++	U
	Progressive motor phenotype. Mid-life onset. Preferential striatal degeneration and NII expression. Striatal neurotransmitter receptor changes precede neurodegeneration.	Core feature – polyQ expansion. Appropriate surrounding protein context. Native murine regulatory elements. Transcriptome alterations similar to HD.	

Table II.2 Wilner's criteria of validity.

Chapter III

Longitudinal Evaluation of the $Hdh^{(CAG)150}$ Knock-in Murine Model of Huntington's Disease

Abstract

Several murine genetic models of Huntington Disease (HD) have been developed. Murine genetic models are crucial for identifying mechanisms of neurodegeneration in HD and for preclinical evaluation of possible therapies for HD. Longitudinal analysis of mutant phenotypes is necessary to validate models and to identify appropriate periods for analysis of early events in the pathogenesis of neurodegeneration. Here we report longitudinal characterization of the murine $Hdh^{(CAG)150}$ knock-in model of HD. A series of behavioral tests at five different time points (20, 40, 50, 70, and 100 weeks) demonstrate an age-dependent, late onset behavioral phenotype with significant motor abnormalities at 70 and 100 weeks of age. Pathologic analysis demonstrated loss of striatal dopamine D1 and D2 receptor binding sites at 70 and 100 weeks of age, and stereological analysis showed significant loss of striatal neuron number at 100 weeks. Late onset behavioral abnormalities, decrease in striatal dopamine receptors, and diminished striatal neuron number observed in this

mouse model recapitulate key features of HD. The $Hdh^{(CAG)150}$ knock-in mouse is a valid model to evaluate early events in the pathogenesis of neurodegeneration in HD.

Introduction

Huntington disease (HD) is a dominantly inherited human neurodegenerative disorder characterized by progressive motor impairment, cognitive decline, and psychiatric problems. Early degeneration of striatal medium spiny neurons (MSNs) and striatal atrophy are hallmarks of HD, though cortical degeneration may also occur prior to the onset of clinical features of HD (N. W. Kowall et al., 1993; J. P. Vonsattel and M. DiFiglia, 1998; H. D. Rosas et al., 2002; H. D. Rosas et al., 2004a; H. D. Rosas et al., 2005). With disease progression, neuronal loss becomes more global, affecting numerous brain areas. HD is caused by a CAG repeat expansion in exon 1 of the *huntingtin* gene, which encodes a widely expressed protein (huntingtin; htt; Huntington's Disease Collaborative Research Group, (H. D. C. R. Group, 1993b). HD belongs to a family of inherited trinucleotide repeat disorders including Spinobulbar Muscular Atrophy (SMBA; Kennedy's disease), Dentatorubro-pallidal Luysian Atrophy, and Spinocerebellar Ataxias 1, 2, 3, 6, 7, and 17 (A. R. La Spada et al., 1991; C. J. Cummings and H. Y. Zoghbi, 2000). These polyglutamine diseases share similar features, including expanded CAG repeats within translated exons, anticipation, and regionally specific CNS pathology. These diseases may share common mechanisms of pathogenesis (H. T. Orr, 2001; J. Hardy and H. T. Orr, 2006). Since the discovery of the *huntingtin* gene in 1993, a variety of murine genetic models have been generated (L. Mangiarini et al., 1996; P. H. Reddy et al., 1998; J. G. Hodgson et al., 1999; G. Schilling et al., 1999; P. F. Shelbourne et al., 1999; V. C. Wheeler et al., 2000; C. H. Lin et al., 2001), largely replacing older

excitotoxic models. Murine models are potentially valuable as tools in exploring the pathogenesis of HD, enabling the search for potential therapeutic drug targets, and in preclinical evaluation of potential therapies. The available murine models can be separated into two categories: transgenic models (ectopic expression of the *huntingtin* mutation) and knock-in models (expression of the mutant *huntingtin* gene under control of the normal regulatory elements). These models vary in the length of repeat, the level of expression of the mutant htt protein, and whether the mutant allele is truncated, full length, human, or murine. Validation of models requires careful characterization of their phenotypic features. An accurate model should recapitulate key behavioral and pathologic features of HD in an age dependent manner. Longitudinal characterization of murine genetic models is crucial for defining periods when early events are likely to be occurring in the pathogenesis of neurodegeneration, and to identify behavioral and/or pathological milestones for use in trials of proposed interventions.

We report the results of longitudinal behavioral and pathologic evaluation of the $Hdh^{(CAG)150}$ knock-in model. Using a series of behavioral tests at five different time points (20, 40, 50, 70, and 100 weeks), we demonstrate an age-dependent, late onset behavioral phenotype with significant motor abnormalities beginning at 70 weeks of age. Pathologic analysis demonstrated loss of striatal dopamine D1 and D2 receptor binding sites at 70 and 100 weeks of age, and stereological analysis showed significant loss of striatal neuron number at 100 weeks.

Materials and Methods

$Hdh^{(CAG)150}$ Mouse Model

45

All experiments were performed with the $Hdh^{(CAG)150}$ mice murine model of HD maintained on a mixed genetic background, 129/Ola and C57BL/J6 (C. H. Lin et al., 2001) with the current $Hdh^{(CAG)150}$ line expressing 75-90% C57BL/6; (PJD, unpublished data). For all experiments, female and male $Hdh^{(CAG)150}$ mice with the same genetic background were mated to produce F1 homozygous, heterozygous, and wild type $Hdh^{(CAG)150}$ mice. Both male and female $Hdh^{(CAG)150}$ mice and their wild type littermates (WT) were used. All animals were housed in cages grouped by gender and provided with food and water *ad libitum*. Animals were housed in a Specific Pathogenic Free conditions with a 12-h light/dark cycle maintained at 23°C. All procedures were conducted in strict compliance with the Guide for the Care and Use of Laboratory Animals as adopted by the NIH and approved by the Committee on Use and Care of Animals (UCUCA), University of Michigan, and the Veterinary Medical Unit (VMU) at the Ann Arbor Veterans Affairs Medical Center.

Genotyping

All mice studied were genotyped as follows; genotyping protocol was adapted from one used previously (C. H. Lin, Tallaksen-Greene S., Chien W.M., Clearly JA., Jackson W.S., Crouse A.B., Ren S., Li XJ., Albin R.L., Detloff P.J., 2001). DNA was extracted from a 1 cm tail snip using a DNeasy Tissue Kit (Qiagen Inc. Valencia, CA, USA). Polymerase chain reaction (PCR) amplification was performed using a Taq polymerase kit (Invitrogen, Carlsbad, CA) and primers (purchased from Invitrogen, Carlsbad, CA) designed to flank the 150 CAG repeat in the *Hdh* locus
(forward primer: CCCATTCATTGCCTTGCTGCTAGG,

reverse primer: CCTCTGGACAGGGAACAGTGTTGG). PCR conditions were as follows: 94°C for 5 min followed by 29 cycles at 94°C for 30 sec, 63°C for 30 sec, 72°C for 3 min and a final extension at 72° for 5 min. DNA products were separated by standard 1.5% agarose gel electrophoresis and were visualized with ethidium bromide using a Gel Doc system (Bio-Rad Laboratories, Hercules, CA). Expected bands: 379 bp for wild type band, 829 bp for mutant band. PCR products were originally sequenced to ensure flanking primers contained the *Hdh* gene product. To confirm reliability of genotyping over time, periodic CAG sizing was performed outside our laboratory (Laragen Inc., Los Angeles, CA) to confirm consistency of the CAG repeat number, which ranged from 145-150 CAG repeats.

Euthanasia

All animals were euthanized according to national guidelines. Euthanasia was carried out by decapitation. This method was approved by UCUCA and the VMU.

Behavioral Examination

Three cohorts of mice (homozygous, heterozygous, and wild type littermate controls) were used for each time point (20, 40, 50, 70, and 100 weeks). Time points are selected based on previously published neuronal intranuclear inclusion (NII) data (S. J. Tallaksen-Greene et al., 2005). In that study, diffuse nuclear htt immunoreactivity was apparent within MSNs around 20 weeks of age, and some htt immunoreactive NIIs were apparent by 40 weeks. By 70 weeks, many striatal neurons contained NIIs, and by 100 weeks, > 90% of striatal neurons contained NIIs. All behavioral evaluations were videotaped and performed with the examiner blind to genotype. Behavioral evaluations

commenced on Wednesdays and ended on Fridays of the following week, a total of eight days of behavioral trials with the first three days for acclimation and a break on Saturdays and Sundays. All behavioral trials were performed in the mornings between the hours of 9 am and noon. Weights, footprint analysis, and activity cage measurements were taken only on the last day of trials. Brains were collected on the last day of testing.

The six behavioral assays used are described in detail below. They are: 1) the accelerating rotarod, 2) the hanging wire test, 3) the tail suspension test, 4) activity monitoring, 5) footprint analysis, and 6) balance beam tests.

Hanging Wire

A standard wire cage lid is used with masking tape placed around the perimeter of the lid to prevent animals from escaping. After an animal is placed on the lid, the lid is shaken gently to induce a firm grip and the lid inverted. The lid is held horizontally 20 cm above the cage litter. Latency to fall is recorded for up to 2 minutes. As described by Crawley, normal mice are able to hang upside down for several minutes (J. N. Crawley, 2000).

Tail Suspension

Animals are suspended by their tail for a total of 1 minute and the presence of hind leg clasping or hind leg folding into the abdomen (C. H. Lin et al., 2001) greater than 2 seconds is scored as "clasping". Seizures were also noted if any occurred. An "escape" was scored during a trial if a mouse crawled up onto the testers hand within the 60 second trial. To escape an animal must grab its tail while suspended upside down and then crawl up and onto the examiner's hand.

Accelerating Rotarod and Balance Beam

Rotarod: The accelerating rotarod model number 7650 from Ugo Basile was used. Mice are habituated for 3 consecutive daily trials followed by two days of rest and tested once a day for five consecutive daily trials on an accelerating protocol (4-40 rpm over 5 min). The latency to fall is measured in each trial up to 5 minutes.

Balance beam: Motor coordination, balance, and hind-limb placement were evaluated by assessing the ability of mice to traverse two types of balance beams to reach an enclosed safety platform (R. J. Carter et al., 1999). Each mouse was tested for its ability to traverse two different styles of 41 cm long scored Plexiglass beams. One was cylindrical 11mm and diameter and the other square and 5mm wide. Beams were placed horizontally 50 cm above a table. A bright light illuminated the start platform, and a darkened enclosed 8000 cm^3 escape box (20 cm x 20 cm x 20 cm) was situated at the end of the beam (PlasticTech, MI). Time to traverse each beam were recorded for each trial with a 20 second maximum cut-off, and falls were scored as 20 seconds. The number of foot slips and whether a mouse dragged itself across the beam on its abdomen ("hind-leg drag") was also recorded.

Analyses of rotarod and balance beam results: The first three trials were used to assess learning and the last five were used to measure motor performance. In normal animals, the largest improvement in rotarod latency to fall times and time to cross the balance beam are observed in the first three trials with a ceiling by the fourth trial. Trials 4-8 are analyzed separately for motor performance after the animals have been trained in the first three trials.

Footprint Analysis

Fore and hind paws of the animals were painted with different colors of non-toxic paint, and the animals are allowed to walk across a 83 cm long unroofed corridor (7 cm wide by 11 cm tall) lined with paper into an enclosed escape area (36 cm long x 7 cm wide x 11 cm tall). Measurements of stride length (the distance between one stride to the next for the same paw), base length (the distance between the two forepaws or hindpaws), and overlap (the distance between fore- and hindpaw placement) were measured. Measurements were made for seven continuous strides and averaged per animal.

Automated Activity Cages

Activity cages with photo beam sensors (Advanced Concepts, Ann Arbor, MI) were used to measure general activity. Four photo beam sensors are located at each end of the activity cage, 2 cm apart, 2.5 cm high, and 4 cm away from the edge. The pairs of beams are situated 15 cm apart and a normal housing cage is placed into the activity apparatus to contain the mouse for the testing session. Beam breaks are automatically scored when any of the four beams are broken. Animals tested over a 2 hour period.

Brain Harvesting and Storage

Brains were extracted immediately after decapitation and divided in the sagittal plane. One hemisphere was coated with M-1 embedding matrix (Shandon, Pittsburgh, PA), frozen in crushed dry ice, wrapped in aluminum foil, and stored at -80 C. The other hemisphere was immersion fixed in 4% paraformaldehyde for 24 hrs, cryoprotected in 20% sucrose in 0.1M phosphate buffer for an additional 24 hrs 4° C, and then frozen by placing the brains on boats made from aluminum foil that were floating on isopentane (cooled on dry ice at least one-half hour). This hemisphere was also stored at -80°C until

time of sectioning. Fixed hemispheres were used for stereological analysis while the corresponding fresh frozen hemispheres were used for autoradiographic receptor binding analyses.

Receptor Autoradiography

All studies were performed on coded samples with genotype information removed. Autoradiographic studies were performed as described previously (S. Tallaksen-Greene et al., 2003). Fresh frozen brains were serially cut on a cryostat at 15μ sections at −12°C and thaw-mounted onto gelatin-coated slides and stored at -80°C until use. Assays for D1 and D2 dopamine receptors were performed as follows: slides with sections were incubated in 25 mM Tris, 100mM NaCl, 1 mM $MgCl_2$, 0.001% ascorbic acid, 1 μM pargyline, pH 7.2 with radioactive ligand 0.55 nM [³H]SCH23390 (specific activity 89 Ci/mmol) for D1 and 0.75 nM [³H]Spiperone (specific activity 96 Ci/mmol) with 100 nM mianserin for D2 for 2.5 hrs at room temperature. Nonspecific binding was determined in the presence of 1 μM cis-flupenthixol for D1and 50 μM dopamine for D2, respectively. Following incubation, slides were subjected to two cold washes at 4°C and then one 10 min. room temperature wash with incubation buffer lacking radioactive ligand, followed by a quick rinse in double distilled water before drying under a stream of warm air. For dopamine transporters (DAT), slides were pre-washed in a 4°C solution containing 50 mM Tris-HCl, 5mM KCl, 300 mM NaCl, pH 7.9 for 5 min, followed by a 1 hr incubation at 4°C in the same buffer with the addition of 10 nM [³H]Mazindol (specific activity 23.1 Ci/mmol) and 300 nM desipramine. Blank conditions contained 100 μM nomifensine. Slides were subjected to a final wash under the same conditions as the pre-wash for 3 min. For GABA-A/benzodiazepine receptors, slides were prewashed

in 50 mM Tris-citrate buffer, pH 7.2 at 4°C for 30 min, air dried and incubated in 50 mM Tris-citrate buffer, pH 7.2 with 5 nM [^{3}H]flunitrazepam (specific activity 85 Ci/mmol) for 1 hr at 4°C. Nonspecific binding was determined in ligand buffer with 2 μM clonazepam. Slides were subjected to one rapid rinse and then two 5 minute washes in 4°C 50 mM Tris-citrate buffer, pH 7.2 before drying under warm air.

D1 and D2 [^{3}H]ligands were purchased from Amersham (United Kingdom). [^{3}H]Mazindol and [^{3}H]flunitrazepam were purchased from DUPONT Co. Biotechnology Systems (Wilmington, DE).

For receptor autoradiography, three slides per subject were used for each radioligand assay, two slides for total binding and the third to define nonspecific labeling with a minimum of two consecutive sections taken at fixed intervals (15 μm) mounted per slide. Slides and ^{14}C standards are arrayed in a standard X-ray cassette, and an autoradiogram is generated by direct apposition of the tissue to the emulsion side of the tritium imaging plate (BAS-TR2025; Fuji Photo Film, Japan) for a period of 19 to 22 hrs.

Autoradiograms were analysed by quantitative densitometry using an MCID-M2 image analysis system (Interfocus Ltd., England). Anatomic locations of selected regions of interest were determined using an approach designed to ensure accuracy and consistency of structures identified (T. J. Morrow et al., 1998). Briefly, for each brain section, we overlaid a matching transparent stereotaxic template, adapted from the mouse brain atlas (G. Paxinos and K. B. J. Franklin, 2001), on the digitized brain images displayed on the video monitor and aligned the images using prominent anatomical landmarks. Optical density (OD) measurements were taken bilaterally in a minimum of six brain sections and measurements were made in each section in which the structure

was visible, sampling as large an area as possible. Tissue ^{14}C concentrations were determined by comparison of ODs with a calibration curve obtained from co-expressed standards. Specific binding was determined by subtracting nonspecific binding from the total binding.

Immunohistochemistry

Hemispheres previously fixed in 4% paraformaldehyde as described above were serially sectioned at 40 μm sagitally throughout the entire hemisphere. Every fourth section was used for stereological analysis. Free floating sections were then stained with a primary specific neuronal antibody, NeuN (Chemicon Int., Temecula, CA, USA) at a dilution of 1:1000 for 1 hr. Sections were processed without primary NeuN antibody to assess background staining. No staining was visualized in these control sections. Detection of immunoreactivity was performed using the Vectastain Elite kit (Vector laboratories, Burlingame, CA, USA) and diaminobenzidine (DAB) substrate was used as the chromogen according to the manufacturer's protocol. Sections were then mounted on gelatin-coated slides and air dried following dehydration with graded alcohols and xylene. Coverslips were affixed with Permount.

Stereology

Unbiased stereological counts of striatal neurons were obtained from the striatum of animals at 70 and 100 weeks of age using the StereoInvestigator software (Micro-Brightfield, Colchester, VT). The optical fractionator method was used to generate an estimate of neuronal number with only darkly stained NeuN immunoreactive cells counted in an unbiased selection of serial sections in a defined volume of the striatum.

Striatal borders were delineated by on NeuN stained section by reference to a mouse brain atlas (G. Paxinos and K. B. J. Franklin, 2001). The striatum was defined to encompass both the dorsal and ventral striatum. Striatal volume was reconstructed by the StereoInvestigator software using the Cavalieri principle. Serially cut sagittal tissue sections (every fourth section) were analyzed for one entire hemisphere of animals in each genotype cohort (n=4/group).

Statistical Analyses

All studies were performed blind to genotype. Comparisons of different groups (between genotypes) was performed on receptor binding, stereology, and weight data using one-way analysis of variance (ANOVA) with posthoc comparisons being made using Tukey HSD when $p < 0.05$. Repeated measures ANOVA was performed for each behavioral test to determine if there was an effect from genotypes or from repeated training. If there was no change after repeated training, the trials were collapsed and a one-factor ANOVA was performed. A critical $p < 0.05$ was used for statistical significance in all analyses. Huynh-Feldt adjustment was used in correcting for violation of sphericity when necessary to adjust non-uniform variance across days or groups. The Kruskal Wallis test was used for analysis of activity cage data due to the unequal variances of the groups. SPSS (SPSS Inc.) statistical software package was used.

Results

Survival and General Observations

All mice survived to 100 weeks. However, by 100 weeks, homozygous $Hdh^{(CAG)150}$ mice exhibited noticeable resting tremor, unsteady movements and

staggering gait. No seizures were noted in any animal. We analyzed the data for sexual dichotomy in the analyses of all our behavioral evaluations and found no differences between genders.

Homozygous *Hdh*^(CAG)150 Mice Exhibit Weight Loss Over Time

Hdh^(CAG)150 homozygotes exhibited progressive weight loss with age (Fig. III.1a and Table III.1). Significant differences in average body weight between homozygous mutants and wild type were observed at 70 and 100 weeks (70 weeks WT 33.6 ± 1.8 grams [mean ± SEM]; HOM 26.9 ± 0.9 grams, $p < 0.05$; 100 weeks WT 28.9 ± 1.7 grams; HOM 18.75 ±0.76 sec., $p < 0.05$). Similar patterns in weight loss were observed when analyzed separately by gender (data not shown). This weight loss was not apparent at earlier ages, although some non-significant differences in weight were observed around 50 weeks of age.

Hdh^(CAG)150 Mice Show Decreased Motor Activity

Mice were assessed for general locomotion and normal exploratory behavior by 2 hour trials in automated activity cages. At 100 weeks, homozygous mice exhibited significantly reduced activity (371.8 ± 60.2 [mean ± SEM] beam breaks/2hr; Kruskal Wallis chi-square < 0.05) compared to wild type (804.2 ± 138.6 beam breaks/2hr; Fig. III.1b) suggesting that homozygous mice have abnormal motor behavior. This reduction is also observed at 70 weeks, although not as robust (HOM 388.7 ± 43.8 beam breaks/2hr; Kruskal Wallis chi-square > 0.05; WT 540 ± 135.8 beam breaks/2hr; Fig. III.1b). The general activity of heterozygous mice was similar to control mice up to 100 weeks (613.9 ± 115.3 beam breaks/2hr; Kruskal Wallis chi-square > 0.05).
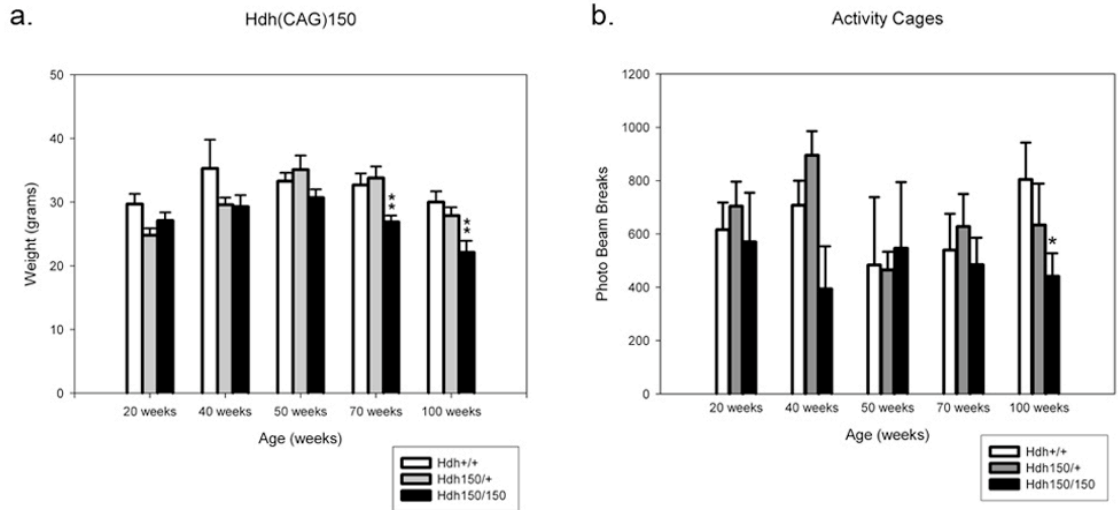
Figure III.1 Hdh(CAG)150 mice exhibit decreased locomotor activity and progressive weight loss. (a) Homozygotes show weight loss over time with significant weight loss at 70 wks and 100 wks compared to heterozygotes and wild type. Weights were taken from three cohorts of mice on the last day of behavioral testing (WT, HET, and HOM) at 20, 40, 50, 70, and 100 weeks. Weights are expressed as mean weight ± SEM. ** denotes a significant difference between wild type and heterozygotes, $p < 0.05$. (b) $Hdh^{(CAG)150}$ heterozygous and homozygous mice exhibit a trend towards decreasing spontaneous activity beginning at 40 weeks. At 100 weeks, differences are significant compared to WT (Kruskall Wallis chi-square < 0.05). Data is expressed as mean ± SEM, n=7-15/group.

Hdh$^{(CAG)150}$ Mice Show Motor Impairment On the Accelerated Rotarod

At 100 weeks, homozygous *Hdh*$^{(CAG)150}$ mice fell significantly earlier during the last five trials (120.34 ± 19.42 sec. [mean ± SEM], $p < 0.05$) compared to wild type (212.38 ± 27.1 sec., (Fig. III.2d) and heterozygous *Hdh*$^{(CAG)150}$ mice (195.28 ± 22.2 sec.).

Weights (grams)	Hdh +/+	Hdh 150/+	Hdh 150/150
20 weeks	29.7 ± 1.6 n=7	24.8 ± 1.1 n=15	27.1 ± 1.3 n=7
40 weeks	35.2 ± 4.5 n=4	30.0 ± 1.1 n=9	29.3 ± 1.8 n=3
50 weeks	33.3 ± 1.3 n=3	35.1 ± 2.2 n=9	30.7 ± 1.3 n=3
70 weeks	33.6 ± 1.8 n=5	33.8 ± 1.8 n=9	*26.9 ± 0.9 n=9
100 weeks	28.9 ± 1.7 n=9	27.9 ± 1.3 n=9	*22.1 ± 1.0 n=10

Table III.1 Mean weights for Hdh(CAG)150 mice. Mean weights of males and females combined. Weights were collected on the last day of behavioral testing. * Denotes $p < 0.05$. All values are presented as mean ± SEM grams.

Motor learning as assessed by improvement over the course of the first three trials was not impaired in *Hdh*$^{(CAG)150}$ homozygotes at 100 weeks of age ($F_{(2,24)} = 5.70$, $p < 0.05$ effect of training). Rotarod performance impairment was dependent on gene dosage, since 100 week old heterozygous *Hdh*$^{(CAG)150}$ mice were able to maintain equal levels of

motor performance as wild type mice ($F_{(2,22)}$ = 3.95, p < 0.05). Furthermore, the impairment of motor performance in 100 week old homozygotes was not found in younger mice, indicating a late-onset deficit. No differences existed between the three cohorts of mice in motor learning or performance at 50 and 70 weeks of age ($F_{(2,11)}$ = 0.56, 50 weeks; $F_{(2,19)}$ = 0.14, 70 weeks, for motor learning, effect of training, p > 0.05) ($F_{(2,10)}$ = 1.14, 50 weeks $F_{(2,19)}$ = 0.18, 70 weeks for motor performance, effect of
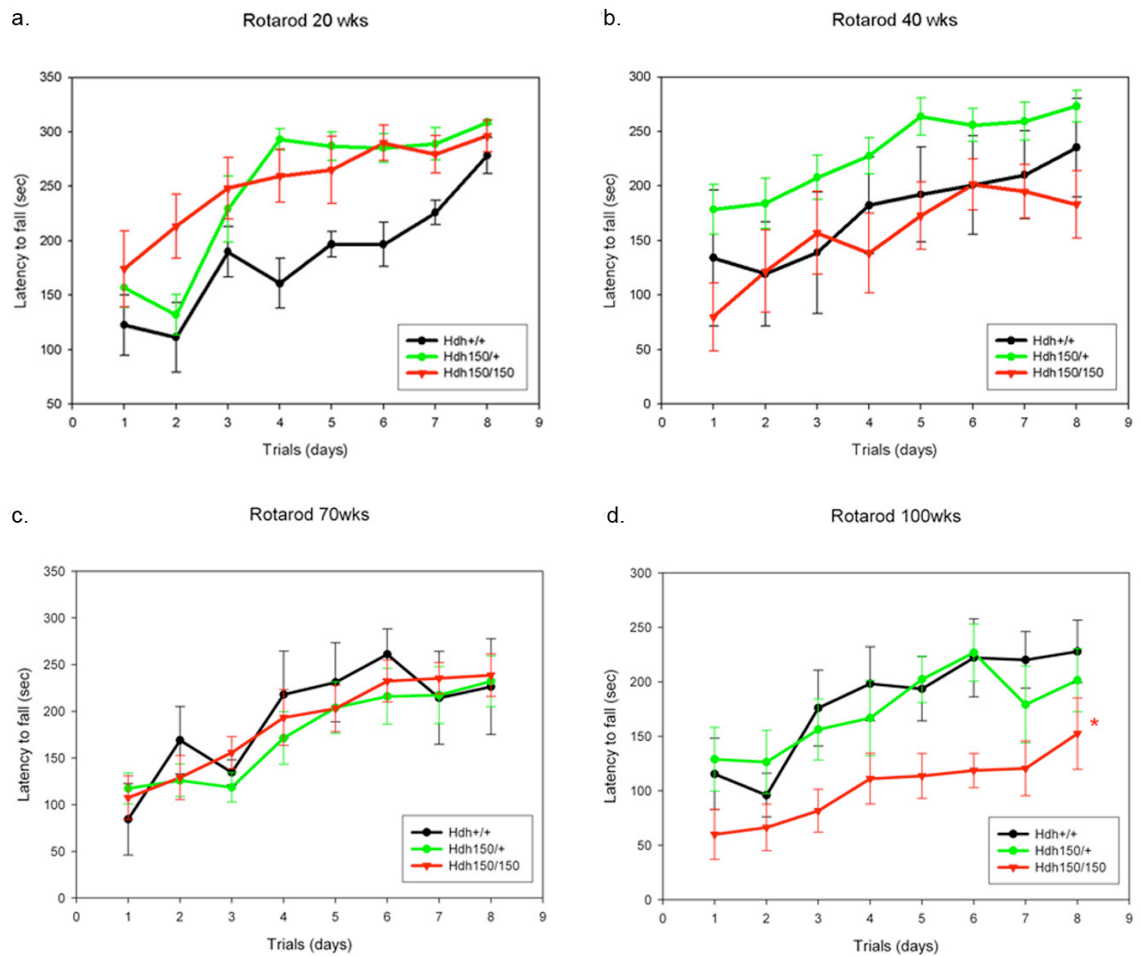
Figure III.2 *Hdh*$^{(CAG)150}$ **mice exhibit decreased motor performance compared to wild type on the accelerating rotarod.** Animals were placed on a rotarod accelerating from 4-40 rpm within 5 minutes. **(a)** 20 weeks **(b)** 40 weeks **(c)** 70 weeks **(d)** 100 weeks. To determine the rate of task learning, the maximum speed at the time of falling off the rotarod was plotted against the trial number over the first 3 days. Performance over days 4-8 measures motor performance. Note that heterozygous and homozygous mice initially learn the rotarod task more rapidly in the first three trials than wild type controls at 20 weeks ($F_{(2,23)}$ =21.2 for effect of trials and $F_{(2,20)}$ = 7.2 for effect of genotype; WT n=6, HET n=13, HOM n=7, p < 0.05). *Hdh*$^{(CAG)150}$ mutant mice show no impairment in rotarod performance earlier than 70 weeks. All groups exhibited significant improvement in performance as training progressed; there were no differences between *Hdh*$^{(CAG)150}$ mutant mice compared to WT at 40 and 70 weeks (WT n=3, HET n=9, HOM n=10, $F_{(2,19)}$ = 0.175 for effect of genotype, p > 0.05). When mice were examined at 100 weeks, homozygotes exhibited a significant decrease in latency to fall (120.34 ± 9.2 sec, p < 0.05 compared to wild type (212.38 ± 27.1 sec. Heterozygotes fell after 195.28 ± 2.2 seconds, not significantly different from wild type controls (p > 0.05; WT n=9, HET n=8, HOM n=8, $F_{(2,22)}$ = 3.98 for effect of genotype). * denotes significance of p < 0.05. Values expressed as mean ± SEM seconds.

genotype, p > 0.05; Fig. III.2c). At 20 weeks the opposite of impairment was seen for *Hdh* heterozygous and homozygous mice, who performed better than wild type controls in both motor learning and motor performance ($F_{(2,23)}$ =21.2 for effect of trials and $F_{(2,20)}$ = 7.2 for effect of genotype; Fig III.2a). This effect was maintained for heterozygotes at 40 weeks but only significant for performance compared to homozygous $F_{(2,20)}$ = 4.27 for genotype effect, p < 0.05; Fig. III.2b).

Hdh$^{(CAG)150}$ Mice Show Abnormal Gait

Footprint analysis was a sensitive indicator of gait abnormalities in *Hdh*$^{(CAG)150}$ mice (Fig. III.3 and Table III.2a). 100 week old *Hdh*$^{(CAG)150}$ homo- and heterozygous mice exhibit statistically significant differences from wild type controls in several measures of gait. Significant differences were found in stride lengths and base lengths (hindpaw stride length WT 6.86 ± 0.22 cm [mean ± SEM]; HET 5.8 ± 0.25 cm; HOM 5.8 ± 0.22, p < 0.05 vs WT; forepaw stride length WT 6.8 ± 0.14 cm; HET 5.8 ± 0.30 cm;

HOM 5.5 ± 0.32 cm, p < 0.05 vs. WT; front base length WT 4.13 ± 0.2 cm; HET 3.47 ±

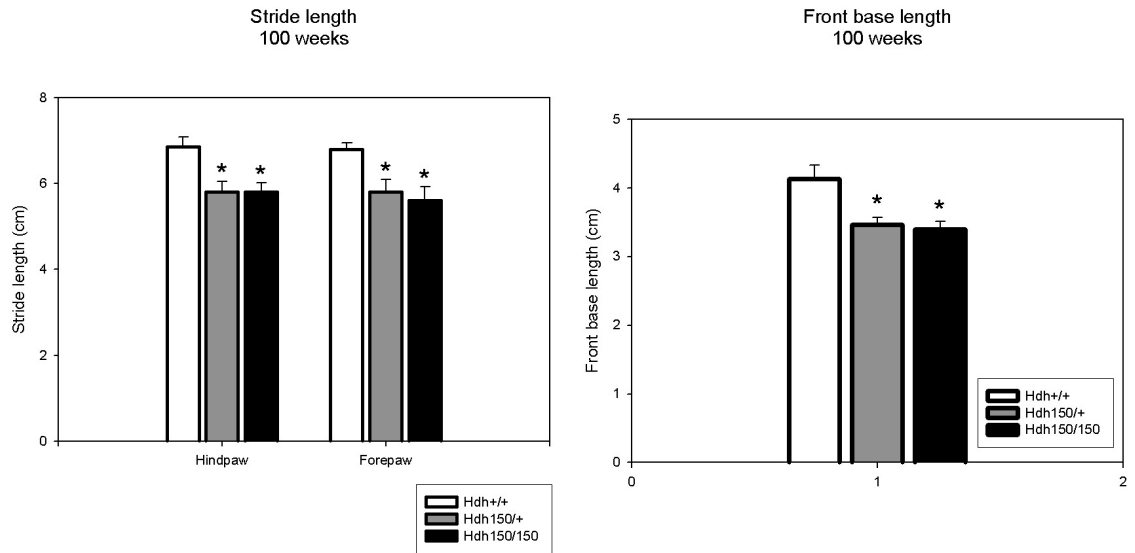0.10 cm; HOM 3.40 ± 0.11 cm, p < 0.05 vs. WT). Gait abnormalities were not as

Figure IIII.3 *Hdh*[(CAG)150] **Mice Show Abnormal Gait.** 100 week old *Hdh*[(CAG)150] homo- and heterozygous mice exhibit statistically significant differences in stride length and base length gait measurements from wild type controls. Significant differences were found in stride lengths and base lengths (hindpaw stride length WT 6.86 ± 0.22 cm [mean ± SEM]; HET 5.8 ± 0.25 cm; HOM 5.8 ± 0.22, p < 0.05 vs WT; forepaw stride length WT 6.8 ± 0.14 cm; HET 5.8 ± 0.30 cm; HOM 5.5 ± 0.32 cm, p < 0.05 vs. WT; front base length WT 4.13 ± 0.2 cm; HET 3.47 ± 0.10 cm; HOM 3.40 ± 0.11 cm, p < 0.05 vs. WT).

profound in younger mutant mice. For example, 70 weeks *Hdh*[(CAG)150] homozygous

and heterozygous mutants did not show statistically significant alterations in these same

measures (WT 4.03 ± 2.0 cm [mean ± SEM]; HET 3.86 ± 0.17 cm, p = 0.092 vs WT;

HOM 3.47 ± 0.09 cm, p = 0.056 vs. WT). *Hdh*[(CAG)150] homozygotes also had more

difficulty traversing the corridor, often leaning on one wall for support, which can be

seen in the bias of gait prints to one side of the paper and the complete loss of gait pattern
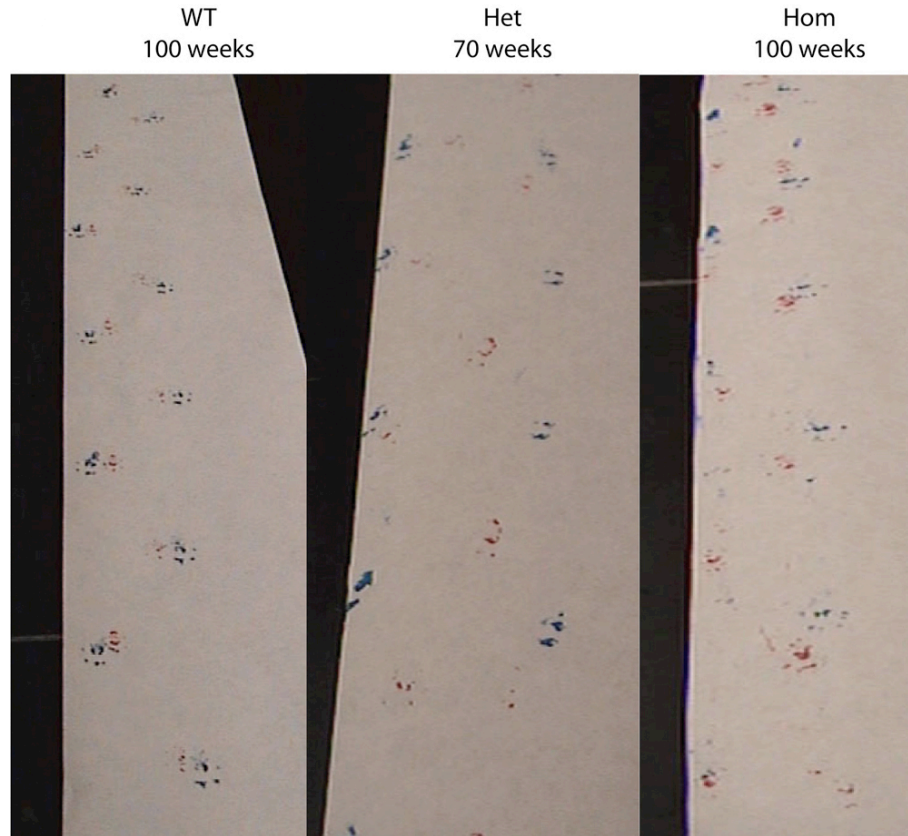
(Fig. III.4).

Figure III.4 *Hdh*$^{(CAG)150}$ **mice show abnormal gait pattern.** Gait was captured by painting the paws of wild type, heterozygous, and homozygous mice with contrasting non-toxic colors prior to walking a paper-lined corridor. Gait pattern was normal in wild type mice. Heterozygotes exhibit incongruent overlaps while homozygotes exhibited complete loss of gait pattern compared to WT.

Wild type mice at 100 weeks showed no loss of gait pattern over the mice tested at earlier ages, maintaining a consistent base length and very little deviance in overlap between hind paw and front paw. However, wild type mice show increased stride length when comparing 20 weeks of age to 100 weeks (Table III.2b; right and left stride lengths 20 weeks 6.25 ± 0.23 cm 3.47 ± 0.10 cm and 6.33 ± 0.2 cm [mean ± SEM], respectively compared to right and left stride lengths 100 weeks 6.84 ± 0.1 and 6.86 ±0.2, respectively, p < 0.05). Measurement of gait features, however, added little to inspection of footprint records. When measurement of gait features showed significant differences,

gait was already qualitatively abnormal and measurements fail to capture qualitative differences between mutant and wild type gaits. Measurements, for example, did not show the tendency of 100 week old homozygous mutants to lean against one wall of the apparatus, a useful qualitative indicator.

a.

Footprint analysis 100 weeks	Hdh +/+ n=9	Hdh 150/+ n=8	Hdh 150/150 n=9
Hindpaw stride length (cm)	6.86 ± 0.22	*5.8 ± 0.25	*5.8 ± 0.22
Forepaw stride length (cm)	6.8 ± 0.14	*5.8 ± 0.30	*5.5 ± 0.32
Front base length (cm)	4.13 ± 0.2	*3.47 ± 0.10	*3.40 ± 0.11

b.

Footprint analysis Hdh +/+	20 weeks n=6	100 weeks n=9
Front base (cm)	3.83 ± 0.14	4.13 ± 0.2
Hind base (cm)	4.18 ± 0.14	4.03 ± 0.15
Right overlap (cm)	0.08 ± 0.12	0.98 ± 0.1
Left overlap (cm)	0.89 ± 0.2	0.74 ± 0.1
Right stride (cm)	6.25 ± 0.23	*6.84 ± 0.1
Left stride (cm)	6.33 ± 0.2	*6.86 ± 0.2

Table III.2 Footprint analysis for *Hdh*$^{(CAG)150}$ mice. Measurements were made for seven continuous strides and averaged per animal. **(a)** Average measurements for *Hdh*$^{(CAG)150}$ mice at 100 weeks. **(b)** Average measurements for WT mice for comparison at 20 weeks and 100 weeks. * Denotes $p < 0.5$ compared to WT. Values presented as mean ± SEM cm.

Hdh$^{(CAG)150}$ Mutants Require More Time to Traverse Balance Beam

Limb coordination and balance was measured with the balance beam task. At 70 weeks *Hdh*$^{(CAG)150}$ homo- and heterozygotes exhibited a trend towards greater time to traverse the 11mm round and 5mm square beams than wild type controls (11 mm round

beam $F_{(2,19)} = 1.38$; 5 mm square beam $F_{(2,18)} = 2.4$ effect for genotype, $p > 0.05$; Fig. III.5a and c respectively). Motor abnormalities became significant at 100 weeks, both heterozygous and homozygous mutants took longer to traverse the beams compared to age-matched wild type littermates (11 mm round beam WT 6.09 ± 0.78 sec. [mean $\pm$ SEM]; HET 9.08 ± 1.69 sec.; HOM 13.92 ± 1.51 sec., $p < 0.05$ and for 5 mm square beam WT 10.11 ± 1.37 sec.; HET 16.77 ± 1.78 sec.; HOM 18.75 ± 0.76 sec., $p < 0.05$) (Fig III.5b and d respectively). When motor learning was assessed for the 70 and 100 week old animals only the 100 week old $Hdh^{(CAG)150}$ homozygotes showed no improvement during the first three trials. 100 week old heterozygotes did, however, decrease their time to traverse the 11 mm round beam in the first three trials demonstrating motor learning was preserved. Deficits in motor performance were not seen in younger mutants. At 20, 40, and 50 weeks, there were no differences between genotypes in latency to cross the balance beams (11 mm round $F_{(2,10)} = 0.013$; 5 mm^2 $F_{(2,10)} = 0.179$ effect for genotype, $p > 0.05$) (Fig. III.6a and b respectively). The penetrance of abnormalities increased with increased gene dosage. For example, at 100 weeks of age 80% of $Hdh^{(CAG)150}$ homozygous mice failed to traverse the 5mm beam while 50% of $Hdh^{(CAG)150}$ heterozygous mice failed compared to 0% of the wild types.
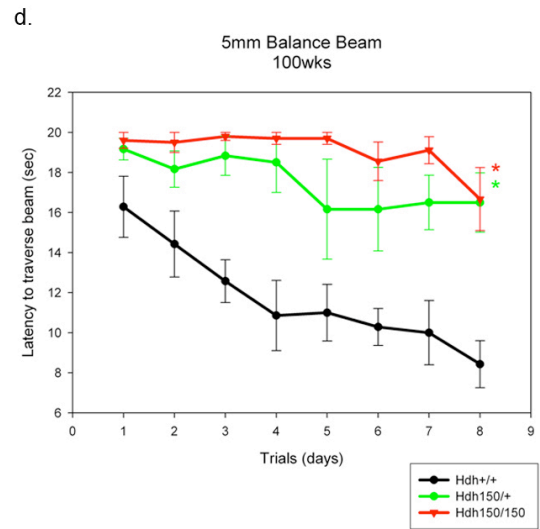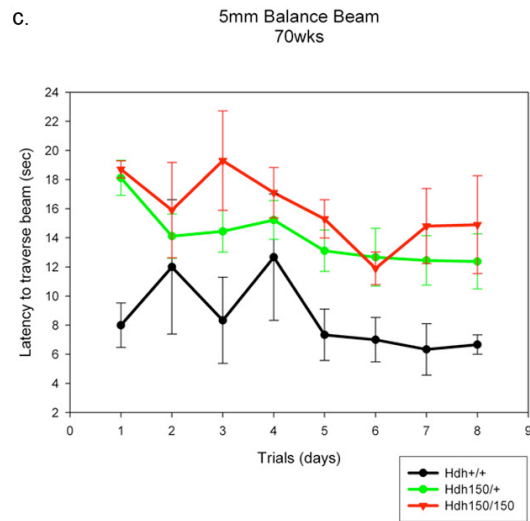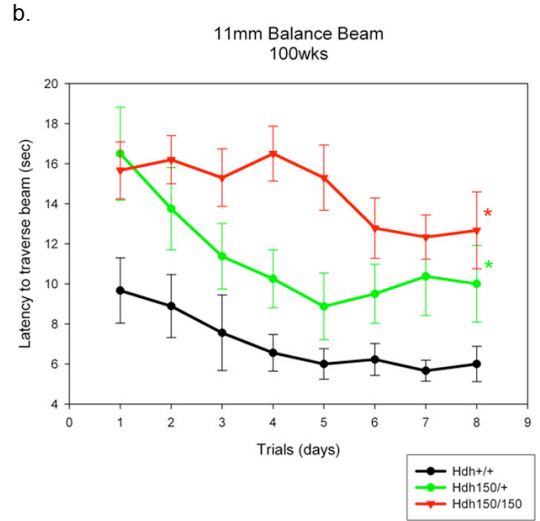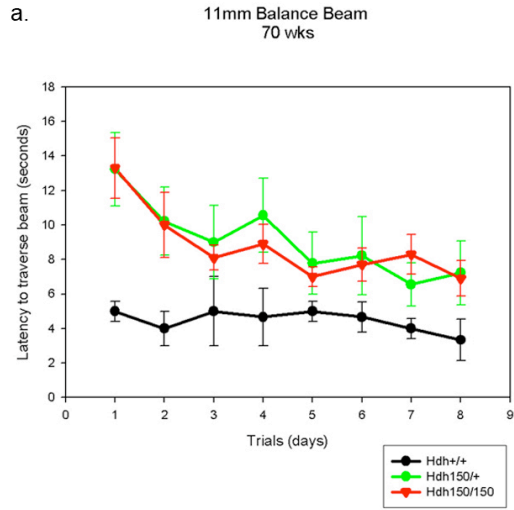
a. 11mm Balance Beam
70 wks

b. 11mm Balance Beam
100wks

c. 5mm Balance Beam
70wks

d. 5mm Balance Beam
100wks

Figure IIII.5 *Hdh*150^{CAG} mice require more time to transverse the balance beam. Mice were placed on a lit platform and traversed beams of different diameters (5mm square and 11mm round) to reach a safe chamber on the far side. Mice were tested at 20, 40, 50, 70 and 100 week time points. **(a)** 11 mm round beam; 70 weeks **(b)** 11 mm round beam; 100 weeks **(c)** 5 mm square beam; 70 weeks **(d)** 5 mm square beam; 100 weeks. Although non-significant, at 70 weeks both heterozygous and homozygous mice required more time to traverse the 11 mm and 5 mm beams compared to wild type mice (11 mm beam $F_{(2,19)}$ = 1.38; 5 mm beam $F_{(2,18)}$ = 2.4 effect for genotype, $p > 0.05$; **(a)** and **(c)**. At 100 weeks, both heterozygous and homozygous mice required significantly more time to traverse the balance beams compared to wild type mice (11 mm beam WT 6.09 ± 0.78; HET 9.08 ± 1.69; HOM 13.92 ± 1.51 sec., $p < 0.05$ and for 5 mm beam WT 10.11 ± 1.37; HET 16.77 ± 1.78; HOM 18.75 ± 0.76 sec., $p < 0.05$; **(b)** and **(d)**. * denotes significance of $p < 0.05$ compared to WT and ** denotes significance of $p < 0.05$ compared to HET. Data is expressed as mean ± SEM in seconds.
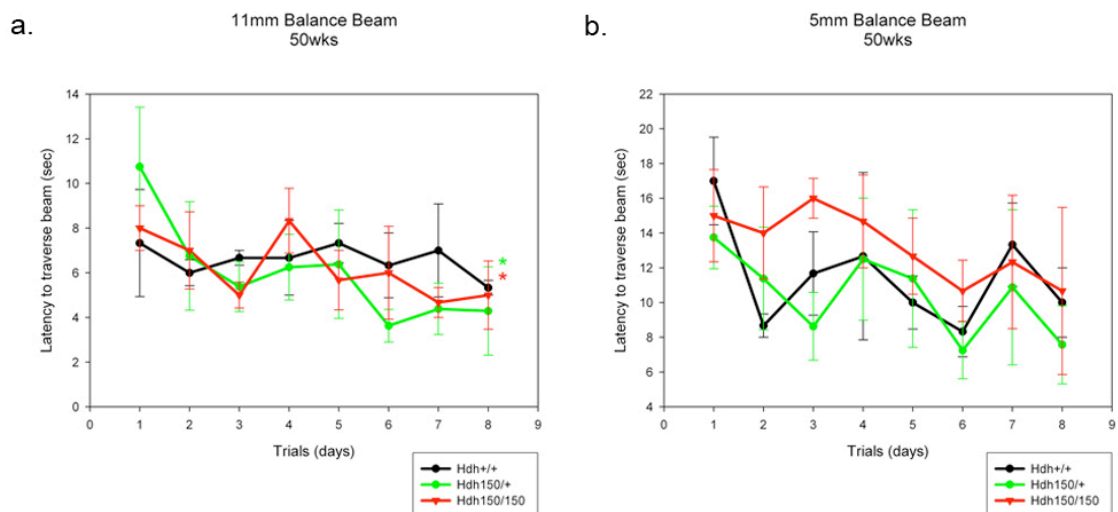

a.

11mm Balance Beam
50wks

b.

5mm Balance Beam
50wks

Figure III.6 *Hdh*150^{CAG} mice exhibit no motor deficits at 50 weeks. *Hdh*^{(CAG)150} mutant mice show no motor abnormalities up to and including 50 weeks of age.

An interesting and obvious difference between *Hdh*^{(CAG)150} mutant mice and wild type littermates was the manner in which they traversed the balance beams. As early as 40 weeks *Hdh*^{(CAG)150} homozygous mice exhibited a "hind-limb drag" behavior where the thorax and abdomen was pressed against the surface of the beam and hind limbs were

laterally wrapped around the beams. The fore limbs were used to pull the mouse across, resulting in a dragging motion across the beams (Fig. III.7a).
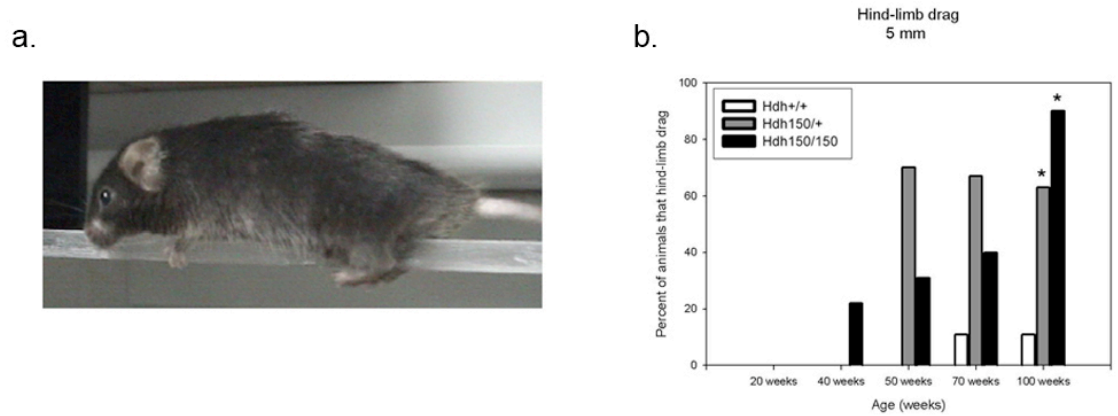

Figure IIII.7 *Hdh*150^{CAG} mice displayed hind-limb drag. *Hdh*150^{CAG} mice displayed hind-limb drag as early as 40 weeks, where the abdomen is pressed against the surface of the beam and hind-limbs are dragged across the beams **(a)**. The percentage of *Hdh*$^{(CAG)150}$ mice presenting hind-limb drag progressively increased with age **(b)**. By 100 weeks, 63% of HET and 90% of HOM displayed hind-limb drag compared to only 11% for WT controls (Pearson chi-square analysis, p < 0.05). Generally, wild type mice displayed an upright posture with exact fore and hind-limb placement on the beams.

Wild type mice displayed an upright posture with exact fore and hind limb placement on the beams. The percentage of mice that displayed "hind-limb drag" increased with age and with the narrower 5 mm square beam (Fig. III.7b). By 100 weeks *Hdh*$^{(CAG)150}$ mutant mice displayed significant differences of hind-limb drag (heterozygotes 63%; homozygotes 90%) compared to wild type controls (11%), Pearson chi-square analysis, p < 0.05. This behavior probably contributed to the increased latency of mutant mice to traverse the beams. The *Hdh*$^{(CAG)150}$ mutant mice display the same type of hind-limb drag that has been previously described in R6/2 mice (R. J. Carter et al., 1999). Hind-limb slips were also scored, however, because *Hdh*$^{(CAG)150}$ mutant mice largely

displayed hind-limb drag instead of showing clear foot slips, this confounded the scoring of hind-leg slips and these results were not useful.

No Loss of Muscle Power in Aged $Hdh^{(CAG)150}$ Mice

To test whether the motor impairments are related to loss of muscle power, the hanging wire test was used. At 100 weeks we found no significant difference in the latency to fall between $Hdh^{(CAG)150}$ homozygotes [Fig. III.8 (92.0 ± 8.5 seconds; mean ± SEM]) and heterozygotes (104.9 ± 6.0) compared to wildtype controls (89.8 ± 11.9). Similarly, no differences existed at any of the earlier time points. Because there was no difference in the repeated measures ANOVA, the last 5 trials were collapsed and averaged, $p > 0.05$.
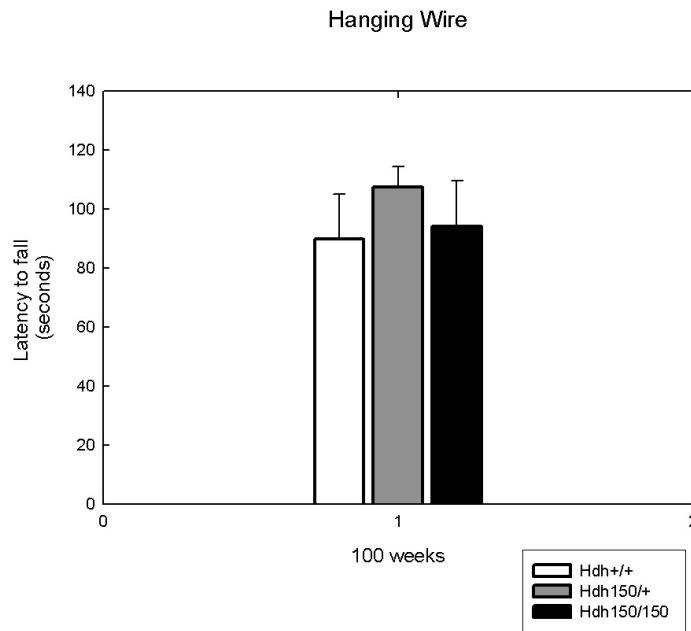

Figure IIII.8 Motor impairments in $Hdh^{(CAG)150}$ mice are not due to muscle weakness. $Hdh^{(CAG)150}$ mice were placed on inverted wire cage lids and latency to fall was recorded up to a maximum cutoff time of 2 minutes. The latency to fall was not significantly different from wild-type animals up to 100 weeks of age. WT (89.8 ± 11.9), He*t* (104.9 ± 6.0), Hom (92.0 ± 8.5), $p > 0.05$.

67

Hdh$^{(CAG)150}$ Mice Exhibit Clasping

We performed a tail suspension test that has been used to detect general neurological abnormalities and has been shown to induce seizures in abnormal mice (C. H. Lin et al., 2001). Animals were suspended by their tail for a total of 1 minute and animals were scored as "clasping" if the paws were held for greater than 2 seconds (Fig. III.9). Only homozygous mice exhibited clasping behavior compared to heterozygous and wild type mice at all time points (Fig. III.10a). A small percentage of homozygous mice exhibited clasping at 20 weeks compared to wild type littermates, however, the clasping phenomenon did not occur at 40 or 50 weeks but was common at 70 and 100 weeks.
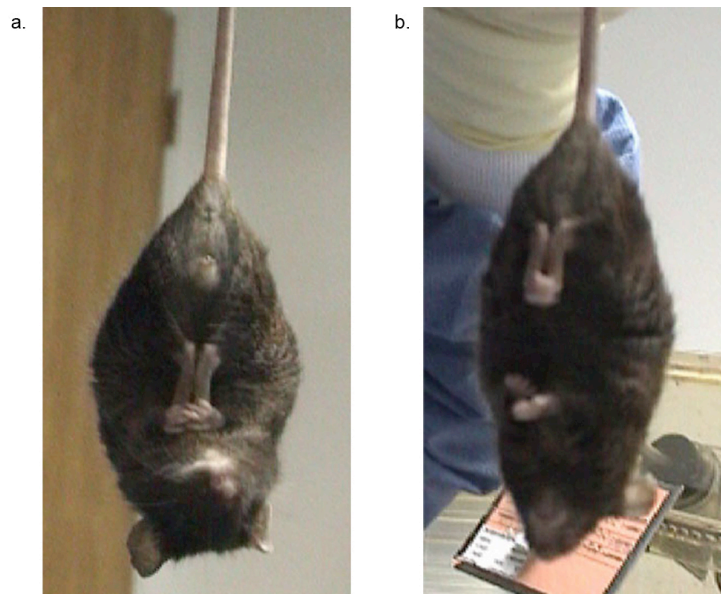

Figure IIII.9 Clasping behavior. Animals were suspended by their tails for a maximum of 60 seconds. Animals were scored as "clasping" if their hind-limbs clasped or folded into the abdomen for a minimum of 2 seconds while suspended with by their tails **(a)** and **(b).**

We did not observe any seizures during this test nor were any seizures reported during routine handling. Additionally, we also looked at the percent of mice that could escape

as described in Lin et al., (2001), a general measure of overall fitness and health. Animals were scored as "escape" if they could crawl up and onto the testers hand within the 60 second clasping trial. We found that the percent of homozygous mice able to escape was actually higher than heterozygous mice compared to wild type controls at 20 and 40 weeks (Fig. III.10b). This effect could be due to the size of the mouse as homozygous mice are generally smaller in size, which may allow them to climb up more easily. Escape was not observed at time points beyond 40 weeks in all groups.
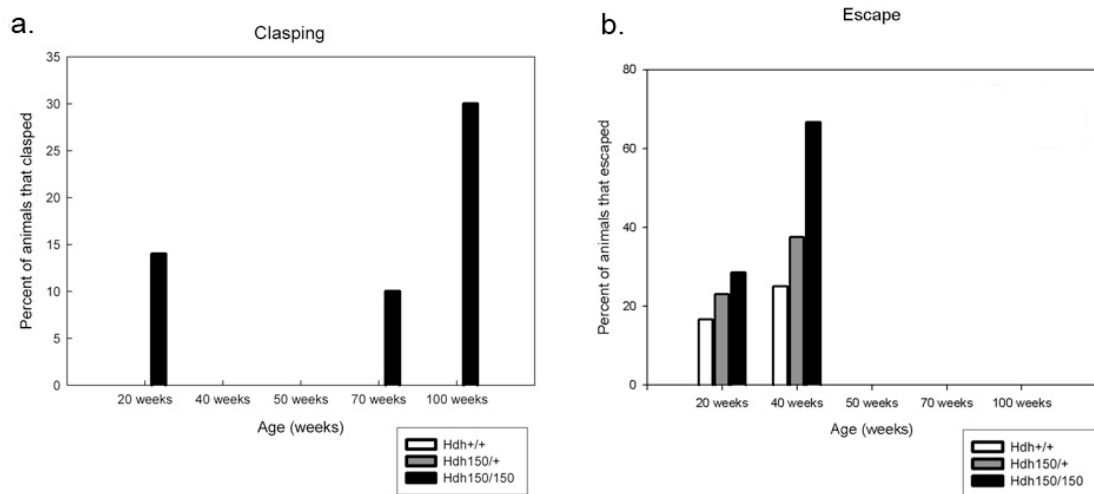

Figure III.10 *Hdh*$^{(CAG)150}$ **homozygous mice display clasping and escape behaviors. (a)** Homozygous mice displayed clasping behavior as early as 20 weeks and the number of mice presenting this behavior increased at 70 and 100 weeks. Clasping was not observed at the 40 or 50 week time points. **(b)** Prior to motor deficits, *Hdh*$^{(CAG)150}$ mice exhibited escape behavior at 20 and 40 weeks. A larger percentage of *Hdh*$^{(CAG)150}$ mice were able to escape compared to wild type controls at both time points.

Neuropathology

Receptor Binding

Autoradiographic receptor analyses provided evidence of significant progressive, mutant allele-dependent morphological alterations in the *Hdh*$^{(CAG)150}$ mouse. Binding

sites were selected based on their regional distribution in the brain. $GABA_A$/benzodiazepine receptor sites were chosen to survey neuronal integrity in many brain regions. These binding sites are highly expressed in most brain regions. An important exception is the striatum, where flunitrazepam binding is relatively low compared to other brain regions. Dopamine D1 and D2 receptor binding sites were chosen for their high expression by MSN dendrites and have shown to be abnormal in HD patients as well as transgenic and other knock-in mouse models of HD (R. A. Weeks et al., 1996; J. H. Cha et al., 1998; L. Kennedy et al., 2005; J. C. H. van Oostrom et al., 2005). Additionally, we chose to look at dopamine reuptake transporters (DAT), a good presynaptic marker for nigrostriatal afferent projections.

Quantitative receptor autoradiographic analyses revealed no differences in $GABA_A$/benzodiazepine binding sites between genotypes in any brain region (Fig. III.11 and Table III.3). We found significant alterations in striatal D1 and D2 receptor binding and in DAT binding at 100 weeks (Fig. III.11 and Table III.3). DAT binding was significantly decreased in the striatum of homozygous mutants to 49% of wild type levels. No DAT reduction was seen in heterozygous mice (WT 81.5 ± 4.9 pCi/g [mean ± SEM]; HOM 41.7 ± 8.2 pCi/g, $p < 0.05$). Striatal D1 receptor binding sites decreased by 50% in heterozygotes and 86% in the homozygotes in the ventral striatum compared to wild type controls and 42% and 79% in the dorsal striatum, respectively (Fig. III.11; ventral striatum WT 36.7 ± 1.7 pCi/g [mean ± SEM]; HET 18.4 ± 4.8 pCi/g; HOM 5.3 ± 0.6; dorsal striatum WT 49.2 ± 5.3 pCi/g; HET 28.5 ± 6.2 pCi/g; HOM 10.5 ± 1.5 pCi/g; $p < 0.05$). Striatal D2 receptor binding sites exhibited a 17% decrease in heterozygotes and 32% decrease in homozygotes in the ventral striatum and a 17% and 42% compared

70

to wild type in the dorsal striatum, respectively (Fig. III.11; ventral striatum WT 101.5 ± 3.6 pCi/g [mean ± SEM]; HET 83.8 ± 4.3 pCi/g; HOM 69.3 ± 0.5; dorsal striatum WT 95.2 ± 2.2 pCi/g; HET 78.6 ± 3.7 pCi/g; HOM 55.6 ± 2.6 pCi/g; $p < 0.05$).   These reductions are late onset. Striatal D1 and D2 receptor binding at earlier time points showed smaller reductions in homozygotes as compared to wild type at 70 weeks (Fig. III.12a and b and Table III.3; ventral striatum
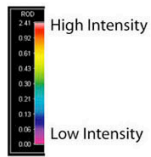
100 weeks GABA receptor binding

100 weeks DAT receptor binding
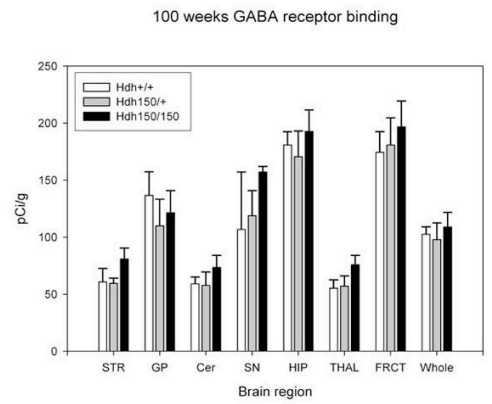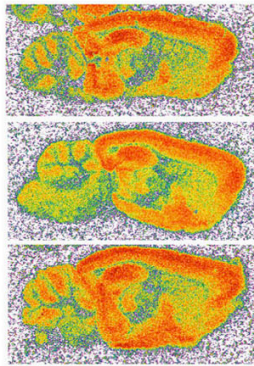
100 weeks D1 receptor binding
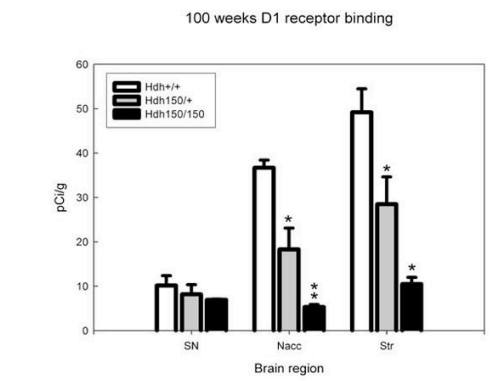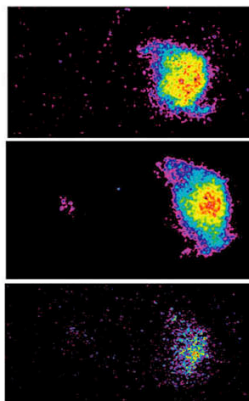
100 weeks D2 receptor binding
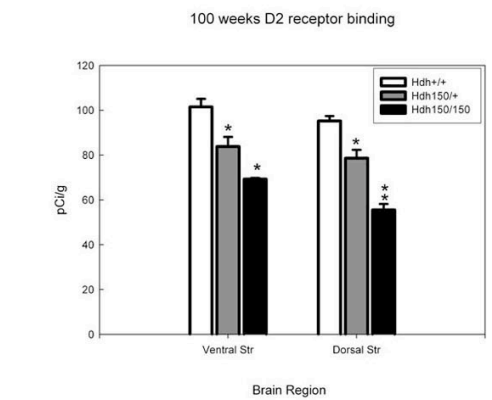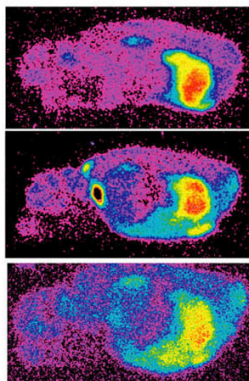
Figure IIII.11 *Hdh*$^{(CAG)150}$ **mice exhibit alterations in striatal DAT binding, D1, and D2 receptor binding at 100 weeks.** Pseudocolor images of receptor binding. Autoradiographs analysed by quantitative densitometry using an MCID-M2 image analysis system. Histograms show the results of densitometric analysis of film im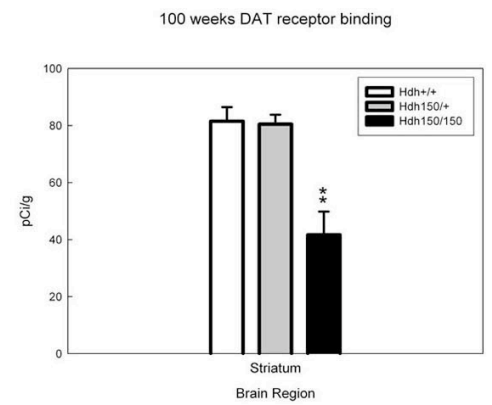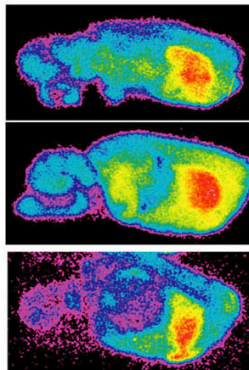ages converted into picomoles of [^{3}H]ligand bound per gram protein. Regions analyzed are the cerebellum (Cer), substantia nigra (SN), globus pallidus (GP), ventral striatum and dorsal striatum (Str), hippocampus (HIP), thalamus (THAL), frontal cortex (FRCT) and whole brain (Whole). * Denotes significant differences between WT and ** denotes significant differences between HET and WT ($p < 0.05$). All values are expressed as mean pCi/g ± SEM).

a. 70 weeks D2 receptor binding

b. 70 weeks D1 receptor binding

Figure III.12 *Hdh*$^{(CAG)150}$ **mice show alterations in D1, and D2 receptor binding as early as 70 weeks.** Homozygous and heterozygous *Hdh*$^{(CAG)150}$ mice exhibit significant reductions of striatal D1 **(a)** and D2 **(b)** receptor binding compared to wild type at 70 weeks. * denotes significance between WT and ** denotes significance between heterozygous and WT ($p < 0.05$). All values are expressed as mean pCi/g ± SEM.

GABA receptor binding (pCi/g) 100 weeks	Hdh +/+ n=4	Hdh 150/+ n=4	Hdh 150/150 n=4
Striatum (Str)	60.0 ± 11.8	60.0 ± 4.6	80.8 ± 9.7
Globus pallidus (GP)	136.6 ± 20.6	109.9 ± 23.4	121.4 ± 19.4
Cerebellum (Cer)	59.1 ± 6.0	57.8 ± 11.7	73.5 ± 10.7
Substantia nigra (SN)	106.8 ± 50.3	118.9 ± 21.9	157.2 ± 4.9
Hippocampus (HIP)	180.8 ± 11.7	170.6 ± 22.5	192.7 ± 18.9
Thalamus (THAL)	55.3 ± 7.3	57.0 ± 8.9	75.8 ± 8.4
Frontal cortex (FRCT)	174.5 ± 18.0	180.8 ± 23.8	196.8 ± 22.7
Whole brain (Whole)	102.6 ± 6.5	98.0 ± 14.5	109.0 ± 12.8

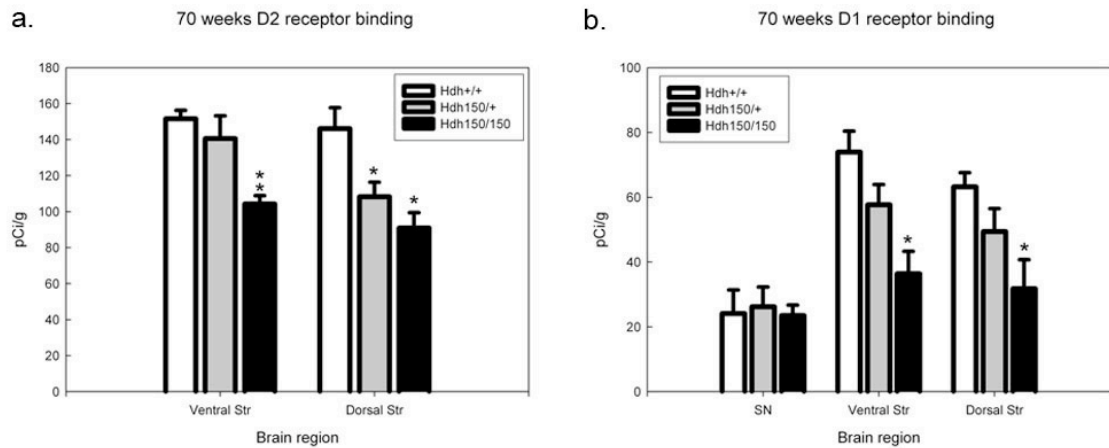| DAT binding (pCi/g) 100 weeks	Hdh +/+ n=4	Hdh 150/+ n=4	Hdh 150/150 n=4
Striatum	81.5 ± 4.9	80.5 ± 3.3	*41.7 ± 8.2

D1 receptor binding (pCi/g) 100 weeks	Hdh +/+ n=4	Hdh 150/+ n=4	Hdh 150/150 n=4
Substantia nigra (SN)	10.2 ± 2.2	8.2 ± 2.1	6.9 ± 0.2
Ventral striatum	36.7 ± 1.7	*18.4 ± 4.8	*5.3 ± 0.6
Dorsal striatum	49.2 ± 5.3	*28.5 ± 6.2	*10.5 ± 1.5

D2 receptor binding (pCi/g) 100 weeks	Hdh +/+ n=4	Hdh 150/+ n=4	Hdh 150/150 n=4
Cerebellum (CBL)	3.3 ± 1.1	6.0 ± 1.5	5.7 ± 0.8
Globus pallidus (GP)	45.8 ± 4.0	41.0 ± 2.1	34.3 ± 5.0
Ventral striatum	101.5 ± 3.6	*83.8 ± 4.3	*69.3 ± 0.5
Dorsal striatum	95.2 ± 2.2	*78.6 ± 3.7	*55.6 ± 2.6

D1 receptor binding (pCi/g) 70 weeks	Hdh +/+ n=4	Hdh 150/+ n=4	Hdh 150/150 n=4
Whole brain (whole)	17.8 ± 2.9	11.5 ± 3.0	9.4 ± 3.0

WT 73.9 ± 6.5 pCi/g [mean ± SEM]; HET 57.7 ± 6.2 pCi/g; HOM 36.4 ± 6.9; dorsal striatum WT 63.2 ± 4.5 pCi/g; HET 49.4 ± 7.1 pCi/g; HOM 31.8 ± 9.0 pCi/g; $p < 0.05$) and no reduction at 40 weeks (data not shown). Heterozygotes showed a lesser effect than homozygotes at 70 weeks with D2 receptor binding showing a greater effect than D1 receptor binding (Fig. III.12a and b and Table III.3; ventral striatum WT 151.6 ± 4.7 pCi/g [mean ± SEM]; HET 140.6 ± 12.6; HOM 104.2 ± 4.7, $p < 0.05$ vs. WT and HOM and HET vs HOM, and for the dorsal striatum WT 146.1 ± 11.7 pCi/g; HET 108.3 ± 8.0 pCi/g; HOM 90.9 ± 8.6 pCi/g, $p < 0.05$ vs. WT), indicating a gene dose effect.

Stereology

Consistent with the receptor binding results, stereological analyses of *Hdh*$^{(CAG)150}$ brains revealed significant reduction in estimated striatal neuron number and striatal volume at 100 weeks of age compared to wild type controls ($p < 0.05$; Fig. III.13a,b,c and Table III.4) (NeuN WT 1,255,311.0 ± 105,371.1 neurons [mean ± SEM]; HET 529,703.7 ± 51,551.75 neurons; HOM 718,355.1 ± 51,257.16; $p < 0.05$ vs. WT). This reflects a mean 42.8% reduction in striatal neuron number in homozygotes and a mean 57.8% reduction in heterozygotes compared to wild type controls. Homozygote striatal neurons were also morphologically distinct. They appeared atrophic and shaped irregularly. Additionally, at 100 weeks of age average striatal volume was significantly reduced for homozygous compared to heterozygous and wild type littermates (Fig. 2.13c

and Table III.4; WT 4.43 x 10^9 ± 2.45x 10^8 μm^3 [mean ± SEM]; HOM 2.64 x 10^9 ± 1.7x 10^8 μm^3; $p < 0.05$ vs. WT). Homozygotes exhibited a mean 40.4% reduction in volume compared to wild type controls. Striatal neuron number and volume were also analyzed at 70 weeks but showed no significant differences in striatal neuron count or volume between groups (data not shown). In summary, $Hdh^{(CAG)150}$ mutant mice showed an approximately 50% loss in striatal perikarya, concomitant with a 40% reduction in striatal volume in homozygotes and this loss occurred between 70 and 100 weeks of age.
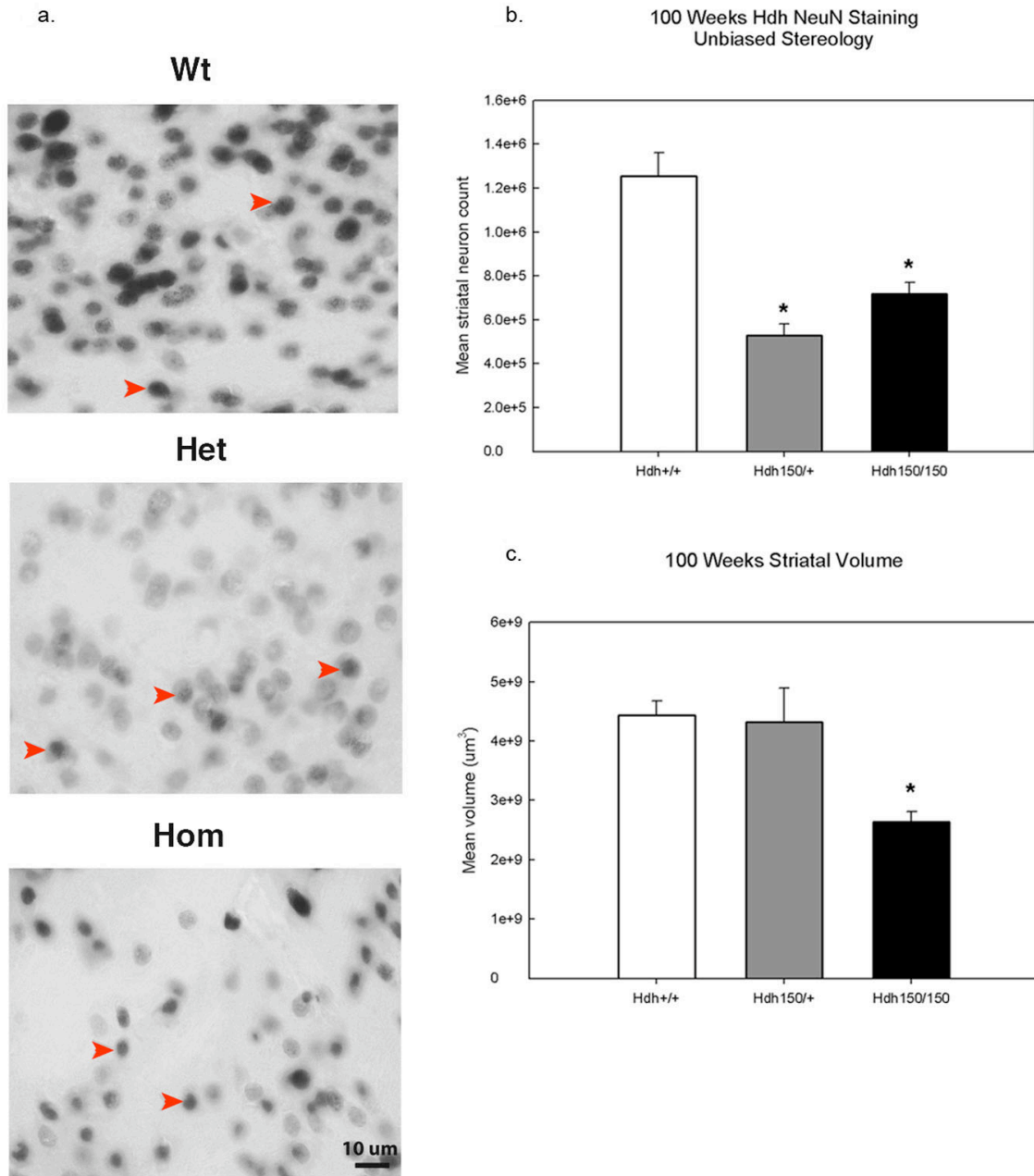
Figure III.13 *Hdh*$^{\text{(CAG)150}}$ mice show reductions in striatal NeuN postitive cells and striatal volume.
(a) Representative images at 100X of NeuN immunoreactive striatal neurons at 100 weeks. Only darkly stained NeuN immunoreactive cells were counted. Arrows indicate typical darkly stained striatal perikarya. Scale bar = 10 μm. **(b)** At 100 weeks, HOM mice show a 42.8% reduction in striatal neuron number and HET mice show a 57.8% reduction compared to WT. **(c)** Striatal volume was also decreased in *Hdh*$^{\text{(CAG)150}}$ mice. Homozygous mice exhibited a 40% reduction in striatal volume at 100 weeks compared to WT (Table 4; n = 4/group, * denotes $p < 0.05$).

Stereology 100 weeks	Hdh +/+ n=3	Hdh 150/+ n=4	Hdh 150/150 n=4
NeuN	$1.3 \times 10^6 \pm 0.11 \times 10^6$ cells	$*5.3 \times 10^5 \pm 0.52 \times 10^5$ cells	$*7.2 \times 10^5 \pm 0.51 \times 10^5$ cells
Striatal volume	$4.43 \times 10^9 \pm 2.45 \times 10^8$ μm^3	$4.3 \times 10^9 \pm 5.63 \times 10^8$ μm^3	$*2.64 \times 10^9 \pm 1.7 \times 10^8$ μm^3

Table III.4 *Hdh*$^{(CAG)150}$ striatal NeuN postitive cells and striatal volume. Striatal NeuN immunoreactive perikarya and striatal volume at 100 weeks. * Denotes $p < 0.5$ compared to WT. All Statistical values are presented as mean ± SEM.

Discussion

We provide a longitudinal characterization of the murine *Hdh*$^{(CAG)150}$ knock-in model of HD. We found that *Hdh*$^{(CAG)150}$ mice exhibit age-dependent weight loss, motor deficits, and striatal pathology that recapitulate important features of HD (Fig. III.14 for a complete timeline of the *Hdh*$^{(CAG)150}$ knock-in line). *Hdh*$^{(CAG)150}$ mice developed motor deficits by 70 weeks. Older *Hdh*$^{(CAG)150}$ mice performed as well as wild type on the rotarod and balance beam during the three days of acclimation, suggesting that motor learning was preserved, and perform normally on the hanging wire test, suggesting absence of muscle weakness or nonspecific debilitation. Behavioral deficits observed in *Hdh*$^{(CAG)150}$ mice parallel decreases in striatal D1 and D2 receptor binding sites at 70 weeks, which precede significant loss of striatal neuron number and volume observed at 100 weeks. The receptor binding data are consistent with imaging studies in human HD

78

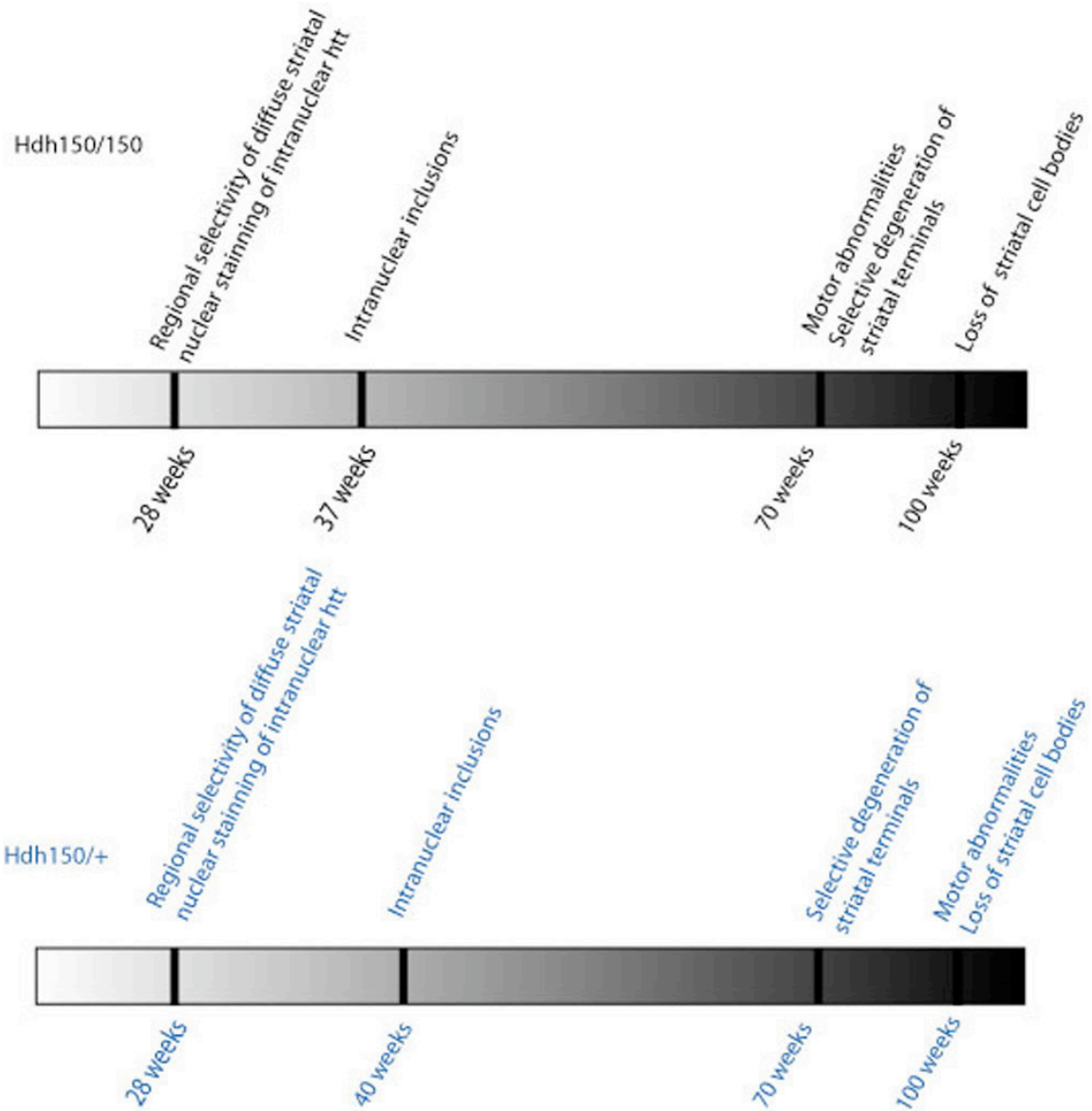**Figure IIII.14 Timeline of the *Hdh*$^{(CAG)150}$ knock-in line.**

patients, as well as other mouse models of HD, which show decreases in D1 and D2 binding (R. A. Weeks et al., 1996; N. Ginovart et al., 1997; J. H. Cha et al., 1998; L. Kennedy et al., 2005; J. C. H. van Oostrom et al., 2005). *Hdh*$^{(CAG)150}$ mice have no overt changes in other brain regions, as shown by GABA$_A$/benzodiazepine binding.

These results are consistent with our earlier description of almost uniquely high expression of striatal NIIs in this line (S. J. Tallaksen-Greene et al., 2005).

We used 6 different methods to evaluate behavior. Accelerating rotarod, balance beam and foot print analysis showed evidence of progressive declines in motor function. The balance beam test was quantitative and sensitive, revealing subtle motor deficits, and demonstrating differences between wild type, heterozygous, and homozygous mice at 100 weeks. Observation of balance beam performance provided complementary qualitative information as mutant mice were not only slower but used a different strategy to cross beams. The rotarod was less predictive of genotype, with similar results for wild type and heterozygous mutant mice. Footprint analysis discriminated wild type and mutants well but quantification of this method is less useful. Measurement of gait features showed significant differences, but these measurements added little to qualitative inspection of footprint patterns. In preliminary experiments, we evaluated younger (< 50 weeks) $Hdh^{(CAG)150}$ mice with a battery of more 'cognitive' tests. No deficiencies were found with the Morris water maze, fear conditioning, or open field tests (McKinney, Murphy, Heng, and Albin, unpublished data).

The original publication of the $Hdh^{(CAG)150}$ mice reported seizures, as well as some behavioral deficits, which occurred earlier than reported here (C. H. Lin et al., 2001). This discrepancy may reflect that our current line has more C57BL/6 background (75-90% C57BL/6; PJD, unpublished data) than the $Hdh^{(CAG)150}$ mice used in the initial study (50-75% C57BL/6). The C57BL/6 background causes reduction in phenotype severity in one other mouse model of HD (J. van Raamsdonk et al., 2007). We never

witnessed seizures in our mice. Absence of epilepsy is congruent with HD and eliminates the possibility that seizures could be the cause of pathologic changes.

Our pathologic analyses suggest that striatal neurons pass through a period of neuronal dysfunction prior to actual neuronal degeneration. At 70 weeks, we found significant declines in both striatal D1 and D2 receptor binding sites in homozygous mutants, and of striatal D2 binding sites in heterozygous mutants, but no change in striatal neuron number or volume. Changes in striatal D1 and D2 receptor binding sites at 70 weeks likely reflect neuronal dysfunction (J. Y. Li et al., 2003; Z. X. Yu et al., 2003) rather than neuronal degeneration. At 100 weeks, D1 and D2 receptor binding sites were diminished significantly in both homozygous and heterozygous mutants, and there was similar loss of neuronal number in both homozygous and heterozygous mutants. Striatal volume measurements, however, were abnormal in 100 week old homozygous mutants only. Since we identified neurons with NeuN immunoreactivity, it is plausible that some striatal neuron perikarya are intact in heterozygous mutants but lost the capacity to express NeuN protein. To maintain consistency across genotypes, only darkly stained striatal neuron perikarya were counted. Given normal striatal volume in 100 week old heterozygotes, this raises the possibility that many striatal neurons in 100 week old heterozygotes are dysfunctional rather than deceased. In homozygous mutants, the concurrent loss of striatal neuron number and volume is strong evidence of striatal neuron degeneration. This result is consistent also with the loss of striatal DAT binding sites in 100 week old homozygous mutants. PET imaging studies indicate that more advanced HD is accompanied by loss of nigrostriatal dopaminergic innervation (L. Backman et al., 1997). The more severe pathologic findings in homozygous mutants is

consistent with data indicating that HD homozygotes and SCA3 homozygotes have more aggressive disease than heterozygotes (A. E. Lang et al., 1994; G. Sobue et al., 1996; F. Squitieri et al., 2003).

Since the great majority of striatal neurons are MSNs, the substantial changes we report in D1/D2 receptor binding, and striatal neuron number in 100 week old homozygotes, imply dysfunction/degeneration of MSNs. The loss of both D1 and D2 binding sites is consistent with dysfunction/degeneration of both major pools of MSNs. The selective loss of striatal D2 binding sites in heterozygous 70 week old mutants is intriguing in view of the probable early loss of MSNs projecting to the lateral globus pallidus in HD (A. Reiner et al., 1988).

Since the identification of *huntingtin*, multiple mouse models have been generated; transgenic chimeric models that express truncated forms of the human mutant HD allele, transgenic chimeric models that express full-length human mutant HD alleles, and knock-in models that express varying length CAG repeat expansions within the murine *huntingtin* homologue. The R6/2 transgenic line, expressing an exon 1 fragment of htt with a range of 148-153 repeats, is widely used because of its aggressive phenotype, and provides clear experimental endpoints (L. Mangiarini et al., 1996; M. A. Hickey et al., 2005; A. J. Morton et al., 2005; E. C. Stack et al., 2005). The aggressive phenotype makes R6/2 very useful for preclinical pharmacology, but it is not an exact genetic or neuropathological analogue of HD. R6/2 mice have widespread NII expression, a high incidence of epilepsy, diabetes, cardiac dysfunction, and neuromuscular junction abnormalities (M. S. Hurlbert et al., 1999; C. A. Meade et al., 2002; R. R. Ribchester et al., 2004; M. J. Mihm et al., 2007). The R6/2 line is a plausible

model of juvenile-onset HD, where the effects of the expanded polyglutamine repeat occurs in the context of a developing brain.

The YAC128 expresses the full-length mutant human HD gene (E. J. Slow et al., 2003), and shows behavioral deficits detectable at 6 months with striatal neuronal loss at 9 and 12 months. YAC 128 mice show a 9% decrease in striatal neuron number at 9 months and a 15% decrease by 12 months. Studies of other striatal neuron markers, such as striatal neuron neurotransmitter receptor binding sites, have not been reported. Results with YAC128 mice may be different from HD, were there is substantial striatal neuron, and probably cortical neuron loss, prior to onset of the overt phenotype (E. H. Aylward et al., 2004; H. D. Rosas et al., 2004b).

Unlike transgenic models of HD, knock-in models provide expression of mutant *huntingtin* in an appropriate genomic and protein context. The $Hdh^{(CAG)150}$ knock-in model is unique from other knock-in models in that it is non-chimeric, expressing only a polyglutamine expansion in the murine Hdh gene and this change is not accompanied by foreign DNA sequences or selectable markers. Behavioral and pathologic data has been published on several knock-in models but none thus far have provided extensive longitudinal behavioral examination and correlative neuropathologic data. A striking feature of the $Hdh^{(CAG)150}$ knock-in model is that the high frequency expression of NIIs is almost unique to the striatum and that neuropil aggregates are expressed probably in striatal projection neuron terminals, even in mice of advanced age (S. J. Tallaksen-Greene et al., 2005). These findings are consistent with the recent reports of the chimeric exon1 140 CAG knock-in mouse model of HD exhibiting late and progressive behavioral

83

and neuropathological phenotype (L. B. Menalled et al., 2003). Other previous knock-in models have reported mild motor behavioral deficits and neurodegeneration.

The relatively specific expression of NIIs within striatal neurons, selective decrease in striatal neurotransmitter receptor binding sites, diminished striatal neuron number, and late onset of behavioral abnormalities observed in $Hdh^{(CAG)150}$ mice recapitulate key features of HD. A recent striatal gene expression study also indicates significant similarity of $Hdh^{(CAG)150}$ mice to HD (A. Kuhn et al., 2007). Because of its milder phenotype and late onset of behavioral abnormalities, the $Hdh^{(CAG)150}$ knock-in line has not widely been used as a model for preclinical pharmacological evaluation. The expedience of an aggressive phenotype must be balanced against the possibility that the phenotype of other mouse models may be driven by molecular processes that do not mimic HD. The $Hdh^{(CAG)150}$ model will be most useful for investigating the pathogenesis of neurodegeneration in HD. We have shown a prolonged period of neuronal dysfunction prior to neuronal death in this line, which will allow examination of the early events in the pathogenesis of HD.

Acknowledgements

Chapter IV

In Vivo Evidence for NMDA Receptor Mediated Excitotoxicity in a Murine Genetic Model of Huntington Disease

Abstract

N-methyl-D-aspartate receptor (NMDAR) mediated excitotoxicity is implicated as a proximate cause of neurodegeneration in Huntington Disease (HD), however, this hypothesis has not been tested rigorously *in vivo*. NMDAR NR2B-subunits are the predominant NR2 subunit expressed by the striatal medium spiny neurons that degenerate in HD. To test this hypothesis, we crossed a well validated murine genetic model of HD - Hdh$^{(CAG)150}$ - with a transgenic line overexpressing NMDAR NR2B-subunits. In the resulting double mutant line, we show exacerbation of selective striatal neuron degeneration. These results provide the first direct *in vivo* evidence of NR2B-NMDAR mediated excitotoxicity in the context of HD. Our results are consistent with prior suggestions that direct and/or indirect interactions of mutant huntingtin with NMDARs are a proximate cause of neurodegeneration in HD.

Introduction

Huntington's disease (HD) is a dominantly inherited neurodegenerative disorder caused by expanded CAG repeat/polyglutamine repeats within the huntingtin locus

resulting in a pathogenic huntingtin protein (htt). Early and prominent neurodegeneration of striatal GABAergic medium spiny neurons (MSNs) is a pathologic hallmark of HD. Clinical manifestations include progressive cognitive decline, psychiatric disturbances, and involuntary movements. HD is incurable and death follows inexorably approximately 15 – 20 years after diagnosis. The striatum is the primary afferent structure of the basal ganglia, composed predominantly of GABAergic MSNs (R. L. Albin et al., 1989; A. M. Graybiel, 1990) and is involved in numerous important functions including habit formation and evaluation of rewarded behaviors. Although the molecular and cellular mechanisms underlying the selective degeneration of MSNs in HD are not yet understood, convergent evidence from a variety of sources supports a role for N-methyl-D-aspartate receptor (NMDAR) mediated excitotoxicity (J. T. Coyle and R. Schwarcz, 1976; E. G. McGeer and P. L. McGeer, 1976; R. Schwarcz et al., 1983; M. F. Beal et al., 1986; M. M. Zeron et al., 2001).

The striatum receives an abundance of glutamatergic corticostriatal and thalamostriatal inputs, and MSNs are endowed heavily with NMDARs and other glutamate receptors (A. M. Graybiel, 1990). Coyle and Schwarcz and the McGeers (McGeer and McGeer, 1976) developed the first chemical model of HD with demonstrations that acute intrastriatal administration of the glutamate agonist kainic acid in rodents produced neurodegeneration with features similar to HD (J. T. Coyle and R. Schwarcz, 1976; E. G. McGeer and P. L. McGeer, 1976). Considerable later work indicated that acute striatal lesions with NMDAR selective agonists reproduced more features of striatal pathology in HD (M. F. Beal et al., 1986; P. Hantraye et al., 1990; M. F. Beal, 1992a; T. J. Bazzett et al., 1993; R. J. Ferrante et al., 1993). This is true for both

NMDAR agonists and metabolic inhibitors whose indirect effects facilitate NMDAR activation (E. Brouillet et al., 1995; J. G. Greene and J. T. Greenamyre, 1995). While the correlation between the effects of acutely administered NMDAR agonists and HD striatal pathology is impressive, the NMDAR excitotoxicity hypothesis of striatal degeneration in HD has not been previously tested rigorously *in vivo*.

NMDARs are hetero-multimeric ionotropic receptors that mediate extracellular calcium entry and consist of NR1 subunits and NR2 (A-D) subunits (R. Dingledine et al., 1999; L. M. Hawkins et al., 1999). Comparative studies confirm that the pharmacological and functional properties of the NMDA receptor depend heavily on the NR2 subunits (S. Cull-Candy et al., 2001; L. Li et al., 2003; J. M. Loftis and A. Janowsky, 2003). In some model systems, NR2B-containing NMDARs have a selective tendency to promote pro-death signaling opposed to the pro-survival promoting pathways of the NR2A-containing NMDARs (G. E. Hardingham and H. Bading, 2002; G. E. Hardingham et al., 2002; G. E. Hardingham and H. Bading, 2003; Y. Liu et al., 2007). NR2B subunit containing NMDARs are highly expressed by MSNs and predominate over other subunit composition, such as the NR1/NR2A, in the striatum (H. Monyer et al., 1992). Previous *in vitro* studies indicate sensitization of NR2B function by mutant htt (N. Chen et al., 1999; M. M. Zeron et al., 2001).

To determine whether striatal pathology and behavioral deficits of HD are caused by NMDAR-mediated excitotoxic injury *in vivo*, we created a modified murine model of excitotoxic injury by crossing a well validated murine genetic model of HD (M.Y. Heng et al., 2007) to a transgenic mouse overexpressing the NR2B-subunit of the NMDAR (Y.

P. Tang et al., 1999). In this double mutant mouse line, we demonstrate exacerbation of striatal pathology characteristic of HD.

Materials and Methods

Hdh150/+; NR2B$^{Tg/WT}$ double mutant mice

Interbreeding the *Hdh*$^{(CAG)150}$ and *NR2B* transgenic lines results in four groups of mice, Hdh+/+; NR2B$^{WT/WT}$ (wild type huntingtin; no transgene), Hdh+/+; NR2B$^{Tg/WT}$ (wild-type huntingtin; one copy of the NR2B transgene), Hdh150/+; NR2B$^{WT/WT}$ (one copy of mutant huntingtin; no transgene), Hdh150/+; NR2B$^{Tg/WT}$ (one copy of mutant huntingtin; one copy of the NR2B transgene).

All four groups were generated from the cross of the *Hdh*$^{(CAG)150}$ mice murine model of HD maintained on a mixed genetic background 129/Ola and C57BL/J6 C. H. Lin et al., 2001) expressing 75-90% C57BL/6; (Peter J. Detloff; unpublished data) with the *NR2B* transgenic mouse maintained on a genetic CBA/C57BL/6 F1 hybrid background (Y. P. Tang et al., 1999) resulting in the F1 mixed background 129/Ola and CBA/C57BL/J6. Both male and female mice and their wild type littermates (WT) were used. All animals were housed in cages grouped by gender and provided with food and water ad libitum. Animals were housed in a Specific Pathogenic Free conditions with a 12-h light/dark cycle maintained at 23°C. All procedures were conducted in strict compliance with the Guide for the Care and Use of Laboratory Animals as adopted by the NIH and approved by the Committee on Use and Care of Animals (UCUCA), University of Michigan, and the Veterinary Medical Unit (VMU) at the Ann Arbor Veterans Affairs Medical Center.

Genotyping

All mice studied were genotyped for both the *Hdh* allele and the *NR2B* transgene. The *Hdh* allele genotyping protocol is previously published in M. Y. Heng et al., 2007. In brief, DNA was extracted from a 1 cm tail biopsy using a DNeasy Tissue Kit (Qiagen Inc. Valencia, CA, USA). Polymerase chain reaction (PCR) amplification was performed using a Taq polymerase kit (Invitrogen, Carlsbad, CA) and primers (purchased from Invitrogen, Carlsbad, CA) designed to flank the 150 CAG repeat in the Hdh locus

Forward primer: CCCATTCATTGCCTTGCTGCTAGG,

Reverse primer: CCTCTGGACAGGGAACAGTGTTGG.

PCR conditions were as follows: 94°C for 5 min followed by 29 cycles at 94°C for 30 sec, 63°C for 30 sec, 72°C for 3 min and a final extension at 72° for 5 min. DNA products were separated by standard 1.5% agarose gel electrophoresis and were visualized with ethidium bromide using a Gel Doc system (Bio-Rad Laboratories, Hercules, CA). Expected bands: 379 bp for wild type band, 829 bp for mutant band. To confirm reliability of genotyping over time, periodic CAG sizing was performed outside our laboratory (Laragen Inc., Los Angeles, CA) to confirm consistency of the CAG repeat number, which ranged from 145-150 CAG repeats. For the *NR2B* transgene, genotyping protocol is taken from (Y. P. Tang et al., 1999). Briefly, genotypes were analyzed by extracting genomic DNA from tail biopsy. The 5' and 3' primers for detecting *NR2B* transgene SV40 polyA sequence (505 bp):

5'-AGAGGATCTTTGTGAAGGAAC-3' and 5'-AAGTAAAACCTCTACAAATG-3', respectively. Mouse tail DNAs (about 1μg) were amplified 30 cycles (1 min, 94ºC; 45 sec, 55 ºC; 1 min, 72 ºC) on a thermal cycler. For zygosity testing, *NR2B* transgene

detection was performed outside our laboratory (Charles River Laboratories Inc., Wilmington, MA).

Euthanasia

All animals were euthanized according to national guidelines. Euthanasia was carried out by decapitation.This method was approved by UCUCA and the VMU.

Behavioral Examination

All four cohorts of mice (Hdh+/+; NR2B$^{WT/WT}$; Hdh+/+; NR2B$^{Tg/WT}$; Hdh150/+; NR2B$^{WT/WT}$; Hdh150/+; NR2B$^{Tg/WT}$) were used for each time point (20, 40, 50, 70, and 100 weeks. Time points are selected based on previously published longitudinal evaluation of the *Hdh*$^{(CAG)150}$ knock-in mice (M. Y. Heng et al., 2007). In that study, behavioral and striatal pathology commenced around 70 weeks of age. All behavioral evaluations were videotaped and performed with the examiner blind to genotype. Behavioral evaluations proceeded on Wednesdays and ended on Fridays of the following week, a total of eight days of behavioral trials with the first three days for acclimation and a break on Saturdays and Sundays. All behavioral trials were performed in the mornings between the hours of 9 am and noon. Weights, footprint analysis, and activity cage measurements were taken only on the last day of trials. Brains were collected on the last day of testing.

The six behavioral assays used are described in detail below. They are: 1) the accelerating rotarod, 2) the hanging wire test, 3) the tail suspension test, 4) activity monitoring, 5) footprint analysis, and 6) balance beam tests previously published in (M. Y. Heng et al., 2007.

Hanging Wire

A standard wire cage lid is used with masking tape placed around the perimeter of the lid to prevent animals from escaping. After an animal is placed on the lid, the lid is shaken gently to induce a firm grip and the lid inverted. The lid is held horizontally 20 cm above the cage litter. Latency to fall is recorded for up to 2 minutes. As described by Crawley, normal mice are able to hang upside down for several minutes (J. N. Crawley, 2000).

Tail Suspension

Animals are suspended by their tail for a total of 1 minute and the presence of hind leg clasping or hind leg folding into the abdomen greater than 2 seconds is scored as "clasping". Seizures were also noted if any occurred. An "escape" was scored during a trial if a mouse crawled up onto the testers hand within the 60 second trial. To escape an animal must grab its tail while suspended upside down and then crawl up and onto the examiner's hand.

Accelerating Rotarod and Balance Beam

Rotarod: The accelerating rotarod model number 7650 from Ugo Basile was used. Mice are habituated for 3 consecutive daily trials followed by two days of rest and tested once a day for five consecutive daily trials on an accelerating protocol (4-40 rpm over 5 min). The latency to fall is measured in each trial up to 5 minutes.

Balance beam: Motor coordination, balance, and hind-limb placement were evaluated by assessing the ability of mice to traverse two types of balance beams to reach an enclosed safety platform (R. J. Carter et al., 1999). Each mouse was tested for its

ability to traverse two different styles of 41 cm long scored Plexiglass beams. One was cylindrical 11mm and diameter and the other square and 5mm wide. Beams were serrated for grip and placed horizontally 50 cm above a table. A bright light illuminated the start platform, and a darkened enclosed 8000 cm^3 escape box (20 cm x 20 cm x 20 cm) was situated at the end of the beam (PlasticTech, MI). Time to traverse each beam were recorded for each trial with a 20 second maximum cut-off, and falls were scored as 20 seconds. The number of foot slips and whether a mouse dragged itself across the beam on its abdomen ("hind-leg drag") was also recorded.

Analyses of rotarod and balance beam results: The first three trials were used to assess learning and the last five were used to measure motor performance. In normal animals, the largest improvement in rotarod latency to fall times and time to cross the balance beam are observed in the first three trials with a ceiling by the fourth trial. Trials 4-8 are analyzed separately for motor performance after the animals have been trained in the first three trials.

Footprint Analysis

Fore and hind paws of the animals were painted with different colors of non-toxic paint, and the animals are allowed to walk across a 83 cm long unroofed corridor (7 cm wide by 11 cm tall) lined with paper into an enclosed escape area (36 cm long x 7 cm wide x 11 cm tall).

Automated Activity Cages

Activity cages with photo beam sensors (Advanced Concepts, Ann Arbor, MI) were used to measure general motor function, spontaneous activity and movement over a two-hour

test session. Four photo beam sensors are located at each end of the activity cage, 2 cm

apart, 2.5 cm high, and 4 cm away from the edge. The pairs of beams are situated 15 cm

apart and a normal housing cage is placed into the activity apparatus to contain the mouse

for the testing session. Beam breaks are automatically scored when any of the four

beams are broken. Animals tested over a 2 hour period.

Brain Harvesting and Storage

Brains were extracted immediately after decapitation and divided in the sagittal

plane. One hemisphere was coated with M-1 embedding matrix (Shandon, Pittsburgh,

PA), frozen in crushed dry ice, wrapped in aluminum foil, and stored at -80 C. The other

hemisphere was immersion fixed in 4% paraformaldehyde for 24 hrs, cryoprotected in

20% sucrose in 0.1M phosphate buffer for an additional 24 hrs 4° C, and then frozen by

placing the brains on boats made from aluminum foil that were floating on isopentane

(cooled on dry ice at least one-half hour). This hemisphere was also stored at -80°C until

time of sectioning. Fixed hemispheres were used for stereological analysis while the

corresponding fresh frozen hemispheres were used for autoradiographic receptor binding

analyses.

Receptor Autoradiography

All studies were performed on coded samples with genotype information

removed. Autoradiographic studies were performed as described previously (Tallaksen-

Greene et al., 2003). Fresh frozen brains were serially cut on a cryostat at 15μ sections at

−12°C and thaw-mounted onto gelatin-coated slides and stored at -80°C until use.

Assays for D1 and D2 dopamine receptors were performed as follows: slides with

sections were incubated in 25 mM Tris, 100mM NaCl, 1 mM $MgCl_2$, 0.001% ascorbic acid, 1 μM pargyline, pH 7.2 with radioactive ligand 0.55 nM [³H]SCH23390 (specific activity 89 Ci/mmol) for D1 and 0.75 nM [³H]Spiperone (specific activity 96 Ci/mmol) with 100 nM mianserin for D2 for 2.5 hrs at room temperature. Nonspecific binding was determined in the presence of 1 μM cis-flupenthixol for D1and 50 μM dopamine for D2, respectively. Following incubation, slides were subjected to two cold washes at 4°C and then one 10 min. room temperature wash with incubation buffer lacking radioactive ligand, followed by a quick rinse in double distilled water before drying under a stream of warm air. For dopamine transporters (DAT), slides were pre-washed in a 4°C solution containing 50 mM Tris-HCl, 5mM KCl, 300 mM NaCl, pH 7.9 for 5 min, followed by a 1 hr incubation at 4°C in the same buffer with the addition of 10 nM [³H]Mazindol (specific activity 23.1 Ci/mmol) and 300 nM desipramine. Blank conditions contained 100 μM nomifensine. Slides were subjected to a final wash under the same conditions as the pre-wash for 3 min. For GABA-A/benzodiazepine receptors, slides were prewashed in 50 mM Tris-citrate buffer, pH 7.2 at 4°C for 30 min, air dried and incubated in 50 mM Tris-citrate buffer, pH 7.2 with 5 nM [³H]flunitrazepam (specific activity 85 Ci/mmol) for 1 hr at 4°C. Nonspecific binding was determined in ligand buffer with 2 μM clonazepam. Slides were subjected to one rapid rinse and then two 5 minute washes in 4°C 50 mM Tris-citrate buffer, pH 7.2 before drying under warm air.

D1 and D2 [³H]ligands were purchased from Amersham (United Kingdom). [³H]Mazindol and [³H]flunitrazepam were purchased from DUPONT Co. Biotechnology Systems (Wilmington, DE).

For receptor autoradiography, three slides per subject were used for each radioligand assay, two slides for total binding and the third to define nonspecific labeling with a minimum of two consecutive sections taken at fixed intervals (15 μm) mounted per slide. Slides and ^{14}C standards are arrayed in a standard X-ray cassette, and an autoradiogram is generated by direct apposition of the tissue to the emulsion side of the tritium imaging plate (BAS-TR2025; Fuji Photo Film, Japan) for a period of 19 to 22 hrs.

Autoradiograms were analysed by quantitative densitometry using an MCID-M2 image analysis system (Interfocus Ltd., England). Anatomic locations of selected regions of interest were determined using an approach designed (T. J. Morrow et al., 1998). Briefly, for each brain section, we overlaid a matching transparent stereotaxic template, adapted from the mouse brain atlas (G. Paxinos and K. B. J. Franklin, 2001), on the digitized brain images displayed on the video monitor and aligned the images using prominent anatomical landmarks. Optical density (OD) measurements were taken bilaterally in a minimum of six brain sections and measurements were made in each section in which the structure was visible, sampling as large an area as possible. Tissue ^{14}C concentrations were determined by comparison of ODs with a calibration curve obtained from co-expressed standards. Specific binding was determined by subtracting nonspecific binding from the total binding.

Immunohistochemistry

Hemispheres previously fixed in 4% paraformaldehyde as described above were serially sectioned at 40 μm sagitally throughout the entire hemisphere. Every fourth section was used for stereological analysis. Free floating sections were processed with either primary antisera against the neuronal antigen NeuN (Chemicon Int., Temecula,

95

CA, USA; 1:100 dilution) or huntingtin (N-18) antibody (Santa Cruz Biotechnology, Inc.,

Santa Cruz, CA, USA; 1:250 dilution).   Sections were processed without primary

antibody to assess background staining.   No staining was visualized in these control

sections.   Detection of immunoreactivity was performed using the Vectastain Elite kit

(Vector laboratories, Burlingame, CA, USA) and diaminobenzidine (DAB) substrate was

used as the chromogen according to the manufacturer's protocol.   Sections were then

mounted on gelatin-coated slides and air dried following dehydration with graded

alcohols and xylene.   Coverslips were affixed with Permount.

Stereology

Unbiased stereological counts of striatal neurons were obtained from the striatum

of animals at 70 and 100 weeks of age using the StereoInvestigator software (Micro-

Brightfield, Colchester, VT).   The optical fractionator method was used to generate an

estimate of neuronal number with only darkly stained NeuN immunoreactive cells

counted in an unbiased selection of serial sections in a defined volume of the striatum.

Striatal borders were delineated by on NeuN stained section by reference to a mouse

brain atlas (G. Paxinos and K. B. J. Franklin, 2001).   The striatum was defined to

encompass both the dorsal and ventral striatum.   Striatal volume was reconstructed by the

StereoInvestigator software using the Cavalieri principle.   Serially cut sagittal tissue

sections (every fourth section) were analyzed for one entire hemisphere of animals in

each genotype cohort (n=4/group).

Statistical Analyses

All studies were performed blind to genotype. Comparisons of different groups (between genotypes) was performed on receptor binding, stereology, and weight data using one-way analysis of variance (ANOVA) with posthoc comparisons being made using Tukey HSD when $p < 0.05$. Repeated measures ANOVA was performed for each behavioral test to determine if there was an effect from genotypes or from repeated training. If there was no change after repeated training, the trials were collapsed and a one-factor ANOVA was performed. A critical $p < 0.05$ was used for statistical significance in all analyses. Huynh-Feldt adjustment was used in correcting for violation of sphericity when necessary to adjust non-uniform variance across days or groups. SPSS (SPSS Inc.) statistical software package was used.

Results

Hdh150/+; NR2B$^{Tg/WT}$ Double Mutant Mice Exhibit Striatal Neuron Loss and Decreased Striatal DA Receptors

At 100 weeks of age, Hdh150/+; NR2B$^{Tg/WT}$ double mutant mice displayed atrophic and irregularly shaped striatal neurons compared to controls (Hdh+/+; NR2B$^{WT/WT}$, Hdh+/+; NR2B$^{Tg/WT}$ and Hdh150/+; NR2B$^{WT/WT}$; Fig. IV.1a-d). The Hdh150/+; NR2B$^{Tg/WT}$ double mutants exhibited marked decreases in striatal volume and neuron number with a mean 51% decrease in striatal volume, and a 36% mean decrease in striatal neuron number compared to all three control groups (Hdh+/+; NR2B$^{WT/WT}$, Hdh+/+; NR2B$^{Tg/WT}$ and Hdh150/+; NR2B$^{WT/WT}$; Fig. IVe and f). At 70 weeks, there was no decrease in striatal neuron number or volume.
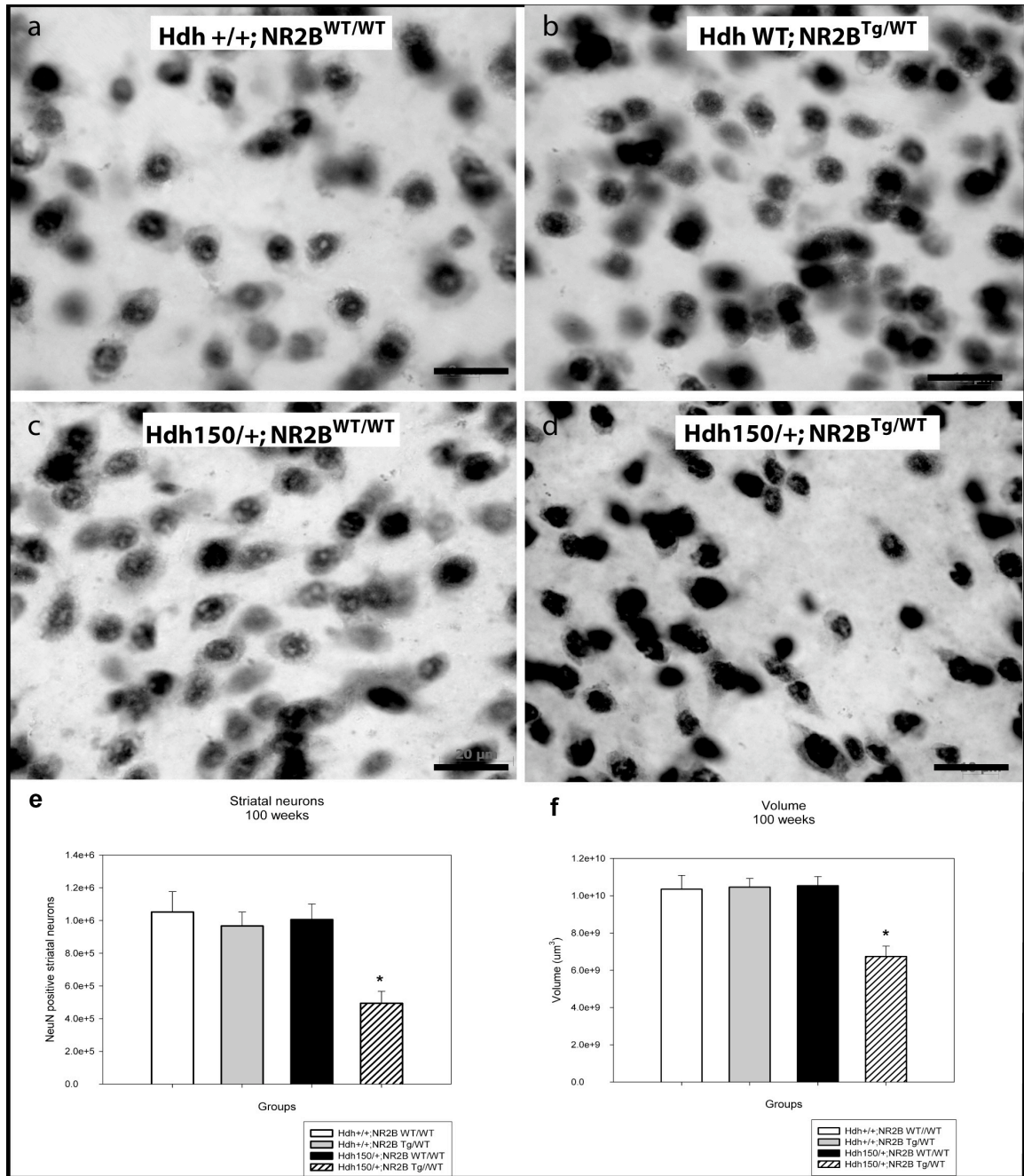
Figure IV.1 Hdh150/+;NR2B$^{Tg/WT}$ double mutant mice exhibit striatal neuron number and volume loss at 100 weeks. (a-d) Hdh150/+;NR2B$^{Tg/WT}$ double mutant mice display atrophic and irregular shaped NeuN postitve stained striatal neurons compared to control groups (Hdh+/+; NR2B$^{WT/WT}$, Hdh+/+; NR2B$^{Tg/WT}$, and Hdh150/+ NR2B$^{WT/WT}$). **(e)** Hdh150/+;NR2B$^{Tg/WT}$ exhibit a 51% loss in striatal neuron number and a 36% reduction in striatal volume **(f)** compared to all three littermate control groups (Hdh+/+; NR2B$^{WT/WT}$, Hdh+/+; NR2B$^{Tg/WT}$, and Hdh150/+ NR2B$^{WT/WT}$). *$p < 0.05$. Values are expressed as mean $\pm$ SEM. N = 4 animals/group

Striatal pathology observed in the double mutant mice was confirmed by loss of striatal dopamine D1 and D2 receptors (Fig. IV.2 and Table IV.1). The Hdh150/+; NR2B$^{Tg/WT}$ double mutant mice exhibited an average 37% reduction of D1 receptor binding in the substantia nigra (SN) compared to both the Hdh+/+; NR2B$^{WT/WT}$ and Hdh+/+; NR2B$^{Tg/WT}$ wild type mice at 100 weeks. The Hdh150/+; NR2B$^{Tg/WT}$ double mutant mice showed a 48% decrease in the ventral striatum and a 43% reduction in the dorsal striatum compared to both Hdh+/+; NR2B$^{WT/WT}$ and Hdh+/+; NR2B$^{Tg/WT}$ wild type mice at 100 weeks (Fig. IV.2a and Table IV.1). Although not significantly different, Hdh150/+; NR2B$^{WT/WT}$ mice exhibit a decrease of D1 receptor binding intermediate between the Hdh+/+; NR2B$^{WT/WT}$, Hdh+/+; NR2B$^{Tg/WT}$ wild type controls and Hdh150/+; NR2B$^{Tg/WT}$ double mutant mice. Hdh150/+; NR2B$^{Tg/WT}$ double mutants exhibited a 44% reduction in the ventral striatum and a 53% reduction in the dorsal striatum of D2 receptor binding at 100 weeks compared to Hdh+/+; NR2B$^{WT/WT}$ wild type controls, and Hdh150/+; NR2B$^{WT/WT}$ again displayed an intermediate effect. Decreased D1 and D2 receptor binding was observed in double mutants at 70 weeks (Fig. IV.2b and Table IV.1). The Hdh150/+; NR2B$^{Tg/WT}$ double mutant mice and Hdh150/+; NR2B$^{WT/WT}$ mice together displayed an average reduction of 29% and 31% of D1 receptor binding in the ventral and dorsal striatum, respectively and similarly for D2 receptor binding with a 30% and 29% average reduction for D2 receptor binding (Fig. IV.2c). GABA$_A$/benzodiazepine receptor binding was used to survey multiple extrastriatal brain regions and revealed no differences between groups at 100 weeks, indicating little or no neuronal loss in these brain regions (Fig. IV.2a). Striatal dopamine transporters were additionally measured and were normal in all groups (data not shown).

a

Hdh+/+; NR2B^WT/WT

Hdh+/+; NR2B^Tg/WT

Hdh150/+; NR2B^WT/WT

Hdh150/+; NR2B^Tg/WT

D1 receptor binding
100 weeks

Hdh+/+; NR2B^WT/WT

Hdh+/+; NR2B^Tg/WT

Hdh150/+; NR2B^WT/WT

Hdh150/+; NR2B^Tg/WT

D2 receptor binding
100 weeks

Hdh+/+; NR2B^WT/WT

Hdh+/+; NR2B^Tg/WT

Hdh150/+; NR2B^WT/WT

Hdh150/+; NR2B^Tg/WT

GABA_A receptor binding
100 weeks

b   D1 receptor binding
70 weeks
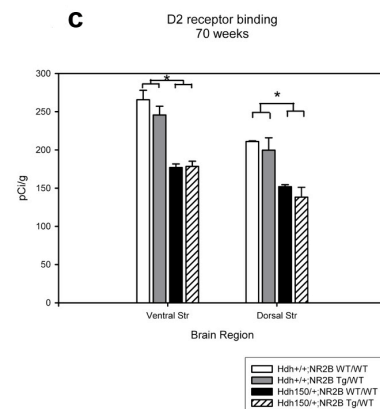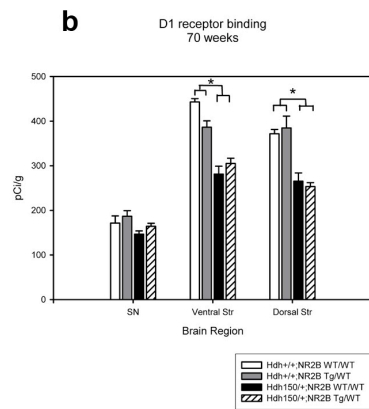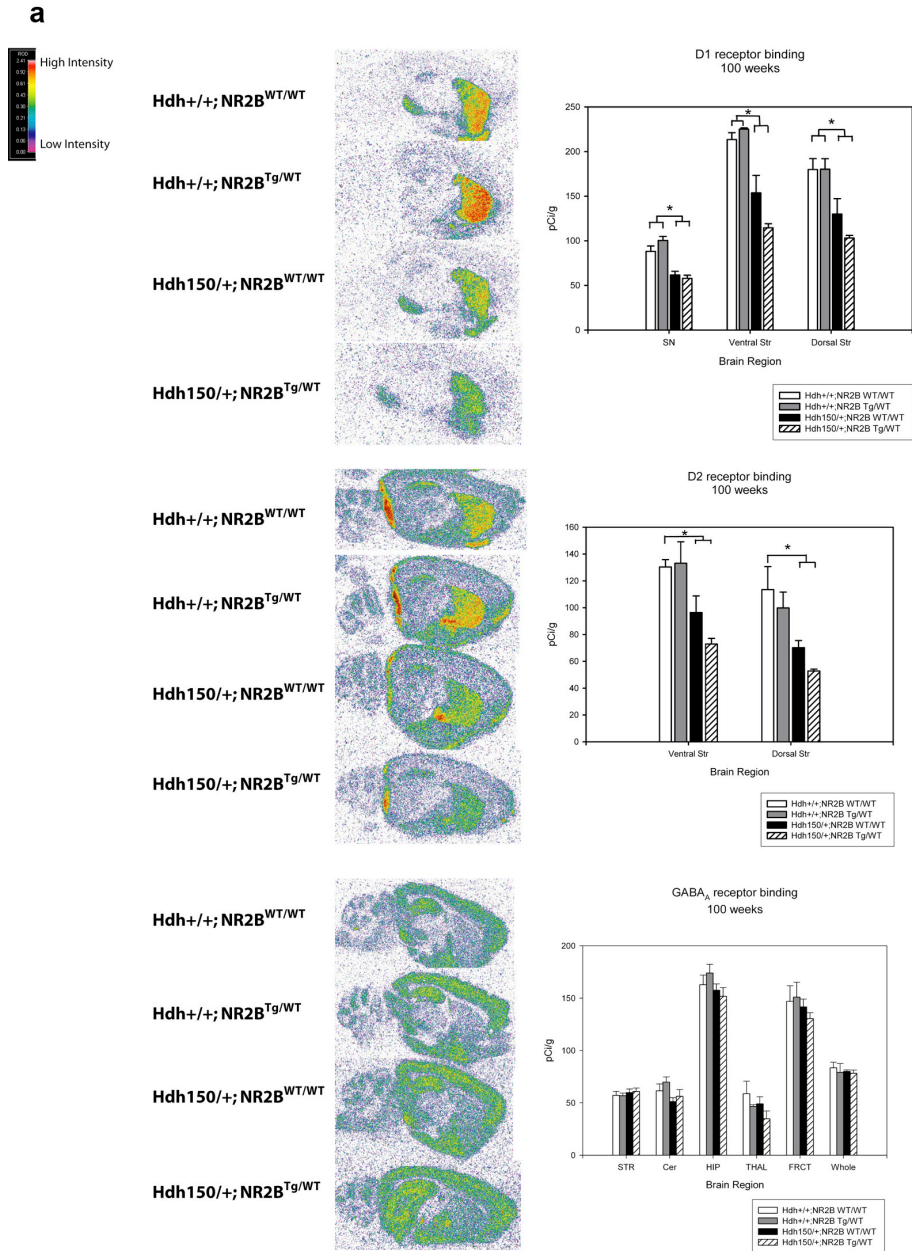
c   D2 receptor binding
70 weeks

Figure IV.2 Hdh150/+;NR2B$^{Tg/WT}$ double mutant mice exhibit reductions in striatal D1 and D2 receptor binding while Hdh150/+;NR2B$^{WT/WT}$ show an intermediate reduction at 100 weeks. Pseudocolor images of receptor binding. Autoradiographs were analyzed by quantitative densitometry using an MCID-M2 image analysis system. Histograms show results of densitometric analysis of film images converted to pCi of ^{3}H-ligand bound per gram of protein. Regions analyzed are the substantia nigra (SN), ventral striatum (ventral Str), dorsal striatum (dorsal Str), whole striatum (STR), cerebellum (Cer), hippocampus (HIP), thalamus (THAL), frontal cortex (FRCT), and whole brain (Whole). (a) D1, D2, and GABA$_A$ receptor binding at 100 weeks (b-c) D1 and D2 receptor binding at 70 weeks. * p < 0.05. Values are expressed as mean pCi/g $\pm$ SEM.

Hdh150/+; NR2B$^{Tg/WT}$ Double Mutant Mice Exhibit No Change in Distribution of NIIs

We determined the distribution of huntingtin aggregates in brain. Neuronal intranuclear inclusions (NIIs) saturated striatal neurons in double mutant and Hdh150/+; NR2B$^{WT/WT}$ mice at 100 weeks (Fig. IV.3). There were only sparse NIIs in other brain regions. This result is consistent with selective striatal pathology in both double mutant and Hdh150/+; NR2B$^{WT/WT}$ mice and is consistent with our prior observations in the Hdh$^{(CAG)150}$ line. With QRT-PCR, we determined that the presence of the NR2B transgene did not affect huntingtin mRNA expression and that the presence of Hdh$^{(CAG)150}$ mutation did not alter transgene mRNA levels (data not shown).

Hdh150/+; NR2B$^{Tg/WT}$ Double Mutant Mice Exhibit Weight Loss and Motor Deficits

Hdh150/+; NR2B$^{Tg/WT}$ double mutant mice exhibited an 18.4% decrease in body weight compared to other groups [Fig. IV.4; Hdh150/+; NR2B$^{Tg/WT}$, 29.4 ± 3.1 g (mean ± SEM); Hdh+/+; NR2B$^{WT/WT}$, 35.7 ± 1.4 g; Hdh+/+; NR2B$^{Tg/WT}$, 36.7 ± 4.5 g; Hdh150/+; NR2B$^{WT/WT}$, 35.6 ± 3.9 g; p < 0.05].

D1 receptor binding (pCi/g) 100 weeks	Hdh+/+; NR2BWT/WT	Hdh+/+; NR2BTg/WT	Hdh150/+; NR2BWT/WT	Hdh150/+; NR2BTg/WT
SN	88.1 +/- 6.1	100.4 +/- 4.6	61.7 +/- 4.1 *	57.9 +/- 3.5 *
Vent Str	213.4 +/- 7.7	225.1 +/- 1.5	153.7 +/- 19.6 *	114.6 +/- 4.5 *
Dors Str	179.8 +/- 12.2	180.2 +/- 11.8	129.9 +/- 17.3 *	103.1 +/- 3.0 *

D2 receptor binding (pCi/g) 100 weeks	Hdh+/+; NR2BWT/WT	Hdh+/+; NR2BTg/WT	Hdh150/+; NR2BWT/WT	Hdh150/+; NR2BTg/WT
Vent Str	130.3 +/- 5.5	133.2 +/- 15.9	96.4 +/- 12.4 *	72.9 +/- 4.2 *
Dors Str	113.5 +/- 17.1	99.8 +/- 11.8	70.2 +/- 5.3 *	52.8 +/- 1.4 *

GABA receptor binding (pCi/g) 100 weeks	Hdh+/+; NR2BWT/WT	Hdh+/+; NR2BTg/WT	Hdh150/+; NR2BWT/WT	Hdh150/+; NR2BTg/WT
STR	57.1 +/- 4.0	56.8 +/- 2.5	60.0 +/- 3.4	60.9 +/- 3.2
CER	61.5 +/- 6.5	70.0 +/- 4.9	51.2 +/- 3.7	56.2 +/- 6.5
HIP	162.7 +/-9.3	173.9 +/- 8.3	157.5 +/- 6.1	151.8 +/- 8.1
THAL	58.7 +/- 11.9	46.6 +/- 1.6	49.0 +/- 6.8	34.8 +/- 7.5
FRCT	146.9 +/- 14.9	150.9 +/- 14.2	141.6 +/- 7.5	130.4 +/- 5.8
WHOLE	83.4 +/- 5.3	79.1 +/- 8.4	79.5 +/- 1.5	78.2 +/- 3.1

D1 receptor binding (pCi/g) 70 weeks	Hdh+/+; NR2BWT/WT	Hdh+/+; NR2BTg/WT	Hdh150/+; NR2BWT/WT	Hdh150/+; NR2BTg/WT
SN	171.4 +/- 16.1	186.8 +/- 12.5	146.6 +/- 7.3	164.4 +/- 6.6
Vent Str	443.0 +/- 7.5	386.4 +/- 14.2	281.3 +/- 17.7 *	305.1 +/- 11.8 *
Dors Str	371.6 +/- 9.7	384.7 +/- 26.4	265.4 +/- 18.4 *	253.2 +/- 8.7 *

D2 receptor binding (pCi/g) 70 weeks	Hdh+/+; NR2BWT/WT	Hdh+/+; NR2BTg/WT	Hdh150/+; NR2BWT/WT	Hdh150/+; NR2BTg/WT
Vent Str	265.7 +/- 12.3	245.7 +/- 11.5	177.0 +/- 4.6 *	178.5 +/- 6.7 *
Dors Str	211.1 +/- 0.82	199.7 +/- 16.2	151.9 +/- 2.6 *	138.3 +/- 12.8 *

Table IV.1 Ligand binding at 100 and 70 weeks. Radioactive ligands: [³H]SCH23390 (D1), [³H]Spiperone (D2), and [³H]Flunitrazepam (GABA). No significant differences between groups in all regions for [³H]Flunitrazepam/GABA binding. * $p < 0.05$ compared to wild type controls. All values are expressed as pCi/g ± SEM.
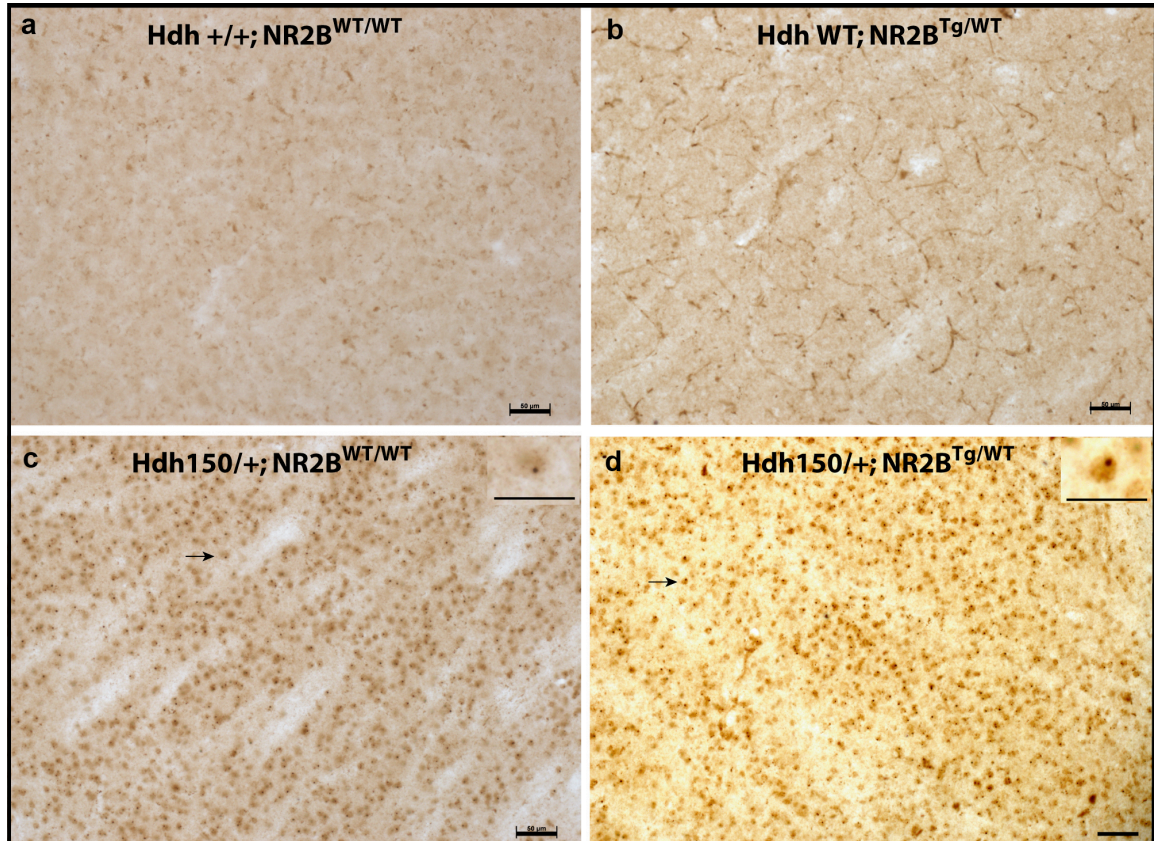
Figure IV.3 Hdh150/+;NR2B^{Tg/WT} double mutant mice and Hdh150/+;NR2B^{WT/WT} exhibit abundant striatal neuronal intranuclear inclusions (NIIs) at 70 weeks. (a-b) No NIIs in Hdh+/+; NR2B^{WT/WT}, Hdh+/+; NR2B^{Tg/WT} mice. **(c-d)** Saturation of NIIs in the striatum of Hdh150/+;NR2B^{Tg/WT} and Hdh150/+ NR2B^{WT/WT} mice. Arrows designate representative inclusions, scale bar = 50 μm. Inset are enlargements of arrows designating NIIs, scale bar = 100 μm.

There were no gross motor abnormalities detected by the accelerated rotarod, all groups displayed similar latencies to fall. The double mutant mice exhibited significantly

reduced general locomotion and exploratory behavior at 100 weeks [Fig. IV.5a; Hdh150/+; NR2B$^{Tg/WT}$, 76.8 ± 17.7 g (mean ± SEM) crossovers/ 2 hr; Hdh+/+; NR2B$^{WT/WT}$, 251.7 ± 30.7; Hdh+/+; NR2B$^{Tg/WT}$, 199.1 ± 43.7 g; Hdh150/+; NR2B$^{WT/WT}$, 102.8 ± 5.1 g; p < 0.01].
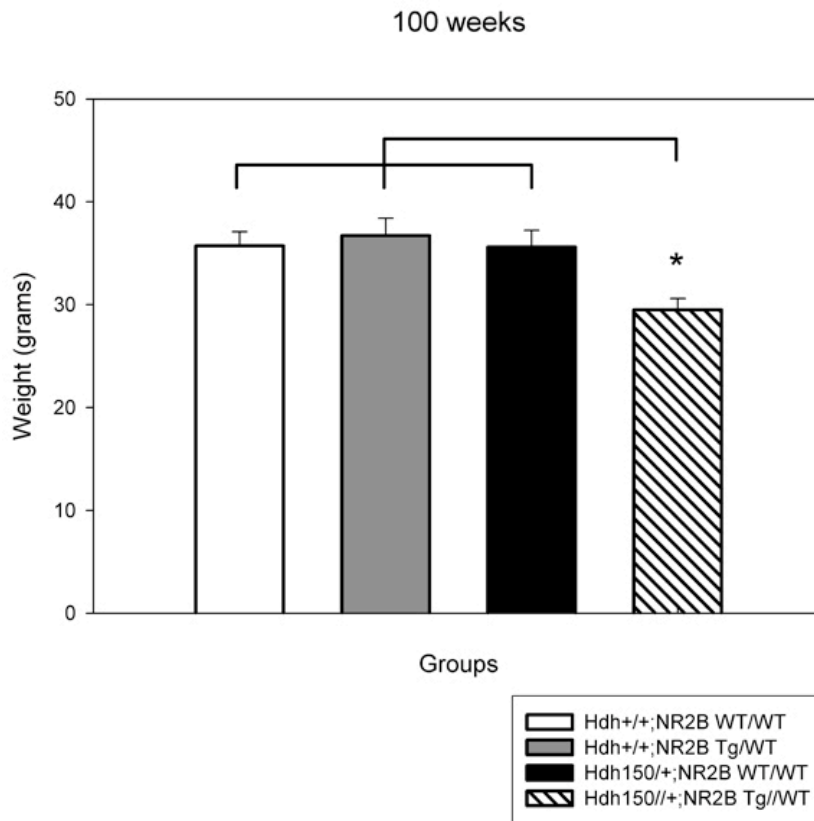
Figure IV.4 Hdh150/+;NR2B$^{Tg/WT}$ bigenic mutant mice exhibit weight loss at 100 weeks. Hdh150/+;NR2B$^{Tg/WT}$ bigenic mutant mice exhibit significant weight loss compared to Hdh+/+; NR2B$^{WT/WT}$, Hdh+/+; NR2B$^{Tg/WT}$, and Hdh150/+ NR2B$^{WT/WT}$ littermate controls. * p < 0.05. Values expressed as mean weight ± SEM.

All groups displayed similar latencies to fall on the hanging wire test, indicating that muscle power was not compromised by the presence of the mutant htt allele or the NR2B transgene (data not shown). Double mutant mice had more difficulty traversing an 11mm

round beam at 100 weeks (Fig. IV.5b). Both Hdh150/+; NR2B$^{Tg/WT}$ and Hdh150/+; NR2B$^{WT/WT}$ require three times as long to traverse the balance beam compared to wild type littermate controls [Hdh150/+; NR2B$^{Tg/WT}$, 5.8 ± 0.4 s (mean ± SEM) seconds;
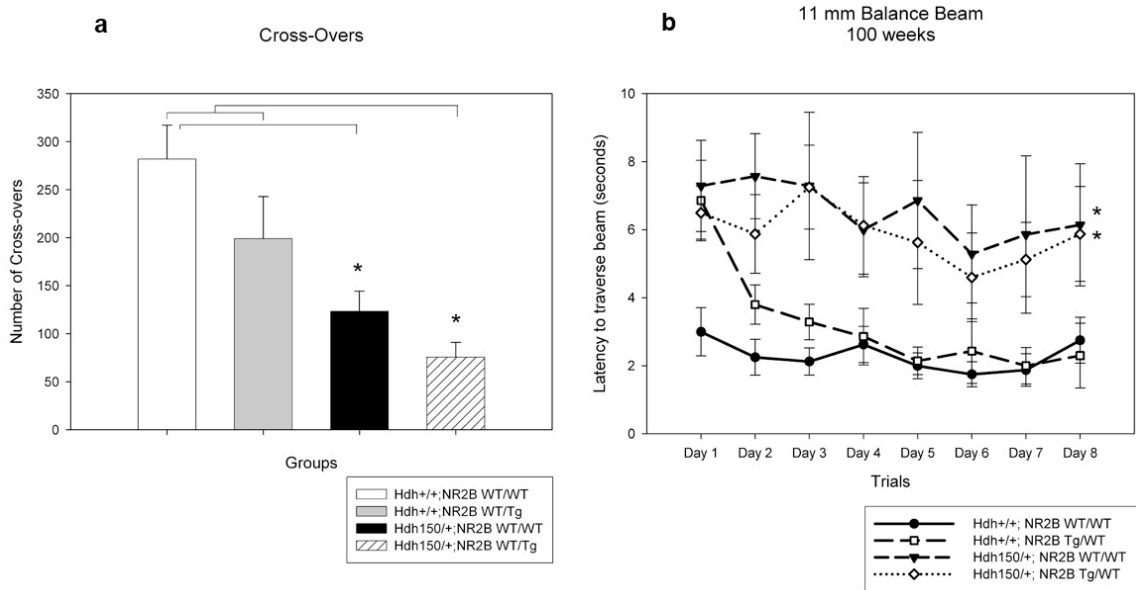
Figure IV.5 Hdh150/+;NR2B$^{Tg/WT}$ double mutant mice and Hdh150/+;NR2B$^{WT/WT}$ exhibit decreased locomotor activity and require more time to traverse the balance beam at 100 weeks. (a) Hdh150/+;NR2B$^{Tg/WT}$ bigenic mutant mice show decreased photo beam breaks as measured in crossovers of activity cages at 100 weeks compared to Hdh+/+; NR2B$^{WT/WT}$, Hdh+/+; NR2B$^{Tg/WT}$. Hdh150/+ NR2B$^{WT/WT}$ also exhibit, to a lesser extent, decreased general activity compared to Hdh+/+; NR2B$^{WT/WT}$. (b) Mice were placed on a lit platform and traversed an 11 mm diameter round balance beam to reach a dark chamber. Animals are tested over eight days (1 trial/day). Both Hdh150/+;NR2B$^{Tg/WT}$ double mutant mice and Hdh150/+;NR2B$^{WT/WT}$ require three times as long to traverse the balance beam compared to controls. Hdh150/+;NR2B$^{Tg/WT}$ and Hdh150/+ NR2B$^{WT/WT}$ require an average of 6.2 sec. ± (SEM) 0.45 sec and Hdh+/+; NR2B$^{WT/WT}$ and Hdh+/+; NR2B$^{Tg/WT}$ require 2.0 sec. + 0.44 sec. to traverse the beam. N = 8-9 animals/group.

Hdh150/+; NR2B$^{WT/WT}$, 6.5 ± 0.6 s; Hdh+/+; NR2B$^{WT/WT}$, 2.0 ± 0.2; p < 0.05]. Footprint analysis revealed that both Hdh150/+; NR2B$^{Tg/WT}$ and Hdh150/+; NR2B$^{WT/WT}$ display a

shortening of stride length and loss of normal gait pattern compared to controls (Fig. IV.6).

Hdh+/+; NR2B$^{WT/WT}$ Hdh+/+; NR2B$^{Tg/WT}$ Hdh150/+; NR2B$^{WT/WT}$ Hdh150/+; NR2B$^{Tg/WT}$

Figure IV.6 Hdh150/+;NR2B$^{Tg/WT}$ double mutant mice display abnormal gait at 100 weeks. Gait was captured by painting the paws of animals with contrasting non-toxic colors prior to walking a paper-lined corridor. Forepaws are painted in red and hindpaws are colored in blue. Hdh150/+;NR2B$^{Tg/WT}$ mice reveal loss of gait pattern and shortening of stride length compared to all groups. Hdh+/+; NR2B$^{WT/WT}$, Hdh+/+; NR2B$^{Tg/WT}$, and Hdh150/+ NR2B$^{WT/WT}$ display congruent overlap paw prints.

Discussion

We tested the hypothesis that the selective striatal degeneration observed in HD is mediated by the NR2B subunit of the NMDAR *in vivo*. In support of this hypothesis, we found that the bigenic mutant mice exhibited a remarkable decrease in striatal neuron number and striatal volume. The striatal degeneration observed in these mice was associated with decreases in dopamine D1 and D2 receptor binding, and with motor deficits. Together, these data demonstrate that synergistic effects of mutant htt and

overexpression of NR2B subunits results in exacerbation of the HD-like phenotype characteristic of $Hdh^{(CAG)150}$ mice. The NR2B transgenic line has previously been shown to exhibit increased NMDAR activation resulting in longer excitatory postsynaptic potentials (EPSPs) and increased calcium flux. *In situ* hybridization reveals increased expression of the NR2B transgene in the cortex, striatum, hippocampus, and amygdala with little increase of expression in thalamus, brainstem, and cerebellum. Within areas of increased NR2B expression, the total number of NR2B-containing NMDAR is increased in individual synapses. These mice display normal growth, body weight, and behavior, and no anatomical abnormalities are reported (Y. P. Tang et al., 1999). Interestingly, while our bigenic mice exhibited exacerbation of striatal neuron degeneration, the time course of their disease was not altered by the addition of the NR2B transgene. We recently generated double bigenics with two copies of the NR2B transgene (Hdh150/+; $NR2B^{Tg/Tg}$) and these mice show even greater deficits in motor impairment (data not shown). Our results are consistent with prior work in other HD murine models supporting a role for NMDAR mediated excitotoxicity in HD.

Studies in transgenic mouse models of HD reveal evidence of increased NMDAR activation. YAC transgenic mice expressing a full length human HD gene (J. G. Hodgson et al., 1999) exhibit increased NMDAR activation followed by increased Ca^{2+} levels and mitochondrial membrane depolarization in MSNs compared to wild type controls (M. M. Zeron et al., 2004; J. Shehadeh et al., 2006). Striatal neurons in these transgenic models appear more susceptible to NMDA agonist mediated toxicity compared to wild type mice, and NMDA induced cell death is abolished by a specific NR2B antagonist (M. S. Levine et al., 1999; M. M. Zeron et al., 2002). Consistent with

these results, the R6/2 transgenic mouse model of HD expressing exon 1 of the human HD (L. Mangiarini et al., 1996) exhibits selective increased NMDA-evoked current and enhancement of intracellular Ca^{2+} (C. Cepeda et al., 2001). Conversely, recent work shows amelioration of behavioral and neuropathological deficits, and increased survival of R6/2 transgenic mice with decortication, an antiexcitotoxic intervention. Inhibition of synthesis of the endogenous NMDAR agonist quinolinic acid markedly extends survival in R6/2 transgenic mice (E. C. Stack et al., 2007). These observations support an important role for NMDAR action, particularly the NR2B subunit, in striatal neuron degeneration in HD.

Single channel measurements and pharmacological studies demonstrate that NR2B subunits dominate other NR2 subunits in determining functional properties of NMDARs Comparative studies confirm that the pharmacological and functional properties of the NMDA receptor depend heavily on the NR2 subunits (S. Cull-Candy et al., 2001; L. Li et al., 2003; J. M. Loftis and A. Janowsky, 2003). In some model systems, NR2B-containing NMDARs have a selective tendency to promote pro-death signaling opposed to the pro-survival promoting pathways of the NR2A-containing NMDARs (G. E. Hardingham and H. Bading, 2002; G. E. Hardingham et al., 2002; G. E. Hardingham and H. Bading, 2003; Y. Liu et al., 2007). NR2B subunit containing NMDARs are highly expressed by MSNs and predominate over other subunit composition, such as the NR1/NR2A, in the striatum (H. Monyer et al., 1992). Previous *in vitro* studies indicate sensitization of NR2B function by mutant htt (N. Chen et al., 1999; M. M. Zeron et al., 2001). NR2B subunit presence influences Mg^{2+} sensitivity and confers high Ca^{+2} permeability. NMDAR activation may either promote neuronal

survival or cause excitotoxic injury (S. Papadia and G. E. Hardingham, 2007). NMDAR effects on survival or death in some CNS neurons heavily depends on NR2 subunit composition. Although extrasynaptic versus synaptic compartmentalization of NR2A- and NR2B-containing NMDAR potentially plays a role in modulating the interplay of cell death and survival pathways (F. X. Soriano and G. E. Hardingham, 2007), recent evidence suggests that subunit composition is more salient in determining the balance between cell death and survival pathways (G. E. Hardingham et al., 2002; C. G. Thomas et al., 2006). Together, these data support that the NR2B NMDA containing receptors are important mediators of neuronal death (G. E. Hardingham and H. Bading, 2003; C. G. Thomas et al., 2006; Y. Liu et al., 2007).

Recent *in vitro* work directly links sensitization of NMDAR-NR2B dysfunction mediated by mutant htt to deranged intracellular Ca^{2+} homeostasis and apoptosis in HD (G. E. Hardingham and H. Bading, 2003; I. Bezprozvanny and M. R. Hayden, 2004; C. G. Thomas et al., 2006; M. M. Fan and L. A. Raymond, 2007). Tang and colleagues demonstrate that overactivation of NR2B containing NMDARs elevates cytosolic Ca^{2+} levels resulting in the activation of cyochrome C and caspases 9 and 3, leading to apoptosis of cultured striatal neurons of a transgenic mouse model of HD (T. S. Tang et al., 2003b). Coexpression of NMDARs with expanded polyglutamine htt in non-neuronal cultured cells enhances excitotoxic cell death, an effect maximized by NR2B subunit expression (M. M. Zeron et al., 2001; L. Li et al., 2004). Similarly, cultured MSNs from a mouse model of HD exhibit increased glutamate evoked peak currents and enhanced Ca^{2+} levels mediated by the NR2B subunit. These findings support the hypothesis that overactivation of NMDARs, particularly those expressing NR2B subunits, in striatal

neurons expressing mutant huntingtin are more vulnerable to NMDAR-mediated Ca^{2+} excitotoxicity (C. Cepeda et al., 2001; M. M. Zeron et al., 2002; L. Li et al., 2003; T. S. Tang et al., 2003b).

NMDAR dysfunction may be only one factor that alters Ca^{2+} homeostasis in HD. Expanded polyQ htt may also perturb other important regulators of intracellular Ca^{2+} homeostasis such as IP3R receptor function and mitochondrial Ca^{2+} uptake (T. S. Tang et al., 2003b; H. B. Fernandes et al., 2007). *In vitro* experiments suggest that direct binding of mutant htt causes abnormal sensitization and activation by type 1 inositol 1,4,5-trisphosphate receptor (InsP3R1), an intracellular Ca^{2+} release channel predominantly expressed in the brain, and results in the detrimental overload of cytosolic Ca^{2+} in MSNs compared to wild type htt (T. S. Tang et al., 2003b). These findings link htt and InsP3R1-mediated neuronal Ca^{2+} signaling and provide an additional explanation for how mutant htt contributes to the unbalanced Ca^{2+} signaling in HD. Other multiple actions of expanded polyQ htt on neuronal Ca^{2+} homeostasis may be involved in neurodegeneration in HD. Dysfunction in brain energy metabolism and homeostasis has also been implicated in HD (M. F. Beal, 1992b; J. M. Oliveira et al., 2007). For example, FDG-PET imaging reveals reduction in glucose metabolism in the cortex and striatum in both manifested HD patients and unaffected carriers, and an increase in cerebral spinal fluid (CSF) lactate. This suggests the possibility of abnormal brain energy metabolism in HD as a result of impaired mitochondrial function (A. Ciarmiello et al., 2006; W. R. Martin et al., 2007). Alterations in PGC-1α, a key regulator of mitochondrial biogenesis and respiration, expression or action have also been suggested as a cause of mitochondrial dysfunction in HD (L. Cui et al., 2006; P. Weydt et al., 2006).

Other mechanistic hypotheses of HD pathogenesis have been suggested, such as transcriptional dysregulation, axonal transport defects, brain-derived neurotropic factor (BDNF) depletion, and proteosomal dysfunction. All these hypotheses have some support (E. Cattaneo et al., 2005; J. H. Cha, 2007; E. C. Stack and R. J. Ferrante, 2007). It is possible that expanded polyQ huntingtin is neurotoxic because it has multiple deleterious effects. While it is important to consider whether there is one pathway leading to neurodegeneration in HD, or a primary pathway resulting in multiple secondary pathways, or an overlapping network of expanded polyQ effects resulting in neurodegeneration, our *in vivo* findings are consistent with previous reports that subunit-specific interaction between NR2B-containing NMDARs and expanded mutant htt potentiate NMDAR-initiated apoptotic cell death and are important mediators of neurodegeneration in HD. NMDAR antagonists are viable candidates as interventions in HD but it seems likely that highly selective NR2B antagonists will be the optimal candidate agents.

The exact mechanism by which mutant htt exacerbates NR2B-NMDAR mediated excitotoxicity in HD is unknown. However, previous studies have suggested altered NMDAR trafficking in human postmortem brains, and in mouse models of HD at early stages of illness. *In vitro* studies of presymptomatic transgenic mouse models of HD demonstrate increased NMDAR insertions of the NR1 and NR2B subunits to the plasma membrane in MSNs compared to wild type controls, and increased functional NR1/NR2B subtypes at the cell surface (N. Chen et al., 1999; M. M. Fan and L. A. Raymond, 2007). Early stage postmortem HD brains exhibit increased levels of NR1/NR2B mRNA in the striatum compared to controls, and with progression of the disease NR1/NR2B mRNA

expression decreased with corresponding neuronal loss in these same regions (T. Arzberger et al., 1997).

Glutamate receptors are tightly regulated by post synaptic density (PSD) proteins and PSD-95 is known to bind and regulate the activity of NMDARs (E. Kim et al., 1996; E. P. Garcia et al., 1998). Normal htt has been shown to mediate the binding of PSD-95 and NMDARs through the binding of the NR2B subunit. Mutant htt may inhibit this interaction (Y. Sun et al., 2001). Interestingly, mutations in key PSD proteins such as PSD-95 and α-CaMKII preferentially displace NR2B subunits to lateral regions of the synapse without affecting changes to the localization of NR2A subunits (C. S. Park et al., 2008). These findings suggest the possibility of subunit-specific NMDAR dynamics and regulation at the synaptic membrane level as an underlying mechanism of glutamate excitoxicity in HD.

Acknowledgements

Chapter V

Conclusion

Summary

In this thesis I present a body of work describing the analysis and use of murine models of HD. I provide the first prospective study of the $Hdh^{(CAG)150}$ knock-in mouse; using a series of sensitive behavioral tests and biochemical assays, I show that it is a valid model of HD. This model is used in the first *in vivo* study of glutamate excitotoxicity, demonstrating that NR2B NMDA receptor mediated excitotoxicity is a proximate underlying mechanism of pathogenesis in HD. The remainder of this chapter will summarize the discussion and experimental results presented in chapters II, III and IV, suggest potential mechanisms by which stimulation striatal NR2B-containing NMDARs may mediate pathogenesis in HD, and pose questions and future directions for research in this area.

Murine Genetic Models of HD

Following the identification of *huntingtin*, various murine models were generated. These models range from transgenic fragment and transgenic full-length models expressing various levels of protein to knock-in models expressing various CAG repeat sizes (Chapter II). The appropriate use of these models depends on how well they recapitulate HD. Validation of models requires careful characterization of their phenotypic features and an accurate model of HD should duplicate key behavioral and pathological features of HD in an age-dependent manner (Chapters II and III). Validation of a model is important because mechanisms of pathogenesis and potential utility of therapeutic interventions are inferred from these models and it is possible that the

113

observed phenotype may be driven by cellular processes unrelated to HD. Unlike transgenic models of HD, knock-in models provide expression of mutant htt in an appropriate genomic and protein context. The $Hdh^{(CAG)150}$ knock-in model is distinguished from other knock-in models in that it is non-chimeric, expressing only a polyglutamine expansion in the murine Hdh gene, unaccompanied by any foreign gene DNA sequences or selectable markers, providing construct validity.

The $Hdh^{(CAG)150}$ knock-in mouse model of HD

In order to maximize the information from the $Hdh^{(CAG)150}$ knock-in mouse model, a longitudinal behavioral and pathological evaluation was undertaken. $Hdh^{(CAG)150}$ heterozygotes exhibited progressive weight loss while homozygotes were unable to gain normal weight compared to wild type controls. The $Hdh^{(CAG)150}$ knock-in line exhibited a progressive, late-onset behavioral phenotype with significant motor abnormalities beginning at 70 weeks, associated with loss of striatal dopamine receptors beginning at 70 weeks and progressing to greater loss of dopamine receptors at 100 weeks of age. Motor abnormalities and neuronal dysfunction preceded significant loss of striatal neuron number at 100 weeks. Sensitive measurements by balance beam and footprint analyses revealed motor impairments in mutant heterozygotes intermediate between wild type controls and mutant homozygotes. These intermediate phenotypic features were previously undetected with the standard behavioral method of the accelerated rotarod. Both behavioral measurements and neuropathological analyses revealed an allele-dependent response, with intermediate deficits in heterozygotes and a more pronounced phenotype in homozygotes. These findings demonstrate that the $Hdh^{(CAG)150}$ knock-in model reproduces key features of HD. Since the $Hdh^{(CAG)150}$ knock-

114

in model exhibits an age-dependent phenotype, this model is advantageous for defining early events in the pathogenesis of neurodegeneration, and posseses behavioral and/or pathological endpoints useful for evaluating therapeutic interventions.

In Vivo Evidence for NMDA Receptor-Mediated Excitotoxicity in HD

After behavioral and neuropathological characterization, the $Hdh^{(CAG)150}$ knock-in model was used to investigate the hypothesis of glutamate excitotoxicity. NMDAR mediated excitotoxicity has long been implicated as a proximate cause of neurodegeneration in HD, however, this hypothesis has not been tested rigorously *in vivo*. NMDAR NR2B-subunits are the predominant NR2 subunit expressed by the striatal medium spiny neurons that degenerate in HD. To investigate the potential role of NR2B NMDAR-mediated excitotoxicity in HD, we crossed the well validated $Hdh^{(CAG)150}$ knock-in mouse model with a transgenic line overexpressing NR2B-subunit receptors (Chapter IV). In the resulting double mutant line, we show exacerbation of selective striatal neuron degeneration. The bigenic mutant mice exhibited a remarkable decrease in striatal neuron number and striatal volume at 100 weeks of age compared to controls. The striatal degeneration observed in these mice was associated with decreases in dopamine D1 and D2 receptor binding at 70 weeks that progressed at 100 weeks, while extrastriatal regions showed no change in benzodiazpine/GABA-A receptor binding. In agreement with these findings, the distribution of huntingtin aggregates/NIIs in brain was saturated in striatal neurons in double mutant and Hdh150/+; $NR2B^{WT/WT}$ mice at 100 weeks while NII expression was relatively sparse in other brain regions. This result is consistent with selective striatal NII pathology in prior work in the $Hdh^{(CAG)150}$ line (Tallaksen-Greene 2005). Double mutants exhibited weight loss and motor deficits at

100 weeks. Interestingly, while our bigenic mice exhibited exacerbation of striatal neuron degeneration, the time course of their disease was not altered by the addition of the NR2B transgene. The interaction between mutant htt and the NR2B transgene exacerbates the motor phenotype and striatal pathology, however, does not accelerate the time course of these abnormalities compared to the $Hdh^{(CAG)150}$ line, at least up to 70 weeks. Differences in behavioral and neurpathological severities are comparable up to 70 weeks between the $Hdh^{(CAG)150}$ line and double mutants, implicating similar mechanisms of pathogenesis at earlier points in the course of the disease. In later stages of the disease, however, double mutants exhibit more severe pathology, suggesting that glutamate excitotoxic mechanisms may be involved in later phases of neurodegenearation, possibly a phase that follows neuronal dysfunction. These results provide the first direct *in vivo* evidence of NR2B NMDAR-mediated excitotoxicity and point towards a mechanism for glutamate-mediated excitotoxicty in HD and suggest possible sequential and temporal differential mechanisms of neuronal degeneration. Our results indicate that NMDA antagonists, particularly those that are selective for NR2B-containing NMDARs, are viable candidates for pharmacological intervention in HD.

Possible Mechanisms Underlying NR2B NMDAR Mediated Excitotoxcity in HD

The exact mechanism by which mutant htt exacerbates NR2B NMDAR-mediated excitotoxicity in HD is unknown. Our findings raise questions about how this interaction may occur. Some possibilities include:

1. Sensitization of the NR2B subunit resulting in overactivation of the NMDAR.

2. Altered NR2B containing NMDAR trafficking resulting in increased expression of NR2B containing NMDAR at the post synaptic membrane.

3. Altered signaling pathways including scaffolding proteins resulting in NMDAR dysregulation at the synaptic membrane.

4. Dysfunction in corticostriatal inputs.

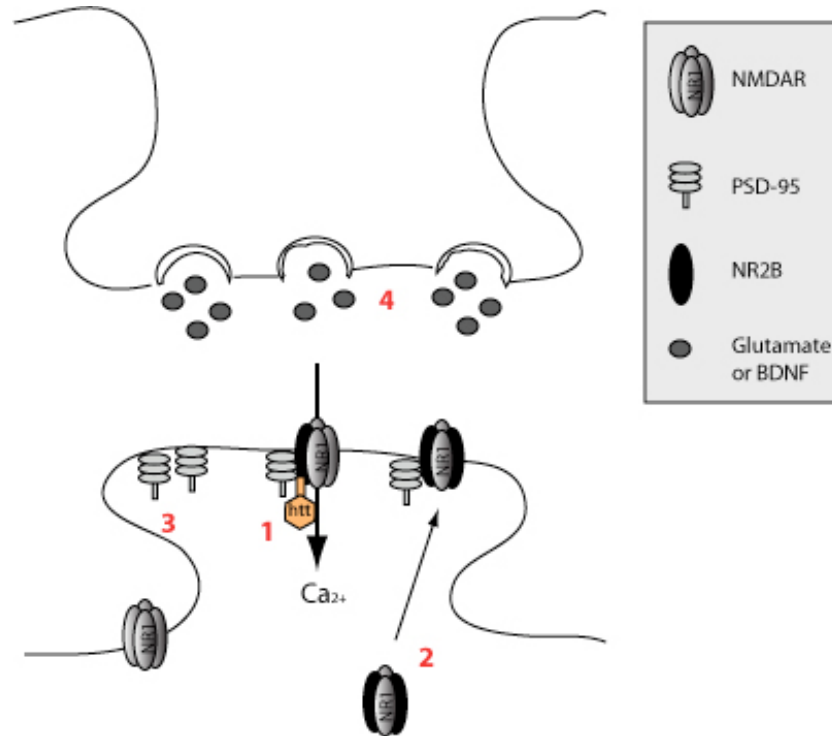**Figure V.1 Possible Mechanisms of NR2B NMDAR Mediated Excitotoxicity:** 1. Sensitization of the NR2B subunit 2. Altered NR2B containing NMDAR 3. Altered signaling pathways including scaffolding proteins 4. Dysfunction in corticostriatal inputs.

The following are several approaches that may be used to unravel the mechanisms underlying NMDAR excitotoxicity.

Sensitization of the NR2B Subunit

It is possible that enhanced activity of the NR2B-containing NMDA receptors may result from sensitization of the NR2B subunit. It has been demonstrated, for example, that wild type htt directly interacts with the NR2B subunit of the NMDAR and that mutant htt alters the normal interaction of the NR2B subunit with PSD-95 (Y. Sun et al., 2001). Tang and colleagues demonstrated that mutant htt sensitizes normal binding of inositol triphosphate to the InsP3R1 receptor, resulting in toxic increases of intracellular calcium (T. S. Tang et al., 2003a). It is plausible that mutant htt may be interacting similarly with the NR2B subunit. Further analysis with electrophysiological recording and Ca^{2+} imaging would be a possible approach to measure NR2B NMDAR sensitization in murine models of HD. One approach would be to use single bouton recording in double bigenics compared to the $Hdh^{(CAG)150}$ knock-in mouse model and littermate controls to examine the complete charge transfer through a single synapse of the NMDAR and to additionally examine receptor channel function by patch-clamp recording in primary dissociated striatal cells and slice culture. Patch clamp recordings would allow measure of several biophysical parameters, including peak currents, decay kinetics, and desensitization. Pharmacologic methods could be used to dissect the specific role of NR2B-containing NMDARs. I would expect significantly larger currents and greater charge transfer in double mutants with $Hdh^{(CAG)150}$ knock-in mouse exhibiting an intermediate effect compared to wild type controls and that these effects would be ameliorated with a selective NR2B antagonist. I would expect similar findings with Ca^{2+} imaging in dissociated striatal cultured neurons. It would be advantageous to perform these experiments at the similar age timepoints 20, 40, 50, 70, and 100 weeks of age to determine when these changes occur. However, with previous findings suggesting that

glutamate excitotoxic mechanisms may be a driving force of toxicity at later stages of neuronal degeneration, I would predict that alterations in Ca^{2+} entry and electrophysiological recording would occur between 70 and 100 weeks; a perioid following neuronal dysfunction at 70 weeks but preceding neurodegneration at 100 weeks.

Alterations in NMDA Receptor Trafficking

Alternatively, NR2B NMDAR-mediated excitotoxicity could result from increased expression of NR2B containing NMDARs at the synaptic membrane. Alterations in NMDA receptor trafficking resulting in changes in synaptic subunit composition could prolong Ca^{2+} entry could possibly contribute to the observed toxicity. Previous studies have suggested altered NMDAR trafficking in human postmortem brains with findings of altered NMDAR subunit expression, and in mouse models of HD at early stages of illness. *In vitro* studies of presymptomatic transgenic mouse models of HD demonstrate increased NMDAR insertions of the NR1 and NR2B subunits to the plasma membrane in MSNs compared to wild type controls, and increased functional NR1/NR2B subtypes at the cell surface (N. Chen et al., 1999; M. M. Fan and L. A. Raymond, 2007). Early stage postmortem HD brains exhibit increased levels of NR1/NR2B mRNA in the striatum compared to controls, and with progression of the disease NR1/NR2B mRNA expression decreases with corresponding neuronal loss in these same regions (T. Arzberger et al., 1997). Given that activation stimulates NR2B pro-death pathways while NR2A stimulates anti-apoptotic cascades (G. E. Hardingham et al., 2002), increased NR2B subunit expression is a possible mechanism for NR2B NMDA receptor-mediated excitotoxicty. This could be further evaluated using optical,

biochemical or electrophysiological techniques. One approach would be to use biotinylation assays to estimate surface NR2B subunit expression on striatal cultures from double mutants, $Hdh^{(CAG)150}$ knock-in mouse, and littermate controls. Another approach could be electrophysiological recording of synaptic NMDAR excitotatory post synaptic currents (EPSCs) in response to pharmacological blockade of either exocytosis or endocytosis in all groups. In double mutants, I would expect to find significant increase of NR2B containing NMDAR insertion at the synapse. An approach to explore subtype specific NMDAR receptor trafficking in synaptic versus extra-synaptic pools is to use photoinactivation. I would expect that this technique would reveal that NR2B containing NMDAR insertion would would be increased extra-synaptically in animals containing mutant htt compared to littermate controls and even more so in double mutants.

Alterations in Signaling Proteins and NMDAR Regulations

Another potential avenue of examining NR2B NMDA receptor-mediated excitotoxicity are alterations in signaling proteins involved in NMDAR signal transduction. Glutamate receptors are tightly regulated by post synaptic density (PSD) proteins and PSD-95 is known to bind and regulate the activity of NMDARs (E. Kim et al., 1996; E. P. Garcia et al., 1998). Synaptic NMDA receptors are localized to the PSDs where they dynamically interact with scaffolding and adaptor proteins, kinases, phosphatases, and other signaling proteins forming an NMDAR signaling complex (S. Kim et al., 2006; S. Lee et al., 2006). It has been proposed that neuron-specific enzymes or substrates responsible for Ca^{2+}-dependent excitotoxicity are co-localized with NMDARs. Postmortem HD brains show that degeneration of the striatum is associated with extensive remodeling of MSNs with

abnormal increases in spine number and dendritic branching (G. A. Graveland et al., 1985) possibly involving alterations in NMDAR regulation. Normal htt has been shown to mediate the binding of PSD-95 and NMDARs through the direct interaction of the NR2B subunit. Mutant htt may inhibit this interaction (Y. Sun et al., 2001). Interestingly, mutations in key PSD proteins such as PSD-95 and α-CaMKII preferentially displace NR2B subunits to lateral regions of the synapse without affecting changes to the localization of NR2A subunits (C. S. Park et al., 2008). These findings suggest the possibility of subunit-specific NMDAR dynamics and regulation at the synaptic membrane level involving as an underlying mechanism of glutamate excitotoxicity in HD. To address mechanisms involving scaffolding proteins and downstream signaling pathways a possible approach would be to investigate downstream pathways involving NR2B promoting pro-death pathways including NMDAR activity-regulated overactivation of the Ca^{2+}-dependent nNOS (neuronal nitric oxide synthase), calpains promoting toxic downstream reponses, and the p38 mitogen-activated protein kinase (MAPK). One approach would be using proteonomics and western analysis to examine the expression of these proteins in the double mutants and the $Hdh^{(150)CAG}$ knock-in mice compared to littermate controls as well as immunohistochemistry for scaffolding proteins including PSD-95, NR2B and synaptophysin (for an internal control) and confocal microscopy for analyses in these same groups. I would expect a significant increase in protein expression that are involved in the pro-death promoting pathways including NOS, MAPK, and calpains in animals containing mutant htt compared to controls and even more so in double mutants. With confocal microscopy I would expect similar increases in PSD-95 and NR2B expression at the synapse in animals containing

mutant htt consistent with degenerative and regenerative changes reported by Graveland et al., 1985. I would predict these changes to occur similarly at the same time points in double mutant and Hdh$^{(150)CAG}$ knock-in mice prior to neurodegenerative at 100 weeks and more closely to 70 weeks, a time where neuronal dysfunction is occurring given the significant reductions of receptor binding on striatal dendrites. Because double mutant and Hdh$^{(150)CAG}$ knock-in mice share similar pathology up to 70 weeks I would expect that mechanisms underyling neuronal dysfunction to be similarly driven at earlier time points of the disease process.

Dysfunction in corticostriatal inputs

The NR2B subunit is highly expressed in cortical regions and altered interaction between mutant htt and NR2B could result in possible corticostriatal circuitry dysfunction including loss of cortical brain-derived-neurotrophic factor (BDNF) trophic support (C. Zuccato and E. Cattaneo, 2007; C. Zuccato et al., 2007) or aberrant synaptic currents resulting in altered coticostriatal communication (C. Cepeda et al., 2003).

The corticostriatal pathway provides most of the excitatory glutamatergic input into the striatum and cortical BDNF production is required for the correct activity of the corticostriatal synapse and for the survival of MSNs that degenerate in HD. Imaging studies in HD patients reveal cortical degeneration prior to the onset of overt clinical features, suggesting that corticolstriatal dysfunction may subsequently contribute to the early striatal specific degeneration observed in HD. There is significant evidence suggesting that excitotoxicity is exerted through altered afferent corticostriatal projections (C. Cepeda et al., 2003; C. Cepeda et al., 2007). Additionally, postmortem HD brains and animal models of HD exhibit significant reductions in BDNF protein and

mRNA levels, particularly the cortex and BDNF vesicle transport and secretion is enhanced by wild type htt (C. Zuccato and E. Cattaneo, 2007). Recent work shows amelioration of behavioral and neuropathological deficits, and increased survival of R6/2 transgenic HD mice with decortication of the corticostriatal pathway (E. C. Stack et al., 2007). A striatal specific NR1 subunit of the NMDAR knockout mouse has recently been generated (M. T. Dang et al., 2006). This line has normal striatal neurons and corticostriate function except for absent NMDA receptor action. Crossing this mouse to the $Hdh^{(150)CAG}$ line would be an *in vivo* approach to differentially examine cortical excitotoxic contributions versus loss of other corticostriate functions. Performing similar longitudinal behavioral characterization with correlative neuropathologic analyses similarly to the $Hdh^{(150)CAG}$ line should establish whether striatal NMDARs alone contribute to early or late stages of striatal neurodegeneration.

Given recent findings of dysfunction in cortical EPSCs in early stages of the disease in some mouse models of HD and imaging studies of HD patients exhibiting early cortical atrophy preceding clinical symptoms, I predict changes in relevant cortical excitatory glutamatergic input to occur early in the disease stage. However, these same mouse models of HD also report altered corticostriatal EPSCs later in the disease and reports on BDNF show decreases in BDNF protein and mRNA levels in HD postmortem brains, particularly the striatum. These findings suggest that perhaps there is a biphasic alteration that the corticostriatal pathway contributes to disease both in early and late phases of HD. Striatal neurons require BDNF for healthy activity and survival, depletion of BDNF in the striatum suggests that impaired anterograde transport of BDNF to its striatal targets via the corticostriatal afferents may contribute to HD pathology. The

corticostriatal pathway is important in both excitatory glutamatergic communication and normal BDNF delivery to striatal neurons and perturbation in this pathway may contribute to the pathogenesis in HD. Dysfunctions of striatal circuits and cortical neurons that make up the corticostriatal pathway may contribute to the age-related transient temporal progression of the HD phenotype.

Final Conclusions

In summary, the $Hdh^{(CAG)150}$ knock-in mouse model recapitulates key features of HD and is a valid model to study disease based mechanisms in HD and that glutamate excitotoxicity is a proximate cause of pathogenesis in HD. The results presented in this dissertation support an important role for NR2B-NMDA receptor-mediated excitotoxicity and suggest several potential and interesting avenues for future research in this area. These alternative hypotheses suggest means by which mutant htt may exert toxicity via NR2B NMDARs.

References

Albin RL, Young AB, Penney JB (1989) The functional anatomy of basal ganglia disorders. Trends Neurosci 12:366-375.

Alexander GE, Crutcher MD (1990) Functional architecture of basal ganglia circuits: neural substrates of parallel processing. Trends Neurosci 13:266-271.

Andrade MA, Bork P (1995) HEAT repeats in the Huntington's disease protein. Nat Genet 11:115-116.

Andreassen OA, Ferrante RJ, Hughes DB, Klivenyi P, Dedeoglu A, Ona VO, Friedlander RM, Beal MF (2000) Malonate and 3-nitropropionic acid neurotoxicity are reduced in transgenic mice expressing a caspase-1 dominant-negative mutant. J Neurochem 75:847-852.

Andresen JM, Gayan J, Djousse L, Roberts S, Brocklebank D, Cherny SS, Cardon LR, Gusella JF, MacDonald ME, Myers RH, Housman DE, Wexler NS (2007) The relationship between CAG repeat length and age of onset differs for Huntington's disease patients with juvenile onset or adult onset. Ann Hum Genet 71:295-301.

Andrew SE, Goldberg YP, Kremer B, Telenius H, Theilmann J, Adam S, Starr E, Squitieri F, Lin B, Kalchman MA, et al. (1993) The relationship between trinucleotide (CAG) repeat length and clinical features of Huntington's disease. Nat Genet 4:398-403.

Antonini A, Leenders KL, Spiegel R, Meier D, Vontobel P, Weigell-Weber M, Sanchez-Pernaute R, de Yebenez JG, Boesiger P, Weindl A, Maguire RP (1996) Striatal glucose metabolism and dopamine D2 receptor binding in asymptomatic gene carriers and patients with Huntington's disease. Brain 119 (Pt 6):2085-2095.

Arrasate M, Mitra S, Schweitzer ES, Segal MR, Finkbeiner S (2004) Inclusion body formation reduces levels of mutant huntingtin and the risk of neuronal death. Nature 431:805-810.

Arzberger T, Krampfl K, Leimgruber S, Weindl A (1997) Changes of NMDA receptor subunit (NR1, NR2B) and glutamate transporter (GLT1) mRNA expression in Huntington's disease--an in situ hybridization study. J Neuropathol Exp Neurol 56:440-454.

Aylward EH, Codori AM, Rosenblatt A, Sherr M, Brandt J, Stine OC, Barta PE, Pearlson GD, Ross CA (2000) Rate of caudate atrophy in presymptomatic and symptomatic stages of Huntington's disease. Mov Disord 15:552-560.

Aylward EH, Sparks BF, Field KM, Yallapragada V, Shpritz BD, Rosenblatt A, Brandt J, Gourley LM, Liang K, Zhou H, Margolis RL, Ross CA (2004) Onset and rate of striatal atrophy in preclinical Huntington disease. Neurology 63:66-72.

Backman L, Robins-Wahlin TB, Lundin A, Ginovart N, Farde L (1997) Cognitive deficits in Huntington's disease are predicted by dopaminergic PET markers and brain volumes. Brain 120 (Pt 12):2207-2217.

Bates GP, Harper P, Jones L (2002) Huntington disease. New York: Oxford University Press.

Bazzett TJ, Becker JB, Kaatz KW, Albin RL (1993) Chronic intrastriatal dialytic administration of quinolinic acid produces selective neural degeneration. Exp Neurol 120:177-185.

Beal MF (1992a) Mechanisms of excitotoxicity in neurologic diseases. FASEB J 6:3338-3344.

Beal MF (1992b) Does impairment of energy metabolism result in excitotoxic neuronal death in neurodegenerative illnesses? Ann Neurol 31:119-130.

Beal MF (1994) Huntington's disease, energy, and excitotoxicity. Neurobiol Aging 15:275-276.

Beal MF, Ferrante RJ, Swartz KJ, Kowall NW (1991) Chronic quinolinic acid lesions in rats closely resemble Huntington's disease. J Neurosci 11:1649-1659.

Beal MF, Kowall NW, Ellison DW, Mazurek MF, Swartz KJ, Martin JB (1986) Replication of the neurochemical characteristics of Huntington's disease by quinolinic acid. Nature 321:168-171.

Becher MW, Kotzuk JA, Sharp AH, Davies SW, Bates GP, Price DL, Ross CA (1998) Intranuclear neuronal inclusions in Huntington's disease and dentatorubral and pallidoluysian atrophy: correlation between the density of inclusions and IT15 CAG triplet repeat length. Neurobiol Dis 4:387-397.

Beglinger LJ, Nopoulos PC, Jorge RE, Langbehn DR, Mikos AE, Moser DJ, Duff K, Robinson RG, Paulsen JS (2005) White matter volume and cognitive dysfunction in early Huntington's disease. Cogn Behav Neurol 18:102-107.

Benn CL, Slow EJ, Farrell LA, Graham R, Deng Y, Hayden MR, Cha JH (2007) Glutamate receptor abnormalities in the YAC128 transgenic mouse model of Huntington's disease. Neuroscience 147:354-372.

Bercovich B, Stancovski I, Mayer A, Blumenfeld N, Laszlo A, Schwartz AL, Ciechanover A (1997) Ubiquitin-dependent degradation of certain protein substrates in vitro requires the molecular chaperone Hsc70. J Biol Chem 272:9002-9010.

Brinkman RR, Mezei MM, Theilmann J, Almqvist E, Hayden MR (1997) The likelihood of being affected with Huntington disease by a particular age, for a specific CAG size. Am J Hum Genet 60:1202-1210.

Brouillet E, Jacquard C, Bizat N, Blum D (2005) 3-Nitropropionic acid: a mitochondrial toxin to uncover physiopathological mechanisms underlying striatal degeneration in Huntington's disease. J Neurochem 95:1521-1540.

Brouillet E, Hantraye P, Ferrante RJ, Dolan R, Leroy-Willig A, Kowall NW, Beal MF (1995) Chronic mitochondrial energy impairment produces selective striatal degeneration and abnormal choreiform. Proc Natl Acad Sci U S A 92:7105-7109.

Browne SE, Bowling AC, MacGarvey U, Baik MJ, Berger SC, Muqit MM, Bird ED, Beal MF (1997) Oxidative damage and metabolic dysfunction in Huntington's disease: selective vulnerability of the basal ganglia. Ann Neurol 41:646-653.

Canals JM, Checa N, Marco S, Akerud P, Michels A, Perez-Navarro E, Tolosa E, Arenas E, Alberch J (2001) Expression of brain-derived neurotrophic factor in cortical neurons is regulated by striatal target area. J Neurosci 21:117-124.

Canals JM, Pineda JR, Torres-Peraza JF, Bosch M, Martin-Ibanez R, Munoz MT, Mengod G, Ernfors P, Alberch J (2004) Brain-derived neurotrophic factor regulates the onset and severity of motor dysfunction associated with enkephalinergic neuronal degeneration in Huntington's disease. J Neurosci 24:7727-7739.

Carter RJ, Lione LA, Humby T, Mangiarini L, Mahal A, Bates GP, Dunnett SB, Morton AJ (1999) Characterization of progressive motor deficits in mice transgenic for the human Huntington's disease mutation. J Neurosci 19:3248-3257.

Cattaneo E, Zuccato C, Tartari M (2005) Normal huntingtin function: an alternative approach to Huntington's disease. Nat Rev Neurosci 6:919-930.

Cepeda C, Wu N, Andre VM, Cummings DM, Levine MS (2007) The corticostriatal pathway in Huntington's disease. Prog Neurobiol 81:253-271.

Cepeda C, Ariano MA, Calvert CR, Flores-Hernandez J, Chandler SH, Leavitt BR, Hayden MR, Levine MS (2001) NMDA receptor function in mouse models of Huntington disease. J Neurosci Res 66:525-539.

Cepeda C, Hurst RS, Calvert CR, Hernandez-Echeagaray E, Nguyen OK, Jocoy E, Christian LJ, Ariano MA, Levine MS (2003) Transient and progressive electrophysiological alterations in the corticostriatal pathway in a mouse model of Huntington's disease. J Neurosci 23:961-969.

Cha JH (2007) Transcriptional signatures in Huntington's disease. Prog Neurobiol 83:228-248.

Cha JH, Frey AS, Alsdorf SA, Kerner JA, Kosinski CM, Mangiarini L, Penney JB, Jr., Davies SW, Bates GP, Young AB (1998) Altered neurotransmitter receptor expression in transgenic mouse models of Huntington's disease. Philos Trans R Soc Lond B Biol Sci 354:981-989.

Chen N, Luo T, Wellington C, Metzler M, McCutcheon K, Hayden MR, Raymond LA (1999) Subtype-specific enhancement of NMDA receptor currents by mutant huntingtin. J Neurochem 72:1890-1898.

Ciarmiello A, Cannella M, Lastoria S, Simonelli M, Frati L, Rubinsztein DC, Squitieri F (2006) Brain white-matter volume loss and glucose hypometabolism precede the clinical symptoms of Huntington's disease. J Nucl Med 47:215-222.

Conneally PM (1984) Huntington disease: genetics and epidemiology. Am J Hum Genet 36:506-526.

Cooper JK, Schilling G, Peters MF, Herring WJ, Sharp AH, Kaminsky Z, Masone J, Khan FA, Delanoy M, Borchelt DR, Dawson VL, Dawson TM, Ross CA (1998) Truncated N-terminal fragments of huntingtin with expanded glutamine repeats form nuclear and cytoplasmic aggregates in cell culture. Hum Mol Genet 7:783-790.

Coyle JT, Schwarcz R (1976) Lesion of striatal neurones with kainic acid provides a model for Huntington's chorea. Nature 263:244-246.

Crawley JN (2000) What's wrong with my mouse? New York: Whiley-Liss.

Cui L, Jeong H, Borovecki F, Parkhurst CN, Tanese N, Krainc D (2006) Transcriptional repression of PGC-1alpha by mutant huntingtin leads to mitochondrial dysfunction and neurodegeneration. Cell 127:59-69.

Cull-Candy S, Brickley S, Farrant M (2001) NMDA receptor subunits: diversity, development and disease. Curr Opin Neurobiol 11:327-335.

Cummings CJ, Zoghbi HY (2000) Fourteen and counting: unraveling trinucleotide repeat diseases. Hum Mol Genet 9:909-916.

Cummings CJ, Orr HT, Zoghbi HY (1999) Progress in pathogenesis studies of spinocerebellar ataxia type 1. Philos Trans R Soc Lond B Biol Sci 354:1079-1081.

Dang MT, Yokoi F, Yin HH, Lovinger DM, Wang Y, Li Y (2006) Disrupted motor learning and long-term synaptic plasticity in mice lacking NMDAR1 in the striatum. Proc Natl Acad Sci U S A 103:15254-15259.

Dawbarn D, De Quidt ME, Emson PC (1985) Survival of basal ganglia neuropeptide Y-somatostatin neurones in Huntington's disease. Brain Res 340:251-260.

de Pril R, Fischer DF, Maat-Schieman ML, Hobo B, de Vos RA, Brunt ER, Hol EM, Roos RA, van Leeuwen FW (2004) Accumulation of aberrant ubiquitin induces aggregate formation and cell death in polyglutamine diseases. Hum Mol Genet 13:1803-1813.

DeLong MR (1990) Primate models of movement disorders of basal ganglia origin. Trends Neurosci 13:281-285.

DiFiglia M, Sapp E, Chase KO, Davies SW, Bates GP, Vonsattel JP, Aronin N (1997) Aggregation of huntingtin in neuronal intranuclear inclusions and dystrophic neurites in brain. Science 277:1990-1993.

DiFiglia M, Sapp E, Chase K, Schwarz C, Meloni A, Young C, Martin E, Vonsattel JP, Carraway R, Reeves SA, et al. (1995) Huntingtin is a cytoplasmic protein associated with vesicles in human and rat brain neurons. Neuron 14:1075-1081.

Dingledine R, Borges K, Bowie D, Traynelis SF (1999) The glutamate receptor ion channels. Pharmacol Rev 51:7-61.

Duff K, Paulsen JS, Beglinger LJ, Langbehn DR, Stout JC, Group P-HIotHS (2007) Psychiatric symptoms in Huntington's disease before diagnosis: the predict-HD study. Biol Psychiatry 62:1341-1346.

Fan MM, Raymond LA (2007) N-methyl-D-aspartate (NMDA) receptor function and excitotoxicity in Huntington's disease. Prog Neurobiol 81:272-293.

Fan MM, Fernandes HB, Zhang LY, Hayden MR, Raymond LA (2007) Altered NMDA receptor trafficking in a yeast artificial chromosome transgenic mouse model of Huntington's disease. J Neurosci 27:3768-3779.

Fernandes HB, Baimbridge KG, Church J, Hayden MR, Raymond LA (2007) Mitochondrial sensitivity and altered calcium handling underlie enhanced NMDA-induced apoptosis in YAC128 model of Huntington's disease. J Neurosci 27:13614-13623.

Ferrante RJ, Kowall NW, Cipolloni PB, Storey E, Beal MF (1993) Excitotoxin lesions in primates as a model for Huntington's disease: histopathologic and neurochemical characterization. Exp Neurol 119:46-71.

Ferrante RJ, Andreassen OA, Dedeoglu A, Ferrante KL, Jenkins BG, Hersch SM, Beal MF (2002) Therapeutic effects of coenzyme Q10 and remacemide in transgenic mouse models of Huntington's disease. J Neurosci 22:1592-1599.

Ferrer I, Goutan E, Marin C, Rey MJ, Ribalta T (2000) Brain-derived neurotrophic factor in Huntington disease. Brain Res 866:257-261.

Fink JS, Weaver DR, Rivkees SA, Peterfreund RA, Pollack AE, Adler EM, Reppert SM (1992) Molecular cloning of the rat A2 adenosine receptor: selective co-expression with D2 dopamine receptors in rat striatum. Brain Res Mol Brain Res 14:186-195.

Garcia EP, Mehta S, Blair LA, Wells DG, Shang J, Fukushima T, Fallon JR, Garner CC, Marshall J (1998) SAP90 binds and clusters kainate receptors causing incomplete desensitization. Neuron 21:727-739.

Gauthier LR, Charrin BC, Borrell-Pages M, Dompierre JP, Rangone H, Cordelieres FP, De Mey J, MacDonald ME, Lessmann V, Humbert S, Saudou F (2004) Huntingtin controls neurotrophic support and survival of neurons by enhancing BDNF vesicular transport along microtubules. Cell 118:127-138.

Ginovart N, Lundin A, Farde L, Halldin C, Backman L, Swahn CG, Pauli S, Sedvall G (1997) PET study of the pre- and post-synaptic dopaminergic markers for the neurodegenerative process in Huntington's disease. Brain 120 (Pt 3):503-514.

Graveland GA, Williams RS, DiFiglia M (1985) Evidence for degenerative and regenerative changes in neostriatal spiny neurons in Huntington's disease. Science 227:770-773.

Graybiel AM (1990) Neurotransmitters and neuromodulators in the basal ganglia. Trends Neurosci 13:244-254.

Greene JG, Greenamyre JT (1995) Characterization of the excitotoxic potential of the reversible succinate dehydrogenase inhibitor malonate. J Neurochem 64:430-436.

Group HDCR (1993a) A novel gene containing a trinucleotide repeat that is expanded and unstable on Huntington's disease chromosomes. The Huntington's Disease Collaborative Research Group. Cell 72:971-983.

Group HS (2001) A randomized, placebo-controlled trial of coenzyme Q10 and remacemide in Huntington's disease. Neurology 57:397-404.

Gu M, Gash MT, Mann VM, Javoy-Agid F, Cooper JM, Schapira AH (1996) Mitochondrial defect in Huntington's disease caudate nucleus. Ann Neurol 39:385-389.

Gusella JF, MacDonald ME (1995) Huntington's disease: CAG genetics expands neurobiology. Curr Opin Neurobiol 5:656-662.

Gutekunst CA, Li SH, Yi H, Ferrante RJ, Li XJ, Hersch SM (1998) The cellular and subcellular localization of huntingtin-associated protein 1 (HAP1): comparison with huntingtin in rat and human. J Neurosci 18:7674-7686.

Gutekunst CA, Levey AI, Heilman CJ, Whaley WL, Yi H, Nash NR, Rees HD, Madden JJ, Hersch SM (1995) Identification and localization of huntingtin in brain and human lymphoblastoid cell lines with anti-fusion protein antibodies. Proc Natl Acad Sci U S A 92:8710-8714.

Gutekunst CA, Li SH, Yi H, Mulroy JS, Kuemmerle S, Jones R, Rye D, Ferrante RJ, Hersch SM, Li XJ (1999) Nuclear and neuropil aggregates in Huntington's disease: relationship to neuropathology. J Neurosci 19:2522-2534.

Halliday GM, McRitchie DA, Macdonald V, Double KL, Trent RJ, McCusker E (1998) Regional specificity of brain atrophy in Huntington's disease. Exp Neurol 154:663-672.

Hantraye P, Riche D, Maziere M, Isacson O (1990) A primate model of Huntington's disease: behavioral and anatomical studies of unilateral excitotoxic lesions of the caudate-putamen in the baboon. Exp Neurol 108:91-104.

Hardingham GE, Bading H (2002) Coupling of extrasynaptic NMDA receptors to a CREB shut-off pathway is developmentally regulated. Biochem Biophys Acta 1600:148-153.

Hardingham GE, Bading H (2003) The yin and yang of NMDA receptor signalling. Trends Neurosci 26:81-89.

Hardingham GE, Fukunaga Y, Bading H (2002) Extrasynaptic NMDARs oppose synaptic NMDARs by triggering CREB shut-off and cell death pathways. Nat Neurosci 5:405-414.

Hardy J, Orr HT (2006) The genetics of neurodegenerative diseases. J Neurochem 97:1690-1699.

Harjes P, Wanker EE (2003) The hunt for huntingtin function: interaction partners tell many different stories. Trends Biochem Sci 28:425-433.

Harper PS (1992) The epidemiology of Huntington's disease. Hum Genet 89:365-376.

Hawkins LM, Chazot PL, Stephenson FA (1999) Biochemical evidence for the co-association of three N-methyl-D-aspartate (NMDA) R2 subunits in recombinant NMDA receptors. J Biol Chem 274:27211-27218.

Hayden MR, Martin WR, Stoessl AJ, Clark C, Hollenberg S, Adam MJ, Ammann W, Harrop R, Rogers J, Ruth T, et al. (1986) Positron emission tomography in the early diagnosis of Huntington's disease. Neurology 36:888-894.

Heng MY, Tallaksen-Greene SJ, Detloff PJ, Albin RL (2007) Longitudinal evaluation of the Hdh(CAG)150 knock-in murine model of Huntington's disease. J Neurosci 27:8989-8998.

Hickey MA, Gallant K, Gross GG, Levine MS, Chesselet MF (2005) Early behavioral deficits in R6/2 mice suitable for use in preclinical drug testing. Neurobiol Dis 20:1-11.

Hinault MP, Ben-Zvi A, Goloubinoff P (2006) Chaperones and proteases: cellular fold-controlling factors of proteins in neurodegenerative diseases and aging. J Mol Neurosci 30:249-265.

Hodgson JG, Agopyan N, Gutekunst CA, Leavitt BR, LePiane F, Singaraja R, Smith DJ, Bissada N, McCutcheon K, Nasir J, Jamot L, Li XJ, Stevens ME, Rosemond E, Roder JC, Phillips AG, Rubin EM, Hersch SM, Hayden MR (1999) A YAC mouse model for Huntington's disease with full-length mutant huntingtin, cytoplasmic toxicity, and selective striatal neurodegeneration. Neuron 23:181-192.

Hunter JM, Lesort M, Johnson GV (2007) Ubiquitin-proteasome system alterations in a striatal cell model of Huntington's disease. J Neurosci Res 85:1774-1788.

Hurlbert MS, Zhou W, Wasmeier C, Kaddis FG, Hutton JC, Freed CR (1999) Mice transgenic for an expanded CAG repeat in the Huntington's disease gene develop diabetes. Diabetes 48:649-651.

Johnson SA, Stout JC, Solomon AC, Langbehn DR, Aylward EH, Cruce CB, Ross CA, Nance M, Kayson E, Julian-Baros E, Hayden MR, Kieburtz K, Guttman M, Oakes D, Shoulson I, Beglinger L, Duff K, Penziner E, Paulsen JS (2007) Beyond disgust: impaired recognition of negative emotions prior to diagnosis in Huntington's disease. Brain 130:1732-1744.

Kaytor MD, Wilkinson KD, Warren ST (2004) Modulating huntingtin half-life alters polyglutamine-dependent aggregate formation and cell toxicity. J Neurochem 89:962-973.

Kennedy L, Shelbourne PF, Dewar D (2005) Alterations in dopamine and benzodiazepine receptor binding precede overt neuronal pathology in mice modelling early Huntington disease pathogenesis. Brain Res 1039:14-21.

Kim E, Cho KO, Rothschild A, Sheng M (1996) Heteromultimerization and NMDA receptor-clustering activity of Chapsyn-110, a member of the PSD-95 family of proteins. Neuron 17:103-113.

Kim MO, Chawla P, Overland RP, Xia E, Sadri-Vakili G, Cha JH (2008) Altered histone monoubiquitylation mediated by mutant huntingtin induces transcriptional dysregulation. J Neurosci 28:3947-3957.

Kim S, Burette A, Chung HS, Kwon SK, Woo J, Lee HW, Kim K, Kim H, Weinberg RJ, Kim E (2006) NGL family PSD-95-interacting adhesion molecules regulate excitatory synapse formation. Nat Neurosci 9:1294-1301.

Klement IA, Skinner PJ, Kaytor MD, Yi H, Hersch SM, Clark HB, Zoghbi HY, Orr HT (1998) Ataxin-1 nuclear localization and aggregation: role in polyglutamine-induced disease in SCA1 transgenic mice. Cell 95:41-53.

Kowall NW, Quigley BJ, Jr., Krause JE, Lu F, Kosofsky BE, Ferrante RJ (1993) Substance P and substance P receptor histochemistry in human neurodegenerative diseases. Regul Pept 46:174-185.

Kremer B, Goldberg P, Andrew SE, Theilmann J, Telenius H, Zeisler J, Squitieri F, Lin B, Bassett A, Almqvist E, et al. (1994) A worldwide study of the Huntington's disease mutation. The sensitivity and specificity of measuring CAG repeats. N Engl J Med 330:1401-1406.

Kuemmerle S, Gutekunst CA, Klein AM, Li XJ, Li SH, Beal MF, Hersch SM, Ferrante RJ (1999) Huntington aggregates may not predict neuronal death in Huntington's disease. Ann Neurol 46:842-849.

Kuhn A et al. (2007) Mutant huntingtin's effects on striatal gene expression in mice recapitulate changes observed in human Huntington's disease brain and do not differ with mutant huntingtin length or wild-type huntingtin dosage. Hum Mol Genet 16:1845-1861.

Kuhn A. GDR, Hodges A., Strand A.D., Sengstag T., Kooperberg C., Becanovic K., Pouladi M.A., Sathasivam K., Cha J.H., Hannan A.J., Hayden, M. R., Leavitt B.R., Dunnett S.B., Ferrante R.J., Albin, R. L., Shelbourne P., Delorenzi M., Augood S.J., Faull R.L., Olson J.M., Bates B.P., Jones, L., Luthi-Carter R. (2007) Mutant huntingtin's effect on striatal gene expression in mice recapitulate changes observed in human Huntington's disease brain and do not differ with mutant huntingtin length or wild-type huntingtin dosage. Hum Mol Genet in press.

Kuppenbender KD, Standaert DG, Feuerstein TJ, Penney JB, Jr., Young AB, Landwehrmeyer GB (2000) Expression of NMDA receptor subunit mRNAs in

neurochemically identified projection and interneurons in the human striatum. J Comp Neurol 419:407-421.

La Spada AR, Wilson EM, Lubahn DB, Harding AE, Fischbeck KH (1991) Androgen receptor gene mutations in X-linked spinal and bulbar muscular atrophy. Nature 352:77-79.

Landwehrmeyer GB, McNeil SM, Dure LSt, Ge P, Aizawa H, Huang Q, Ambrose CM, Duyao MP, Bird ED, Bonilla E, et al. (1995) Huntington's disease gene: regional and cellular expression in brain of normal and affected individuals. Ann Neurol 37:218-230.

Lang AE, Rogaeva EA, Tsuda T, Hutterer J, St George-Hyslop P (1994) Homozygous inheritance of the Machado-Joseph disease gene. Ann Neurol 36:443-447.

Langbehn DR, Brinkman RR, Falush D, Paulsen JS, Hayden MR (2004) A new model for prediction of the age of onset and penetrance for Huntington's disease based on CAG length. Clin Genet 65:267-277.

Lee S, Lee K, Hwang S, Kim SH, Song WK, Park ZY, Chang S (2006) SPIN90/WISH interacts with PSD-95 and regulates dendritic spinogenesis via an N-WASP-independent mechanism. EMBO J 25:4983-4995.

Levine MS, Klapstein GJ, Koppel A, Gruen E, Cepeda C, Vargas ME, Jokel ES, Carpenter EM, Zanjani H, Hurst RS, Efstratiadis A, Zeitlin S, Chesselet MF (1999) Enhanced sensitivity to N-methyl-D-aspartate receptor activation in transgenic and knockin mouse models of Huntington's disease. J Neurosci Res 58:515-532.

Li H, Li SH, Cheng AL, Mangiarini L, Bates GP, Li XJ (1999) Ultrastructural localization and progressive formation of neuropil aggregates in Huntington's disease transgenic mice. Hum Mol Genet 8:1227-1236.

Li JY, Plomann M, Brundin P (2003) Huntington's disease: a synaptopathy? Trends Mol Med 9:414-420.

Li L, Murphy TH, Hayden MR, Raymond LA (2004) Enhanced striatal NR2B-containing N-methyl-D-aspartate receptor-mediated synaptic currents in a mouse model of Huntington's disease. J Neurophysiol 92:2738-2746.

Li L, Fan MM, Icton CD, Leavitt BR, Hayden MR, Murphy TH, Raymond LA (2003) Role of NR2B-type NMDA receptors in selective neurodegeneration in Huntington disease. Neurobiol Aging 24:1113-1121.

Li SH, Li XJ (2004) Huntingtin-protein interactions and the pathogenesis of Huntington's disease. Trends Genet 20:146-154.

Li XJ, Li SH, Sharp AH, Nucifora FC, Jr., Schilling G, Lanahan A, Worley P, Snyder SH, Ross CA (1995) A huntingtin-associated protein enriched in brain with implications for pathology. Nature 378:398-402.

Lim J, Crespo-Barreto J, Jafar-Nejad P, Bowman AB, Richman R, Hill DE, Orr HT, Zoghbi HY (2008) Opposing effects of polyglutamine expansion on native protein complexes contribute to SCA1. Nature 452:713-718.

Lin CH, Tallaksen-Greene S, Chien WM, Cearley JA, Jackson WS, Crouse AB, Ren S, Li XJ, Albin RL, Detloff PJ (2001) Neurological abnormalities in a knock-in mouse model of Huntington's disease. Hum Mol Genet 10:137-144.

132

Lin CH, Tallaksen-Greene S., Chien W.M., Clearly JA., Jackson W.S., Crouse A.B., Ren S., Li XJ., Albin R.L., Detloff P.J. (2001) Neurological abnormalities in a knock-in mouse model of Hungtington's disease. Hum Mol Genet 10:137-144.

Lin X, Cummings CJ, Zoghbi HY (1999) Expanding our understanding of polyglutamine diseases through mouse models. Neuron 24:499-502.

Lione LA, Carter RJ, Hunt MJ, Bates GP, Morton AJ, Dunnett SB (1999) Selective discrimination learning impairments in mice expressing the human Huntington's disease mutation. J Neurosci 19:10428-10437.

Liu Y, Wong TP, Aarts M, Rooyakkers A, Liu L, Lai TW, Wu DC, Lu J, Tymianski M, Craig AM, Wang YT (2007) NMDA receptor subunits have differential roles in mediating excitotoxic neuronal death both in vitro and in vivo. J Neurosci 27:2846-2857.

Loftis JM, Janowsky A (2003) The N-methyl-D-aspartate receptor subunit NR2B: localization, functional properties, regulation, and clinical implications. Pharmacol Ther 97:55-85.

Lunkes A, Mandel JL (1997) Polyglutamines, nuclear inclusions and neurodegeneration. Nat Med 3:1201-1202.

Maat-Schieman ML, Dorsman JC, Smoor MA, Siesling S, Van Duinen SG, Verschuuren JJ, den Dunnen JT, Van Ommen GJ, Roos RA (1999) Distribution of inclusions in neuronal nuclei and dystrophic neurites in Huntington disease brain. J Neuropathol Exp Neurol 58:129-137.

Macdonald V, Halliday G (2002) Pyramidal cell loss in motor cortices in Huntington's disease. Neurobiol Dis 10:378-386.

Mangiarini L, Sathasivam K, Seller M, Cozens B, Harper A, Hetherington C, Lawton M, Trottier Y, Lehrach H, Davies SW, Bates GP (1996) Exon 1 of the HD gene with an expanded CAG repeat is sufficient to cause a progressive neurological phenotype in transgenic mice. Cell 87:493-506.

Mann VM, Cooper JM, Javoy-Agid F, Agid Y, Jenner P, Schapira AH (1990) Mitochondrial function and parental sex effect in Huntington's disease. Lancet 336:749.

Martin WR, Wieler M, Hanstock CC (2007) Is brain lactate increased in Huntington's disease? J Neurol Sci 263:70-74.

McGeer EG, McGeer PL (1976) Duplication of biochemical changes of Huntington's chorea by intrastriatal injections of glutamic and kainic acids. Nature 263:517-519.

Meade CA, Deng YP, Fusco FR, Del Mar N, Hersch S, Goldowitz D, Reiner A (2002) Cellular localization and development of neuronal intranuclear inclusions in striatal and cortical neurons in R6/2 transgenic mice. J Comp Neurol 449:241-269.

Menalled LB (2005) Knock-in mouse models of Huntington's disease. NeuroRx 2:465-470.

Menalled LB, Sison JD, Dragatsis I, Zeitlin S, Chesselet MF (2003) Time course of early motor and neuropathological anomalies in a knock-in mouse model of Huntington's disease with 140 CAG repeats. J Comp Neurol 465:11-26.

Menalled LB, Sison JD, Wu Y, Olivieri M, Li XJ, Li H, Zeitlin S, Chesselet MF (2002) Early motor dysfunction and striosomal distribution of huntingtin

microaggregates in Huntington's disease knock-in mice. J Neurosci 22:8266-8276.

Metzger S, Rong J, Nguyen HP, Cape A, Tomiuk J, Soehn AS, Propping P, Freudenberg-Hua Y, Freudenberg J, Tong L, Li SH, Li XJ, Riess O (2008) Huntingtin-associated protein-1 is a modifier of the age-at-onset of Huntington's disease. Hum Mol Genet 17:1137-1146.

Mihm MJ, Amann DM, Schanbacher BL, Altschuld RA, Bauer JA, Hoyt KR (2007) Cardiac dysfunction in the R6/2 mouse model of Huntington's disease. Neurobiol Dis 25:297-308.

Milakovic T, Quintanilla RA, Johnson GV (2006) Mutant huntingtin expression induces mitochondrial calcium handling defects in clonal striatal cells: functional consequences. J Biol Chem 281:34785-34795.

Monyer H, Sprengel R, Schoepfer R, Herb A, Higuchi M, Lomeli H, Burnashev N, Sakmann B, Seeburg PH (1992) Heteromeric NMDA receptors: molecular and functional distinction of subtypes. Science 256:1217-1221.

Morfini G, Pigino G, Brady ST (2005) Polyglutamine expansion diseases: failing to deliver. Trends Mol Med 11:64-70.

Morrow TJ, Paulson PE, Danneman PJ, Casey KL (1998) Regional changes in forebrain activation during the early and late phase of formalin nociception: analysis using cerebral blood flow in the rat. Pain 75:355-365.

Morton AJ, Hunt MJ, Hodges AK, Lewis PD, Redfern AJ, Dunnett SB, Jones L (2005) A combination drug therapy improves cognition and reverses gene expression changes in a mouse model of Huntington's disease. Eur J Neurosci 21:855-870.

Moseley ML, Zu T, Ikeda Y, Gao W, Mosemiller AK, Daughters RS, Chen G, Weatherspoon MR, Clark HB, Ebner TJ, Day JW, Ranum LP (2006) Bidirectional expression of CUG and CAG expansion transcripts and intranuclear polyglutamine inclusions in spinocerebellar ataxia type 8. Nat Genet 38:758-769.

Moulder KL, Onodera O, Burke JR, Strittmatter WJ, Johnson EM, Jr. (1999) Generation of neuronal intranuclear inclusions by polyglutamine-GFP: analysis of inclusion clearance and toxicity as a function of polyglutamine length. J Neurosci 19:705-715.

Nucifora FC, Jr., Sasaki M, Peters MF, Huang H, Cooper JK, Yamada M, Takahashi H, Tsuji S, Troncoso J, Dawson VL, Dawson TM, Ross CA (2001) Interference by huntingtin and atrophin-1 with cbp-mediated transcription leading to cellular toxicity. Science 291:2423-2428.

Oliveira JM, Jekabsons MB, Chen S, Lin A, Rego AC, Goncalves J, Ellerby LM, Nicholls DG (2007) Mitochondrial dysfunction in Huntington's disease: the bioenergetics of isolated and in situ mitochondria from transgenic mice. J Neurochem 101:241-249.

Ordway JM, Tallaksen-Greene S, Gutekunst CA, Bernstein EM, Cearley JA, Wiener HW, Dure LSt, Lindsey R, Hersch SM, Jope RS, Albin RL, Detloff PJ (1997) Ectopically expressed CAG repeats cause intranuclear inclusions and a progressive late onset neurological phenotype in the mouse. Cell 91:753-763.

Orr HT (2001) Beyond the Qs in the polyglutamine diseases. Genes Dev 15:925-932.

Orr HT, Zoghbi HY (2007) Trinucleotide repeat disorders. Annu Rev Neurosci 30:575-621.

Panov AV, Lund S, Greenamyre JT (2005) Ca2+-induced permeability transition in human lymphoblastoid cell mitochondria from normal and Huntington's disease individuals. Mol Cell Biochem 269:143-152.

Panov AV, Gutekunst CA, Leavitt BR, Hayden MR, Burke JR, Strittmatter WJ, Greenamyre JT (2002) Early mitochondrial calcium defects in Huntington's disease are a direct effect of polyglutamines. Nat Neurosci 5:731-736.

Papadia S, Hardingham GE (2007) The dichotomy of NMDA receptor signaling. Neuroscientist 13:572-579.

Park CS, Elgersma Y, Grant SG, Morrison JH (2008) alpha-Isoform of calcium-calmodulin-dependent protein kinase II and postsynaptic density protein 95 differentially regulate synaptic expression of NR2A- and NR2B-containing N-methyl-d-aspartate receptors in hippocampus. Neuroscience 151:43-55.

Paulson HL, Perez MK, Trottier Y, Trojanowski JQ, Subramony SH, Das SS, Vig P, Mandel JL, Fischbeck KH, Pittman RN (1997) Intranuclear inclusions of expanded polyglutamine protein in spinocerebellar ataxia type 3. Neuron 19:333-344.

Pavese N, Andrews TC, Brooks DJ, Ho AK, Rosser AE, Barker RA, Robbins TW, Sahakian BJ, Dunnett SB, Piccini P (2003) Progressive striatal and cortical dopamine receptor dysfunction in Huntington's disease: a PET study. Brain 126:1127-1135.

Paxinos G, Franklin KBJ (2001) The mouse brain in stereotaxic coordinates, Second Edition. San Diego: Academic Press.

Penney JB, Jr., Young AB, Shoulson I, Starosta-Rubenstein S, Snodgrass SR, Sanchez-Ramos J, Ramos-Arroyo M, Gomez F, Penchaszadeh G, Alvir J, et al. (1990) Huntington's disease in Venezuela: 7 years of follow-up on symptomatic and asymptomatic individuals. Mov Disord 5:93-99.

Perez-Navarro E, Canals JM, Gines S, Alberch J (2006) Cellular and molecular mechanisms involved in the selective vulnerability of striatal projection neurons in Huntington's disease. Histol Histopathol 21:1217-1232.

Perutz MF, Pope BJ, Owen D, Wanker EE, Scherzinger E (2002) Aggregation of proteins with expanded glutamine and alanine repeats of the glutamine-rich and asparagine-rich domains of Sup35 and of the amyloid beta-peptide of amyloid plaques. Proc Natl Acad Sci U S A 99:5596-5600.

Powers WJ, Haas RH, Le T, Videen TO, Hershey T, McGee-Minnich L, Perlmutter JS (2007a) Normal platelet mitochondrial complex I activity in Huntington's disease. Neurobiol Dis 27:99-101.

Powers WJ, Videen TO, Markham J, McGee-Minnich L, Antenor-Dorsey JV, Hershey T, Perlmutter JS (2007b) Selective defect of in vivo glycolysis in early Huntington's disease striatum. Proc Natl Acad Sci U S A 104:2945-2949.

Reddy PH, Williams M, Charles V, Garrett L, Pike-Buchanan L, Whetsell WO, Jr., Miller G, Tagle DA (1998) Behavioural abnormalities and selective neuronal loss in HD transgenic mice expressing mutated full-length HD cDNA. Nat Genet 20:198-202.

Reiner A, Albin RL, Anderson KD, D'Amato CJ, Penney JB, Young AB (1988) Differential loss of striatal projection neurons in Huntington disease. Proc Natl Acad Sci U S A 85:5733-5737.

Ribchester RR, Thomson D, Wood NI, Hinks T, Gillingwater TH, Wishart TM, Court FA, Morton AJ (2004) Progressive abnormalities in skeletal muscle and neuromuscular junctions of transgenic mice expressing the Huntington's disease mutation. Eur J Neurosci 20:3092-3114.

Rosas HD, Feigin AS, Hersch SM (2004a) Using advances in neuroimaging to detect, understand, and monitor disease progression in Huntington's disease. NeuroRx 1:263-272.

Rosas HD, Hevelone ND, Zaleta AK, Greve DN, Salat DH, Fischl B (2005) Regional cortical thinning in preclinical Huntington disease and its relationship to cognition. Neurology 65:745-747.

Rosas HD, Liu AK, Hersch S, Glessner M, Ferrante RJ, Salat DH, van der Kouwe A, Jenkins BG, Dale AM, Fischl B (2002) Regional and progressive thinning of the cortical ribbon in Huntington's disease. Neurology 58:695-701.

Rosas HD, Koroshetz WJ, Chen YI, Skeuse C, Vangel M, Cudkowicz ME, Caplan K, Marek K, Seidman LJ, Makris N, Jenkins BG, Goldstein JM (2004b) Evidence for more widespread cerebral pathology in early HD: an MRI-based morphometric analysis. Neurology 60:1615-1620.

Rubinsztein DC et al. (1996) Phenotypic characterization of individuals with 30-40 CAG repeats in the Huntington disease (HD) gene reveals HD cases with 36 repeats and apparently normal elderly individuals with 36-39 repeats. Am J Hum Genet 59:16-22.

Sapp E, Schwarz C, Chase K, Bhide PG, Young AB, Penney J, Vonsattel JP, Aronin N, DiFiglia M (1997) Huntingtin localization in brains of normal and Huntington's disease patients. Ann Neurol 42:604-612.

Saudou F, Finkbeiner S, Devys D, Greenberg ME (1998) Huntingtin acts in the nucleus to induce apoptosis but death does not correlate with the formation of intranuclear inclusions. Cell 95:55-66.

Sawa A, Wiegand GW, Cooper J, Margolis RL, Sharp AH, Lawler JF, Jr., Greenamyre JT, Snyder SH, Ross CA (1999) Increased apoptosis of Huntington disease lymphoblasts associated with repeat length-dependent mitochondrial depolarization. Nat Med 5:1194-1198.

Scherzinger E, Lurz R, Turmaine M, Mangiarini L, Hollenbach B, Hasenbank R, Bates GP, Davies SW, Lehrach H, Wanker EE (1997) Huntingtin-encoded polyglutamine expansions form amyloid-like protein aggregates in vitro and in vivo. Cell 90:549-558.

Schiffmann SN, Vanderhaeghen JJ (1991) Does the absence of clinical expression of choreoathetosis, despite severe striatal atrophy, correlate with plasticity of neuropeptide synthesis? J Neural Transm Suppl 33:99-103.

Schilling G, Becher MW, Sharp AH, Jinnah HA, Duan K, Kotzuk JA, Slunt HH, Ratovitski T, Cooper JK, Jenkins NA, Copeland NG, Price DL, Ross CA, Borchelt DR (1999) Intranuclear inclusions and neuritic aggregates in transgenic mice expressing a mutant N-terminal fragment of huntingtin. Hum Mol Genet 8:397-407.

Schwarcz R, Whetsell WOJ, Mangano RM (1983) Quinolinic acid: an endogenous metabolite that produces axon-sparing lesions in rat brain. Science 219:316-318.

Semaka A, Creighton S, Warby S, Hayden MR (2006) Predictive testing for Huntington disease: interpretation and significance of intermediate alleles. Clin Genet 70:283-294.

Seneca S, Fagnart D, Keymolen K, Lissens W, Hasaerts D, Debulpaep S, Desprechins B, Liebaers I, De Meirleir L (2004) Early onset Huntington disease: a neuronal degeneration syndrome. Eur J Pediatr 163:717-721.

Sharp AH, Loev SJ, Schilling G, Li SH, Li XJ, Bao J, Wagster MV, Kotzuk JA, Steiner JP, Lo A, et al. (1995) Widespread expression of Huntington's disease gene (IT15) protein product. Neuron 14:1065-1074.

Shehadeh J, Fernandes HB, Zeron Mullins MM, Graham RK, Leavitt BR, Hayden MR, Raymond LA (2006) Striatal neuronal apoptosis is preferentially enhanced by NMDA receptor activation in YAC transgenic mouse model of Huntington disease. Neurobiol Dis 21:392-403.

Shelbourne PF, Killeen N, Hevner RF, Johnston HM, Tecott L, Lewandoski M, Ennis M, Ramirez L, Li Z, Iannicola C, Littman DR, Myers RM (1999) A Huntington's disease CAG expansion at the murine Hdh locus is unstable and associated with behavioural abnormalities in mice. Hum Mol Genet 8:763-774.

Slow EJ, Graham RK, Hayden MR (2006) To be or not to be toxic: aggregations in Huntington and Alzheimer disease. Trends Genet 22:408-411.

Slow EJ, Graham RK, Osmand AP, Devon RS, Lu G, Deng Y, Pearson J, Vaid K, Bissada N, Wetzel R, Leavitt BR, Hayden MR (2005) Absence of behavioral abnormalities and neurodegeneration in vivo despite widespread neuronal huntingtin inclusions. Proc Natl Acad Sci U S A 102:11402-11407.

Slow EJ, van Raamsdonk J, Rogers D, Coleman SH, Graham RK, Deng Y, Oh R, Bissada N, Hossain SM, Yang YZ, Li XJ, Simpson EM, Gutekunst CA, Leavitt BR, Hayden MR (2003) Selective striatal neuronal loss in a YAC128 mouse model of Huntington disease. Hum Mol Genet 12:1555-1567.

Sobue G, Doyu M, Nakao N, Shimada N, Mitsuma T, Maruyama H, Kawakami S, Nakamura S (1996) Homozygosity for Machado-Joseph disease gene enhances phenotypic severity. J Neurol Neurosurg Psychiatry 60:354-356.

Solomon AC, Stout JC, Johnson SA, Langbehn DR, Aylward EH, Brandt J, Ross CA, Beglinger L, Hayden MR, Kieburtz K, Kayson E, Julian-Baros E, Duff K, Guttman M, Nance M, Oakes D, Shoulson I, Penziner E, Paulsen JS (2007) Verbal episodic memory declines prior to diagnosis in Huntington's disease. Neuropsychologia 45:1767-1776.

Soong BW, Paulson HL (2007) Spinocerebellar ataxias: an update. Curr Opin Neurol 20:438-446.

Soriano FX, Hardingham GE (2007) Compartmentalized NMDA receptor signalling to survival and death. J Physiol 584:381-387.

Squitieri F, Gellera C, Cannella M, Mariotti C, Cislaghi G, Rubinsztein DC, Almqvist EW, Turner D, Bachoud-Levi AC, Simpson SA, Delatycki M, Maglione V, Hayden MR, Donato SD (2003) Homozygosity for CAG mutation in Huntington disease is associated with a more severe clinical course. Brain 126:946-955.

Stack EC, Ferrante RJ (2007) Huntington's disease: progress and potential in the field. Expert Opin Investig Drugs 16:1933-1953.

Stack EC, Kubilus JK, Smith K, Cormier K, Del Signore SJ, Guelin E, Ryu H, Hersch SM, Ferrante RJ (2005) Chronology of behavioral symptoms and neuropathological sequela in R6/2 Huntington's disease transgenic mice. J Comp Neurol 490:354-370.

Stack EC, Dedeoglu A, Smith KM, Cormier K, Kubilus JK, Bogdanov M, Matson WR, Yang L, Jenkins BG, Luthi-Carter R, Kowall NW, Hersch SM, Beal MF, Ferrante RJ (2007) Neuroprotective effects of synaptic modulation in Huntington's disease R6/2 mice. J Neurosci 27:12908-12915.

Starling AJ, Andre VM, Cepeda C, de Lima M, Chandler SH, Levine MS (2005) Alterations in N-methyl-D-aspartate receptor sensitivity and magnesium blockade occur early in development in the R6/2 mouse model of Huntington's disease. J Neurosci Res 82:377-386.

Steffan JS, Kazantsev A, Spasic-Boskovic O, Greenwald M, Zhu YZ, Gohler H, Wanker EE, Bates GP, Housman DE, Thompson LM (2000) The Huntington's disease protein interacts with p53 and CREB-binding protein and represses transcription. Proc Natl Acad Sci U S A 97:6763-6768.

Stine OC, Pleasant N, Franz ML, Abbott MH, Folstein SE, Ross CA (1993) Correlation between the onset age of Huntington's disease and length of the trinucleotide repeat in IT-15. Hum Mol Genet 2:1547-1549.

Strand AD, Baquet ZC, Aragaki AK, Holmans P, Yang L, Cleren C, Beal MF, Jones L, Kooperberg C, Olson JM, Jones KR (2007) Expression profiling of Huntington's disease models suggests that brain-derived neurotrophic factor depletion plays a major role in striatal degeneration. J Neurosci 27:11758-11768.

Strong TV, Tagle DA, Valdes JM, Elmer LW, Boehm K, Swaroop M, Kaatz KW, Collins FS, Albin RL (1993) Widespread expression of the human and rat Huntington's disease gene in brain and nonneural tissues. Nat Genet 5:259-265.

Sun Y, Savanenin A, Reddy PH, Liu YF (2001) Polyglutamine-expanded huntingtin promotes sensitization of N-methyl-D-aspartate receptors via post-synaptic density 95. J Biol Chem 276:24713-24718.

Szebenyi G, Morfini GA, Babcock A, Gould M, Selkoe K, Stenoien DL, Young M, Faber PW, MacDonald ME, McPhaul MJ, Brady ST (2003) Neuropathogenic forms of huntingtin and androgen receptor inhibit fast axonal transport. Neuron 40:41-52.

Tabrizi SJ, Cleeter MW, Xuereb J, Taanman JW, Cooper JM, Schapira AH (1999) Biochemical abnormalities and excitotoxicity in Huntington's disease brain. Ann Neurol 45:25-32.

Tallaksen-Greene S, Ordway JM, Crouse AB, Jackson WS, Detloff PJ, Albin RL (2003) Hprt(CAG)146 mice: age of onset of behavioral abnormalities, time course of neuronal intranuclear inclusion accumulation, neurotransmitter marker alterations, mitochondrial function markers, and susceptibility to 1-methyl-4-phenyl-1,2,3,6-tetrahydropyridine. J Comp Neurol 465:205-219.

Tallaksen-Greene SJ, Crouse AB, Hunter JM, Detloff PJ, Albin RL (2005) Neuronal intranuclear inclusions and neuropil aggregates in HdhCAG(150) knockin mice. Neuroscience 131:843-852.

Tang TS, Tu H, Chan EY, Maximov A, Wang Z, Wellington CL, Hayden MR, Bezprozvanny I (2003a) Huntingtin and huntingtin-associated protein 1 influence

neuronal calcium signaling mediated by inositol-(1,4,5) triphosphate receptor type 1. Neuron 39:227-239.

Tang YP, Shimizu E, Dube GR, Rampon C, Kerchner GA, Zhuo M, Lui G, Tsien JZ (1999) Genetic enhancement of learning and memory in mice. Nature 401:63-69.

Thomas CG, Miller AJ, Westbrook GL (2006) Synaptic and extrasynaptic NMDA receptor NR2 subunits in cultured hippocampal neurons. J Neurophysiol 95:1727-1734.

Thomas EA (2006) Striatal specificity of gene expression dysregulation in Huntington's disease. J Neurosci Res 84:1151-1164.

Trushina E et al. (2004) Mutant huntingtin impairs axonal trafficking in mammalian neurons in vivo and in vitro. Mol Cell Biol 24:8195-8209.

van Oostrom JCH, Maquire RP, Verschuuren-Bemelmans CC, Veenma-van der Duin L, Pruim J, Roos R, Leenders KL (2005) Striatal dopamine D2 receptors, metabolism, and volume in preclinical Huntington disease. Neurology 65:941-943.

van Raamsdonk J, Metzler M, Slow E, Pearson J, Schwab C, Carroll J, Graham R, Leavitt BR, Hayden MR (2007) Phenotypic abnormalities in the YAC128 mouse model of Huntington disease are penetrant on multiple genetic backgrounds and modulated by strain. Neurobiol Dis 26:189-200.

Van Raamsdonk JM, Murphy Z, Slow EJ, Leavitt BR, Hayden MR (2005a) Selective degeneration and nuclear localization of mutant huntingtin in the YAC128 mouse model of Huntington disease. Hum Mol Genet 14:3823-3835.

Van Raamsdonk JM, Pearson J, Slow EJ, Hossain SM, Leavitt BR, Hayden MR (2005b) Cognitive dysfunction precedes neuropathology and motor abnormalities in the YAC128 mouse model of Huntington's disease. J Neurosci 25:4169-4180.

Vonsattel JP, DiFiglia M (1998) Huntington disease. J Neuropathol Exp Neurol 57:369-384.

Vonsattel JP, Myers RH, Stevens TJ, Ferrante RJ, Bird ED, Richardson EP, Jr. (1985) Neuropathological classification of Huntington's disease. J Neuropathol Exp Neurol 44:559-577.

Warby S, Graham R, Hayden MR (2008) Huntington disease. wwwgenetestsorg.

Weeks RA, Piccini P, Harding AE, Brooks DJ (1996) Striatal D1 and D2 dopamine receptor loss in asymptomatic mutation carriers of Huntington's disease. Ann Neurol 40:49-54.

Wexler NS et al. (2004) Venezuelan kindreds reveal that genetic and environmental factors modulate Huntington's disease age of onset. Proc Natl Acad Sci U S A 101:3498-3503.

Weydt P, Pineda VV, Torrence AE, Libby RT, Satterfield TF, Lazarowski ER, Gilbert ML, Morton GJ, Bammler TK, Strand AD, Cui L, Beyer RP, Easley CN, Smith AC, Krainc D, Luquet S, Sweet IR, Schwartz MW, La Spada AR (2006) Thermoregulatory and metabolic defects in Huntington's disease transgenic mice implicate PGC-1alpha in Huntington's disease neurodegeneration. Cell Metab 4:349-362.

Wheeler VC, Gutekunst CA, Vrbanac V, Lebel LA, Schilling G, Hersch S, Friedlander RM, Gusella JF, Vonsattel JP, Borchelt DR, MacDonald ME (2002) Early

phenotypes that presage late-onset neurodegenerative disease allow testing of modifiers in Hdh CAG knock-in mice. Hum Mol Genet 11:633-640.

Wheeler VC, White JK, Gutekunst CA, Vrbanac V, Weaver M, Li XJ, Li SH, Yi H, Vonsattel JP, Gusella JF, Hersch S, Auerbach W, Joyner AL, MacDonald ME (2000) Long glutamine tracts cause nuclear localization of a novel form of huntingtin in medium spiny striatal neurons in HdhQ92 and HdhQ111 knock-in mice. Hum Mol Genet 9:503-513.

White JK, Auerbach W, Duyao MP, Vonsattel JP, Gusella JF, Joyner AL, MacDonald ME (1997) Huntingtin is required for neurogenesis and is not impaired by the Huntington's disease CAG expansion. Nat Genet 17:404-410.

Willner P (1991) Neuromethods 18.

Woodman B, Butler R, Landles C, Lupton MK, Tse J, Hockly E, Moffitt H, Sathasivam K, Bates GP (2007) The Hdh(Q150/Q150) knock-in mouse model of HD and the R6/2 exon 1 model develop comparable and widespread molecular phenotypes. Brain Res Bull 72:83-97.

Yamamoto A, Lucas JJ, Hen R (2000) Reversal of neuropathology and motor dysfunction in a conditional model of Huntington's disease. Cell 101:57-66.

Yamanaka T, Miyazaki H, Oyama F, Kurosawa M, Washizu C, Doi H, Nukina N (2008) Mutant Huntingtin reduces HSP70 expression through the sequestration of NF-Y transcription factor. EMBO J 27:827-839.

Yu ZX, Li SH, Evans J, Pillarisetti A, Li H, Li XJ (2003) Mutant huntingtin causes context-dependent neurodegeneration in mice with Huntington's disease. J Neurosci 23:2193-2202.

Zeron MM, Chen N, Moshaver A, Lee AT, Wellington CL, Hayden MR, Raymond LA (2001) Mutant huntingtin enhances excitotoxic cell death. Mol Cell Neurosci 17:41-53.

Zeron MM, Hansson O, Chen N, Wellington CL, Leavitt BR, Brundin P, Hayden MR, Raymond LA (2002) Increased sensitivity to N-methyl-D-aspartate receptor-mediated excitotoxicity in a mouse model of Huntington's disease. Neuron 33:849-860.

Zeron MM, Fernandes HB, Krebs C, Shehadeh J, Wellington CL, Leavitt BR, Baimbridge KG, Hayden MR, Raymond LA (2004) Potentiation of NMDA receptor-mediated excitotoxicity linked with intrinsic apoptotic pathway in YAC transgenic mouse model of Huntington's disease. Mol Cell Neurosci 25:469-479.

Zhai W, Jeong H, Cui L, Krainc D, Tjian R (2005) In vitro analysis of huntingtin-mediated transcriptional repression reveals multiple transcription factor targets. Cell 123:1241-1253.

Zoghbi HY, Orr HT (1999) Polyglutamine diseases: protein cleavage and aggregation. Curr Opin Neurobiol 9:566-570.

Zuccato C, Cattaneo E (2007) Role of brain-derived neurotrophic factor in Huntington's disease. Prog Neurobiol 81:294-330.

Zuccato C, Marullo M, Conforti P, Macdonald ME, Tartari M, Cattaneo E (2007) Systematic Assessment of BDNF and Its Receptor Levels in Human Cortices Affected by Huntington's Disease. Brain Pathol.

Zuccato C, Tartari M, Crotti A, Goffredo D, Valenza M, Conti L, Cataudella T, Leavitt BR, Hayden MR, Timmusk T, Rigamonti D, Cattaneo E (2003) Huntingtin

interacts with REST/NRSF to modulate the transcription of NRSE-controlled neuronal genes. Nat Genet 35:76-83.

Zuccato C, Ciammola A, Rigamonti D, Leavitt BR, Goffredo D, Conti L, MacDonald ME, Friedlander RM, Silani V, Hayden MR, Timmusk T, Sipione S, Cattaneo E (2001) Loss of huntingtin-mediated BDNF gene transcription in Huntington's disease. Science 293:493-498.